Mesoscopic particles in polymer solutions

Inaugural-Dissertation

zur

Erlangung des Doktorgrades der

Mathematisch-Naturwissenschaftlichen Fakultät

der Heinrich-Heine-Universität Düsseldorf

vorgelegt von

Ralph Maaßen

aus Mönchengladbach

Grafische Betriebe des Forschungszentrums Jülich, Jülich

2002

Gedruckt mit der Genehmigung der Mathematisch-Naturwissenschaftlichen Fakultät der Heinrich-Heine-Universität Düsseldorf

Referent: Prof. E. Eisenriegler

Koreferent: Prof. H.K. Janssen

Tag der mündlichen Prüfung: 22. Mai 2002

Abstract

In this work I study a single mesoscopic colloidal particle immersed in a solution of long, flexible, and free non-adsorbing polymer chains. For entropic reasons the chains avoid the space close to the surface of the particle which leads to a depletion layer around the particle.

For a spherical particle I investigate the solvation free energy and the polymer density depletion profiles and discuss the corresponding crossover functions which interpolate between the limits of small and large particle to polymer size ratio and of dilute and semi-dilute embedding polymer solutions. In a first step, a mean-field approach is used which reveals qualitative features. An important relation between the pressure exerted by the polymers onto the particle surface and the local monomer density close to the surface is also obeyed in mean-field theory. In a second step, a 'renormalized mean-field (or tree) approximation' is used to estimate the solvation free energy of the spherical particle. This employs the renormalization group and leads to scaling functions and power laws with the correct exponents for polymers in a good solvent. For large particle to polymer size ratio the dependence on the inter-chain overlap of the surface tension and the coefficient of spontaneous curvature in a small curvature expansion is calculated. The behavior of the polymer induced surface tension compares well with results that have been obtained from simulations by Louis *et al.* The crossover of the solvation free energy from large to small size ratio is obtained in the dilute and the semi-dilute limit. For small particle radius the solvation free energy

is proportional to the unperturbed monomer density but independent of the inter-chain overlap.

In order to study the effect of anisotropy, a particle of ellipsoidal shape is investigated in a solution of ideal polymer chains. The depletion layer is anisotropic and most pronounced in regions of weak surface curvature.

An exact analytical expression is obtained for the center of mass density profile of free ideal polymer chains in a half space bounded by a hard planar wall. Contrary to the power law behaviors of the monomer density profile and the density profile of chain ends or midpoints, the center of mass profile tends to zero in an exponential fashion on approaching the wall.

Contents

Chapter 1

Introduction

There is an effective interaction between colloidal particles in a solvent which contains non-adsorbing free polymer chains. It was first found by Asakura and Oosawa [1] nearly 50 years ago. Since the chains avoid the space between two close particles, the unbalanced polymer pressure from outside pushes the two particles towards each other. This depletion interaction is believed to be important for a variety of interesting colloids such as casein micelles [2], red blood cells [3], and globular proteins [4]. It is an example of what is termed 'macromolecular crowding' in the biophysical chemistry literature [5, 6]. Thus there has been much interest in calculating or approximating the depletion interaction between colloids in the last years [7]-[15].

The depletion of long flexible polymers near the surface of a colloidal particle is an entropic effect. Immersing a particle into a solution of non-adsorbing polymers reduces the available number of configurations. This leads to a depletion layer around the particle which can be described by means of the bulk normalized polymer density profile $\mathcal{M}$ or the (bulk normalized)

density of chain ends $\mathcal{E}$. Since there is work needed to displace the polymers from the volume of the particle and from the depletion layer, it costs free energy to immerse the particle into the polymer solution. This free energy cost F as well as $\mathcal{M}$ and $\mathcal{E}$ depends in a crucial way on the ratio of the particle and chain sizes and on the degree of overlap between the chains, i.e., on whether the polymer solution is dilute or semi-dilute. The simplest system for studying both effects is a *single* spherical particle or a *single* cylindrical rod with radius R embedded in a monodisperse solution of free non-adsorbing polymer chains. This system includes also the case of a polymer solution in presence of a *planar wall* which can be considered as a particle with infinite radius.

In this work I study the depletion density profiles around a spherical or cylindrical particle and the free energy cost to immerse the particle for arbitrary overlap and size ratio. The overlap between chains may be characterized by n/n^*, where n is the number density of chains in the bulk and n^* is the density at the onset of overlap [16], and the size ratio by

$$\rho \;=\; R \,/\, \mathcal{R}_x \quad . \tag{1.1}$$

Here $d\,\mathcal{R}_x^2$ is the mean square end-to-end distance of a single polymer chain in dilute solution without particles, and d denotes the spatial dimension. For semi-dilute solutions, where the overlap between chains is very large, the chains form a kind of mesh. The typical polymer length scale in this case is the mesh size or screening length ξ [16, 17, 18].

Fig. 1.1 shows various limits of a single spherical or cylindrical particle in a polymer solution. The four corners are related to the cases of a planar wall in a dilute or semi-dilute solution (lower and upper left corner) and of a small

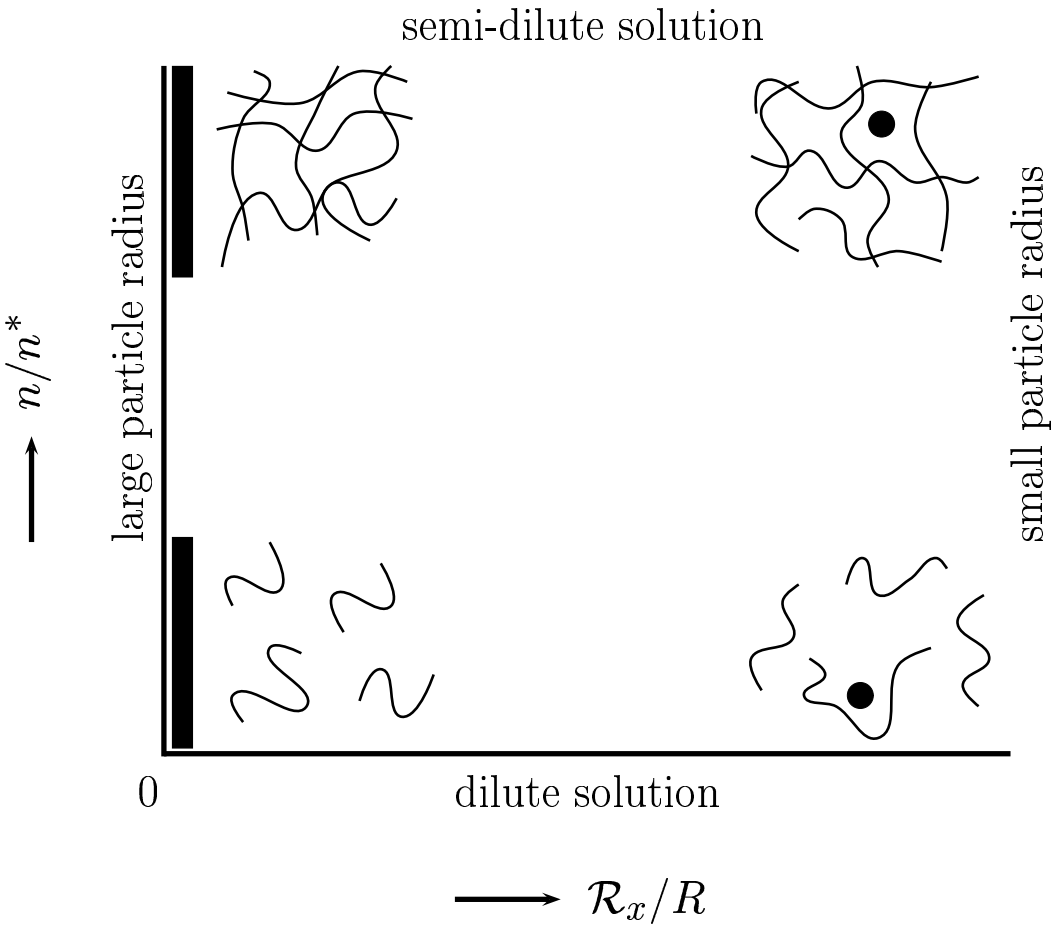

Figure 1.1: Various limits of a single spherical particle or a single cylindrical rod in a solution of non-adsorbing polymers. The sphere or rod becomes a planar wall for vanishing $\mathcal{R}_x/R$ (i.e. for points on the vertical axis), and becomes a 'small' sphere or a 'thin' rod with a radius much smaller than the characteristic polymer lengths (such as the root mean square end-to-end distance $\propto \mathcal{R}_x$ in the dilute solution or the mesh-size ξ in the semi-dilute solution) as $\mathcal{R}_x/R$ becomes large with the inter-chain overlap n/n^* kept fixed. The following limits are shown: planar wall in a dilute solution (lower left corner), planar wall in a semi-dilute solution (upper left corner), small sphere or a thin rod in a dilute solution (lower right corner), and small sphere or a thin rod in a semi-dilute solution (upper right corner).

sphere or a thin rod in a dilute or semi-dilute solution (lower and upper right corner), respectively. The behavior is quite different in these different limits. For example in the semi-dilute limit $n \gg n^*$ the bulk-normalized polymer density profile $\mathcal{M}_{\rm pw}$ near a planar wall reaches its bulk value 1 for distances z from the wall which are of the order of the screening length ξ. In the dilute limit $n \ll n^*$ the corresponding 'healing length' for $\mathcal{M}_{\rm pw}$ is [16, 19] of the order of the end-to-end distance $\propto \mathcal{R}_x$, introduced below Eq. (1.1). For spheres or infinitely long rods with *small* radius $R \ll \xi, \mathcal{R}_x$, corresponding to the right margin of Fig. 1.1, the healing length of $\mathcal{M}$ is of the order of R. For distances r from the center of the small sphere (or $r_\perp$ from the axis of the thin cylinder) which are much smaller than ξ or $\mathcal{R}_x$ the normalized profile $\mathcal{M}_{\rm s}$ is *independent* of the overlap and of $\xi, \mathcal{R}_x$ and only depends [20, 21, 22, 23] on r/R (or $r_\perp/R$). Also the free energy cost F shows qualitative differences [24, 7, 25, 26] in the various limits in Fig. 1.1.

An important relation between the two basic physical quantities $\mathcal{M}$ and F which applies for arbitrary size ratio and overlap is the so-called density-pressure identity. See Refs. [27, 28, 23] and Appendix A. For example, for a cylinder of infinite length $\lambda \to \infty$ it relates the polymer pressure

$$p = \frac{1}{S_\perp} \frac{d}{dR} \frac{F}{\lambda} \tag{1.2}$$

on the surface of the cylinder with surface area $S_\perp \lambda$ to the behavior $\mathcal{M}^{\rm as}(r_\perp)$ of the normalized polymer density profile $\mathcal{M}(r_\perp)$ *near* the surface via

$$\frac{n \mathcal{R}_x^{1/\nu} \mathcal{M}^{(\rm as)}(r_\perp)}{(r_\perp - R)^{1/\nu}} = B \frac{p}{k_B T} \quad . \tag{1.3}$$

Here $S_\perp = 2\pi R$ (or $S_\perp = 4\pi R^2$) is the circumference of the circle (or the

surface area of the sphere) of radius R of the cross-section perpendicular to the axis of the cylinder in three (or four[1]) dimensions, $r_\perp$ is the distance of $\mathbf{r}$ from the axis, ν is the Flory exponent [16, 17, 18] and B is a universal amplitude [28, 29]. The denominator $(r_\perp - R)^{1/\nu}$ on the left-hand side cancels the $r_\perp$-dependence of $\mathcal{M}^{(\mathrm{as})}$, and both sides in Eq. (1.3) only depend on $R, \mathcal{R}_x$, and n. Although the density-pressure identity involves the density at distances $r_\perp - R$ from the surface that are small compared to R and the mesoscopic polymer lengths, these distances are in the scaling regime and still much larger than microscopic lengths such as the monomer size. The identity is free of microscopic parameters and no proportionality factors have been omitted.

Keeping both the size ratio and the degree of inter-chain overlap *arbitrary* one has to resort to approximations. One approximation that I will use in this work is the mean-field approximation that determines the leading order results $\epsilon \searrow 0$ for a polymer embedding space of dimension $d = 4 - \epsilon$. For illustration I recall some known analytical mean-field results valid for some of the limiting cases in Fig. (1.1) for an infinitely long cylinder (rod) in four dimensions:

(i) For *small* radius R ($\rho \to 0$) the normalized density profile and the free energy cost per unit axis length λ are given by [21, 22]

$$\mathcal{M} = \left(1 - \frac{R}{r_\perp}\right)^2 \qquad ; \qquad R\,,\, r_\perp \ll \mathcal{R}_x\,,\, \xi \tag{1.4}$$

and

$$\frac{F}{k_B T \lambda} = 2\pi n R\, \mathcal{R}_x^2 \quad . \tag{1.5}$$

[1]The special interest in the spatial dimension four will be explained in Chapter 2.

These expressions apply for *arbitrary* overlap n/n^*.

(ii) In the mean-field approximation a *dilute* polymer solution ($n/n^* \to 0$) corresponds to a solution of ideal chains without excluded volume interaction between monomers. In this case the bulk-normalized density profile and the free energy cost per unit axis length λ for arbitrary size ratio ρ are given by [24, 22]

$$\mathcal{M}(\mathbf{r}) = 1 - 8\,\frac{R}{r_\perp}\,\mathrm{i}^2\mathrm{erfc}(y) + 4\,\frac{R^2}{r_\perp^2}\,\mathrm{i}^2\mathrm{erfc}(2y) \quad , \tag{1.6}$$

where i^2erfc is the second iterated complementary error function [30],

$$y = \frac{r_\perp - R}{\sqrt{2}\mathcal{R}_x} \tag{1.7}$$

and

$$\frac{F}{k_B T \lambda} \;=\; 2\pi n R\,\mathcal{R}_x^2 \left(1 + 2\sqrt{\frac{2}{\pi}}\rho + \frac{2}{3}\rho^2\right) \quad . \tag{1.8}$$

The profile (1.6) and the free energy cost (1.8) satisfy the density-pressure identity and reduce, for $\rho \to 0$, to the thin cylinder expressions in (i).

Analytical mean-field results for large radius (planar wall) are also available in the *semi-dilute* limit [16, 27] and will be mentioned in Sec. 3.1.4. No analytical mean-field results seem to be known for the dilute - semi-dilute crossover in the planar wall limit (vertical axis in Fig. 1.1) and for the crossover in size ratio in the semi-dilute limit (horizontal line for large n/n^*).

This work is organized as follows. In Chapter 2 I present the model and the methods that will be used in Chapter 3 to calculate scaling functions in the mean-field approximation. Although the leading order results for $d \to 4$

lead to estimates for scaling functions in $d = 3$ with only moderate quantitative success, they are useful due to several reasons. First of all most of the *qualitative* features in d near 4 presumably persist down to $d = 3$. Secondly they demonstrate in a transparent way fundamental properties, such as the density-pressure identity (1.3) or the small radius expansion [22, 7], which should apply along the *whole* route. Furthermore it is possible to improve the mean-field results via the so called renormalized tree approximation [18] which will be introduced in Chapter 4 below. This theory works directly in three dimensions and gives at least semi-quantitative results.

A particle of *ellipsoidal* shape is considered in Chapter 5 in order to study the effect of anisotropy. Both cases of an elongated and a flattened ellipsoid of revolution are considered. In the limit that the smaller axis goes to zero, this geometry includes the cases of an infinitely thin needle and of a circular disk. Because of the lower symmetry the ellipsoidal case is more complicated and I consider only dilute solutions of ideal chains.

Another interesting result for ideal chains is presented in Chapter 6, in which I derive the center of mass distribution of an ideal polymer chain near a planar wall. Since fixing the center of mass close to the wall restricts the polymer configurations much more than fixing an end or the midpoint, there are qualitative differences in the corresponding density profiles.

In Chapter 7 all results will be summarized. Some technical details are relegated to Appendices A-D. Parts of Chapters 1-4 have been published in Ref. [31] and parts of Chapter 6 in Ref. [32].

Chapter 2

Model and Methods

A dilute or semi-dilute solution of long flexible polymer chains displays universal behavior which is independent of most details and depends on only a few qualitative properties, such as the presence of the excluded volume interaction between monomers in a good solvent.

The simplest example for universality is the Gaussian form of the distance distribution between endpoints of a long chain without excluded volume interaction. This applies for arbitrary short range interactions along the chain and is ensured by the central limit theorem.

The universal properties [16, 17, 18, 19] of long flexible polymers in a good solvent that interact with an embedded non-adsorbing mesoscopic colloidal particle can be calculated from a simple model in which each polymer molecule is represented by a 'spring and bead' chain. This means that the polymer molecule is replaced by a sequence of elastic springs connecting point-like beads. The beads are excluded from the space occupied by the particle. Beads of the same chain or of different chains repel each other at

microscopic distances. Despite the simplicity of the model the conformational statistics of the polymers for *arbitrary* size ratio and overlap is quite complex, and one has to resort to approximations. The approximation used in Chapter 3 is called the self-consistent mean-field approximation and goes also under the names of the random-phase or tree approximation [16, 18]. On replacing the excluded volume interaction by a configuration-independent external potential acting on each chain-monomer, the mean-field approximation reduces the many-chain problem to the problem of one ideal chain in a potential to be determined self-consistently.

The spatial dimension four is something special for polymer systems. The reason is that for $d \nearrow 4$ two chains or two parts of one chain rarely cross. This is consistent with the Hausdorff-dimension two for an ideal, random walk like chain [17]. Thus for $d \nearrow 4$ dilute polymers behave like ideal chains, and the dilute - semi-dilute crossover takes place at a very large geometrical inter-chain overlap for which a chain interacts with many other chains and for which mean-field theory applies. Thus the mean-field results of Chapter 3 give quantitative approximations only close to four dimensions. In Sec. 2.5 I introduce briefly the polymer magnet analogy which states that the partition function of the polymer chains is connected with the order parameter correlation function in a Ginzburg-Landau field theory. In the last two sections of this chapter I consider expansions for the cases of very small or large particles.

2.1 The 'spring and bead' model

For introducing the model I first consider the case of the pure polymer solution without imbedded particles. The macromolecule is replaced by a sequence of segments and its configuration is given by the position of all segment endpoints. The chain connectedness is incorporated by a harmonic potential that couples two consecutive segments. Therefore each segment can be viewed as an elastic spring. These springs connect point-like beads, and all beads repel each other via a delta-function repulsion. If one introduces the set of segment endpoints of $\mathcal{N}$ chains, each consisting of N segments, in the form

$$\{\mathbf{r}_j^{(m)}\} = \{\mathbf{r}_0^{(1)}, ..., \mathbf{r}_N^{(1)}; \mathbf{r}_0^{(2)}, ..., \mathbf{r}_N^{(2)}; ...; \mathbf{r}_0^{(\mathcal{N})}, ..., \mathbf{r}_N^{(\mathcal{N})}\} \ , \tag{2.1}$$

the probability to find the system in a specific configuration is given by

$$\begin{aligned} p\{\mathbf{r}_j^{(m)}\} \ &= \ \frac{1}{\mathcal{Z}(\mathcal{N})} \prod_{m=1}^{\mathcal{N}} \prod_{j=1}^{N} P(\mathbf{r}_j^{(m)}, \mathbf{r}_{j-1}^{(m)}) \cdot \\ &\quad \cdot \prod_{(mj,m'j')}{}' \left[1 - b\delta^d(\mathbf{r}_j^{(m)} - \mathbf{r}_{j'}^{(m')})\right] \ , \end{aligned} \tag{2.2}$$

where the function P denotes the normalized Gaussian

$$P(\mathbf{r}, \mathbf{r}') \ = \ (4\pi l^2)^{-\frac{d}{2}} \, \mathrm{e}^{(\mathbf{r}-\mathbf{r}')^2/(4l^2)} \ . \tag{2.3}$$

The product in the second line of Eq. (2.2) extends over all pairs of segments and the prime over the product sign indicates that after multiplying out only terms are kept in which each segment coordinate occurs at most once. The microscopic length l is an effective segment size, d is the space dimension,

and the interaction constant b models the effective strength of the repulsion. For ideal chains b equals zero and the configurational weight is just given by the Gaussians in Eq. (2.2). The partition function $\mathcal{Z}^{(\mathcal{N})}$ is defined as

$$\mathcal{Z}^{(\mathcal{N})} = \int_{\mathcal{U}} d\mathbf{r}_0^{(1)} ... d\mathbf{r}_N^{(\mathcal{N})} \prod_{m=1}^{\mathcal{N}} \prod_{j=1}^{N} P(\mathbf{r}_j^{(m)}, \mathbf{r}_{j-1}^{(m)}) \cdot \tag{2.4}$$

$$\cdot \prod_{(mj,m'j')}{}' \left[1 - b\delta^d(\mathbf{r}_j^{(m)} - \mathbf{r}_{j'}^{(m')})\right] . \tag{2.5}$$

$$\tag{2.6}$$

Here the integration over all segment coordinates has to be carried out over the volume $\mathcal{U}$ of the system.

For the case of an imbedded particle (see Fig. 2.1) $\mathcal{U}$ equals the outer space of the particle and the configurational weight of Eq. (2.2) is set to zero if any of the segment endpoints is in the volume occupied by the particle. Formally this can be achieved by introducing a potential which is infinity inside the particle and zero in the space outside the particle.

For later use I introduce the partition function for an *ideal* chain in an external 'potential' W with the two ends fixed at $\mathbf{r} = \mathbf{r}_0$ and $\mathbf{r}' = \mathbf{r}_N$. This is given by

$$\tilde{\mathcal{Z}}_{L,l}^{[W]}(\mathbf{r}, \mathbf{r}') = \int_{\mathcal{U}} d\mathbf{r}_1 ... d\mathbf{r}_{N-1} \prod_{j=1}^{N} P(\mathbf{r}_j, \mathbf{r}_{j-1}) \cdot$$

$$\cdot \exp\left\{-l^2 \sum_{j=1}^{N} W\left(\frac{\mathbf{r}_j + \mathbf{r}_{j-1}}{2}\right)\right\} \tag{2.7}$$

with $L \equiv N l^2$.

Of most interest is the continuum limit

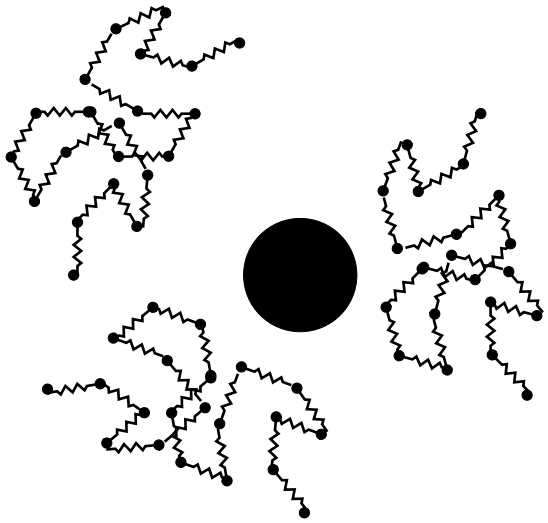

Figure 2.1: An illustration of the 'spring and bead' model. Point like beads are connected by springs, the bead-bead interaction and the bead-particle interaction are pure excluded volume interactions.

$$Z^{[W]}(L,\mathbf{r},\mathbf{r}') \;=\; \lim_{l\to 0}\, \tilde{\mathcal{Z}}^{[W]}_{L,l}(\mathbf{r},\mathbf{r}') \tag{2.8}$$

of the partition function which is determined by a generalized diffusion equation [19, 16]

$$\left(\frac{\partial}{\partial L} - \Delta_{\mathbf{r}} + W(\mathbf{r})\right) Z^{[W]}(L,\mathbf{r},\mathbf{r}') \;=\; 0 \quad \text{for } \mathrm{r},\mathrm{r}' \in \mathcal{U} \tag{2.9}$$

with the 'initial condition'

$$Z^{[W]}(L=0,\mathbf{r},\mathbf{r}') \;=\; \delta(\mathbf{r}-\mathbf{r}') \;\; . \tag{2.10}$$

Of course the model is very simple and neglects all microscopic details of the polymer chains, but this is justified by the experimentally verified concept of universality.

2.2 Self-consistent mean-field theory

As mentioned above the idea of the self-consistent mean-field theory is to describe the many-chain problem as the problem of one ideal chain in an external potential. Due to the contact interaction in Eq. (2.2) the external potential is proportional to the bulk normalized monomer density profile $\mathcal{M}(\mathbf{r})$. This is defined as

$$\mathcal{M}(\mathbf{r}) \;=\; \langle\hat{\rho}(\mathbf{r})\rangle/nN\;, \tag{2.11}$$

where

$$\hat{\rho}(\mathbf{r}) \;=\; \sum_{m=1}^{\mathcal{N}}\sum_{j=0}^{N}\delta^d(\mathbf{r}_j^{(m)}-\mathbf{r}) \tag{2.12}$$

is the monomer density operator and nN is the monomer density in the bulk. The way to handle this problem is presented by De Gennes in Reference [16] and will be sketched briefly here. In the second subsection I introduce the method of auxiliary fields and follow the procedure of Ref. [18] to derive the mean-field expression for the free energy cost of immersing a particle into the polymer solution.

2.2.1 Self-consistent potential

For the determination of the density profile $\mathcal{M}(\mathbf{r})$ in presence of a particle one starts an iteration procedure by associating to a certain 'starting profile' an external potential

$$\mathcal{V}(\mathbf{r}) \;=\; l^{-2}\,b\,N\,n\,\mathcal{M}(\mathbf{r}) \;=\; (\mathcal{S}/L)\,\mathcal{M}(\mathbf{r})\;. \tag{2.13}$$

Here

$$\mathcal{S} = b N^2 n = \frac{b}{l^4} L^2 n \quad . \tag{2.14}$$

The potential in Eq. (2.13) is proportional to the local monomer density and to the strength of the excluded volume interaction b. The factor l^{-2} is necessary due to the definition in Eq. (2.7). The meaning of L derives from

$$L = \frac{1}{2}\mathcal{R}_x^2 \,, \tag{2.15}$$

where $\mathcal{R}_{EE} \equiv d\,\mathcal{R}_x^2$ is the mean square end-to-end distance of a *single, ideal* chain with N segments. The quantity $\mathcal{S}$ occurs also in the mean-field expressions for the screening length ξ and the density correlation length ξ_D. The screening length describes the small p behavior $\sim (1 + p^2\xi^2 + ...)^{-1}$ of the spatial Fourier transform of the polymer density bulk correlation function in the semi-dilute limit. Here the limit of small p is taken after the semi-dilute limit so that $\mathcal{R}_x^{-1} \ll p$. In the mean-field approximation ξ is given by

$$\xi = \sqrt{\frac{L}{2\mathcal{S}}} = \frac{\mathcal{R}_x}{2\sqrt{\mathcal{S}}} \,. \tag{2.16}$$

While ξ is the relevant polymer length scale in the semi-dilute limit, the correlation length ξ_D is a good quantity marking the dilute - semi-dilute crossover. It is defined as the square root of the second moment of the density correlation function divided by the zeroth moment and is in mean-field approximation given by

$$\xi_D = \sqrt{\frac{d}{3(1+\mathcal{S})}}\,\mathcal{R}_x \,. \tag{2.17}$$

Although the mean-field theory does not give a quantitative description and leads to wrong exponents for a polymer solution in three dimensions, we shall see in Chapter 3 that it explains interesting *qualitative* effects of an immersed particle. In this case the meaning of the quantity $\mathcal{S}$ is best defined by means of the ratio correlation length to isolated chain size via Eq. (2.17). Although I will address $\mathcal{S}$ frequently as the 'inter-chain overlap', it is proportional to the *geometrical* overlap

$$s_d^{(x)} \;=\; (\mathcal{R}_x)^d\, n \tag{2.18}$$

with $\mathcal{R}_x$ from Eq. (2.15) only in $d = 4$.

In the following I need the partition function $Z^{[\mathcal{V}]}(L', \mathbf{r})$ of an ideal chain in the potential $\mathcal{V}$ with only one end fixed at $\mathbf{r}$ and with a polymerization index $N' = L'/l^2$ smaller than N. This follows from Eq. (2.8) by integration over the free end as

$$Z^{[\mathcal{V}]}(L', \mathbf{r}) \;=\; \int d\mathbf{r}'\, Z^{[\mathcal{V}]}(L', \mathbf{r}, \mathbf{r}') \;\;, \tag{2.19}$$

where L and W have to be replaced by L' and $\mathcal{V}$. Thus $Z^{[\mathcal{V}]}(L'; \mathbf{r})$ satisfies the diffusion-type equation

$$\left(\frac{\partial}{\partial L'} - \Delta_{\mathbf{r}} + \mathcal{V}(\mathbf{r})\right) Z^{[\mathcal{V}]}(L', \mathbf{r}) \;=\; 0 \quad \text{for } \mathrm{r} \in \mathcal{U} \tag{2.20}$$

with

$$Z^{[\mathcal{V}]}(L' = 0, \mathbf{r}) \;=\; 1 \tag{2.21}$$

and the boundary condition

$$Z^{[\mathcal{V}]}(L', \mathbf{r}_S) \;=\; 0 \tag{2.22}$$

for any point $\mathbf{r}_S$ on the particle surface. The new bulk-normalized polymer density profile in the iteration procedure is that of ideal chains in the external potential $\mathcal{V}$ and is given by [16]

$$\mathcal{M}(\mathbf{r}) = \frac{1}{L} \mathrm{e}^{\mathcal{S}} \int_0^L dL'' \, Z^{[\mathcal{V}]}(L'', \mathbf{r}) \, Z^{[\mathcal{V}]}(L - L'', \mathbf{r}) \quad . \tag{2.23}$$

Note that for $\mathbf{r}$ far from the particle or wall, $Z^{[\mathcal{V}]}(L', \mathbf{r})$ approaches the $\mathbf{r}$-independent value $\mathrm{e}^{-bNN'n}$, so that $\mathcal{M}(\mathbf{r})$ approaches 1. Now one reinserts this new profile into Eq. (2.13) and restarts the procedure to derive again a new profile for the local concentration. By further iterating this procedure until convergence is reached one arrives at a final density profile which is then self-consistent. Besides the segment density this procedure yields also the bulk normalized density of chain ends $\mathcal{E}(\mathbf{r})$ given by

$$\mathcal{E}(\mathbf{r}) = \mathrm{e}^{\mathcal{S}} Z^{[\mathcal{V}]}(L, \mathbf{r}) \, . \tag{2.24}$$

2.2.2 Mean-field expression for the free energy and the method of auxiliary fields

Immersing a single hard colloidal particle in a bath of non-adsorbing polymer chains costs free energy because this immersion reduces the number of possible chain configurations. In order to derive the mean-field expression for the free energy cost F of immersing the particle it is advantageous to use the grand canonical partition function

$$\mathcal{Z}_G \;=\; 1 \,+\, \sum_{\mathcal{N}=1}^{\infty} \frac{1}{\mathcal{N}!}\, \zeta^{\mathcal{N}}\, \mathcal{Z}^{(\mathcal{N})} \tag{2.25}$$

in the presence of the particle, where

$$\zeta \;=\; \frac{\mathrm{e}^{\mu_p/(k_B T)}}{(4\pi l^2)^{d/2}} \tag{2.26}$$

is the chain fugacity, and μ_p is the chemical potential of the chains. Proceeding as in Ref. [18] one formally rewrites the excluded volume interaction from Eq. (2.2) as

$$\begin{aligned} \prod_{(mj,m'j')}{}' \left[1 - b\delta^d(\mathbf{r}_j^{(m)} - \mathbf{r}_{j'}^{(m')})\right] \;&\rightarrow\; \exp\left(-\frac{b}{2}\sum_{j,m}\sum_{j',m'} \delta^d(\mathbf{r}_j^{(m)} - \mathbf{r}_{j'}^{(m')})\right) \\ &=\; \exp\left(-\frac{b}{2}\int d\mathbf{r}\hat{\rho}^2(\mathbf{r})\right) \end{aligned} \tag{2.27}$$

with the monomer density operator $\hat{\rho}(\mathbf{r})$ introduced in Eq. (2.12). Now one can decouple the chains by linearizing the interaction term by means of a fluctuating field φ yielding

$$\exp\left(-\frac{b}{2}\int d\mathbf{r}\hat{\rho}^2(\mathbf{r})\right) \;=\; \int D[\varphi] \exp\left(-\frac{1}{2b}\int d\mathbf{r}\varphi^2(\mathbf{r}) - i\int d\mathbf{r}\hat{\rho}(\mathbf{r})\varphi(\mathbf{r})\right) \;. \tag{2.28}$$

Inserting this into Eqs. (2.4) and (2.25) and using Eqs. (2.7) and (2.8) one finally arrives at

$$\mathcal{Z}_G \;=\; \int D[\varphi] \mathrm{e}^{-S[\varphi]} \;, \tag{2.29}$$

where the new "action" is given by $S[\varphi] = \mathcal{A}[i\varphi/l^2]$ with

$$\mathcal{A}[\mathcal{W}] \;=\; \int_{\mathcal{U}} d\mathbf{r}' \left(-\zeta\, Z^{[\mathcal{W}]}(L\,,\,\mathbf{r}') \;-\; \frac{l^4}{2b}\,\mathcal{W}^2(\mathbf{r}') \right), \tag{2.30}$$

and where $\mathcal{W} = i\varphi/l^2$ has the meaning of a potential field. Here I consider a large but finite volume $\mathcal{U}$. The mean-field approximation is obtained on replacing the functional integration over φ or $\mathcal{W}$ by taking the extremum of $\mathcal{A}$ with respect to $\mathcal{W}$. If the extremum occurs at $\mathcal{W} = \mathcal{V}$, this yields

$$0 \;=\; \left(\frac{\delta\mathcal{A}}{\delta\mathcal{W}(\mathbf{r})}\right)_{\mathcal{W}=\mathcal{V}} \;=\; \zeta\, \mathrm{e}^{-L\mathcal{V}_{\mathrm{bulk}}}\, L\, \mathcal{M}(\mathbf{r}) \;-\; \frac{l^4}{b}\,\mathcal{V}(\mathbf{r}) \quad . \tag{2.31}$$

The chain fugacity is related to the chain density via the bulk relation

$$\begin{aligned} n \;&=\; -\zeta \frac{d}{d\zeta}\,\frac{\mathcal{F}_G}{\mathcal{U}} \;=\; \zeta \frac{d}{d\zeta}\left(\zeta\, \mathrm{e}^{-L\mathcal{V}_{\mathrm{bulk}}} \;+\; \frac{l^4}{2b}\mathcal{V}_{\mathrm{bulk}}^2\right) \\ &=\; \zeta\, \mathrm{e}^{-L\mathcal{V}_{\mathrm{bulk}}} - \left(\frac{d\,\mathcal{V}_{\mathrm{bulk}}}{d\zeta}\right)\left(\zeta\, \mathrm{e}^{-L\mathcal{V}_{\mathrm{bulk}}}\, L \;-\; \frac{l^4}{b}\,\mathcal{V}_{\mathrm{bulk}}\right) \\ &=\; \zeta\, \mathrm{e}^{-L\mathcal{V}_{\mathrm{bulk}}} \quad , \end{aligned} \tag{2.32}$$

where the last step results from the extremum condition in Eq. (2.31) with $\mathcal{M}(\mathbf{r})$ and $\mathcal{V}(\mathbf{r})$ replaced by their bulk values 1 and $\mathcal{V}_{\mathrm{bulk}}$, respectively. Substituting Eq. (2.32) into Eq. (2.31) shows that

$$\mathcal{V}(\mathbf{r}) \;=\; \frac{nLb}{l^4}\,\mathcal{M}(\mathbf{r}) \;=\; \frac{\mathcal{S}}{L}\,\mathcal{M}(\mathbf{r}) \quad , \tag{2.33}$$

i.e. the potential field at the extremum is identical with the mean field (2.13), and

$$L\,\mathcal{V}_{\mathrm{bulk}} \;=\; \mathcal{S} \quad . \tag{2.34}$$

The grand-canonical polymer free energy per k_BT in mean-field approximation is given by

$$\mathcal{F}_G \;=\; \mathcal{A}[\mathcal{V}] \quad . \tag{2.35}$$

The first term on the right hand side of Eq. (2.30), which due to Eq. (2.24) is a spatial integration over the end-density, can also be expressed as an integration over the density profile $\mathcal{M}$, since due to the chain structure [16]

$$\int d\mathbf{r}'\, Z^{[\mathcal{V}]}(L,\mathbf{r}') \;=\; \int d\mathbf{r}\, Z^{[\mathcal{V}]}(L'',\mathbf{r})\, Z^{[\mathcal{V}]}(L-L'',\mathbf{r}) \tag{2.36}$$

for arbitrary $L'' < L$. Thus the free energy in Eq. (2.35) is determined by only the density profile

$$\mathcal{F}_G \;=\; -n \int_{\mathcal{U}} d\mathbf{r}\,[\mathcal{M}(\mathbf{r}) \;+\; \frac{1}{2}\mathcal{S}\,\mathcal{M}^2(\mathbf{r})] \quad , \tag{2.37}$$

and the free energy cost of immersing the particle has the form

$$\begin{aligned} \frac{F}{k_BT} \;&=\; \mathcal{F}_G \;-\; \mathcal{F}_G|_{\text{without particle}} \\ &=\; V\,\frac{\Pi}{k_BT} \;+\; n\int d\mathbf{r}\,\{1-\mathcal{M}(\mathbf{r}) + \frac{\mathcal{S}}{2}[1-\mathcal{M}^2(\mathbf{r})]\} \quad . \end{aligned} \tag{2.38}$$

Here V is the volume occupied by the particle, and the integral extends over the volume outside the particle. Π is the osmotic pressure that in the mean-field approximation takes the Flory-Huggins form

$$\Pi/(k_BT) \;=\; n\,(\,1 \;+\; \mathcal{S}/2\,) \quad . \tag{2.39}$$

Note that the $\mathcal{M}$-dependent terms in the integrand of Eq. (2.38) have the form of the bulk-pressure in Eq. (2.39), with the polymer density in the bulk n replaced by the local density $n\mathcal{M}(\mathbf{r})$. While the first term on the right hand side of Eq. (2.38) is the work needed to displace the polymers from the volume occupied by the particle, the remaining terms describe the formation of a depletion layer around the particle.

2.3 Basic ideas of the renormalization group and the epsilon expansion

The bead and spring model still has a definite microstructure, because it depends on the definition of a segment given by N and l and on the interaction strength b. Since one is interested in universal properties, a change in the definition of l and therefore of N and b should lead to the same macroscopic physics. This implies that there should exist a mapping $l, N, b \to l', N', b'$ which leaves macroscopic observables invariant. The existence of such a mapping is the basic idea of the renormalization group (R.G.) theory. For infinitely long chains one can apply this mapping repeatedly and thus get a sequence b_i of interaction constants. Now power laws, scaling, and universality follow if one makes the crucial assumption that this sequence converges, i.e., that there exists a fixed point b_{FP} for the interaction constant. By constructing explicitly a R.G. mapping this assumption is verified. Here one finds [18] the necessity of a parameter that can make this fixed point value b_{FP} arbitrarily small. The only parameter that can be used for that purpose is $\epsilon = 4 - d$, and therefore one has to introduce an expansion in powers of ϵ. In leading order in ϵ one finds a fixed point value

$$b_{\rm FP} \equiv 2\,\pi^2\,\epsilon\,l^4 \tag{2.40}$$

of b which is consistent with the fact that the excluded volume interaction is negligible above four dimensions.

The quantity $\mathcal{S}$ in Eq. (2.14) that measures the inter-chain overlap is then given by

$$\mathcal{S} = \epsilon\,\frac{\pi^2}{2}\,s_4^{(x)} = \frac{n}{n^*} \quad . \tag{2.41}$$

Here

$$n^* \equiv (A_2)^{-1} = \left(\epsilon\frac{\pi^2}{2}\mathcal{R}_x^4\right)^{-1} \tag{2.42}$$

is a convenient quantity marking the crossover between dilute ($n \ll n^*$) and semi-dilute ($n \gg n^*$) behavior. A_2 is the second virial coefficient which occurs in the density expansion for the osmotic pressure

$$\frac{\Pi}{k_B T} = n + \frac{1}{2}\,A_2\,n^2 + ... \tag{2.43}$$

and which takes the value $A_2 = b_{\rm FP} N^2$ for $\epsilon \to 0$. The expression (2.40) for $b_{\rm FP}$ is consistent with the leading term $\epsilon/8$ in the ϵ-expansion of the universal amplitude ratio $\psi^* = A_2/(\sqrt{2\pi}\mathcal{R}_x)^d$ which is known as the 'interpenetration ratio'. As pointed out above, in $4-\epsilon$ dimensional space with small ϵ two polymer chains rarely cross and the chain density in the crossover region ($n \approx n^*$), where the contribution quadratic in the density to the osmotic pressure is of the same order of magnitude as the linear term, corresponds to a very large geometrical overlap $s_d^{(x)}$ in Eq. (2.18) of order $1/\epsilon$.

2.4 Generalized cylinder

The closed system of Eqs. (2.20)-(2.23) determining $\mathcal{M}(\mathbf{r})$ and Eq. (2.38) for F apply to *arbitrary* particle shapes. For a sphere or an infinitely long cylinder, $\mathcal{M}(\mathbf{r})$ and $Z^{[\nu]}(L', \mathbf{r})$ only depend on the distance r from the center of the sphere or on the distance $r_\perp$ from the axis of the cylinder.

To analyze both situations in one step, Hanke et al. [22, 7] introduced the concept of a 'generalized cylinder' with an 'axis' of $d_\parallel$ dimensions and with the remaining $d - d_\parallel = d_\perp$ dimensions perpendicular to the axis. The outer space of the generalized cylinder is determined by distances $r_\perp$ from the axis larger than its 'radius' R. For $d_\parallel = 0$ the generalized cylinder becomes a sphere. For $d_\parallel = 1$ and $d = 3$ it is a cylinder of radius R , and for $d_\parallel = 2$, $d = 3$ it is a plate of thickness $2R$ in three dimensions. Below we shall consider a generalized cylinder in $d = 4 - \epsilon$ dimensions with

$$d_\parallel = 1 - \epsilon \quad , \quad d_\perp = 3 \tag{2.44}$$

which tends for $\epsilon \searrow 0$ to a cylinder in $d = 4$ dimensions and for $\epsilon \nearrow 1$ to a sphere in $d = 3$ dimensions.

2.5 Polymer magnet analogy

The Laplace transform of the partition function $Z^{[0]}(L, \mathbf{r}, \mathbf{r}')$ of an ideal chain with ends fixed at $\mathbf{r}$ and $\mathbf{r}$' is given by

$$G_S(t; \mathbf{r}, \mathbf{r}') = \int_0^\infty dL\, \mathrm{e}^{-Lt}\, Z^{[0]}(L; \mathbf{r}, \mathbf{r}'\,;\, R) \equiv \mathcal{L}Z^{[0]}(L; \mathbf{r}, \mathbf{r}'\,;\, R) \tag{2.45}$$

and satisfies an Ornstein-Zernike type equation

$$(-\Delta_{\mathbf{r}} + t)\, G_S(t;\mathbf{r},\mathbf{r}') = \delta(\mathbf{r}-\mathbf{r}')\ , \tag{2.46}$$

where G_S vanishes on the surface S of the particle. De Gennes [33] made the extremely useful observation that this Laplace transform can be identified as

$$G_S(t;\mathbf{r},\mathbf{r}')\ =\ C(\mathbf{r},\mathbf{r}')\,, \tag{2.47}$$

where C is a two point correlation function

$$C(\mathbf{r},\mathbf{r}')\ =< \phi(\mathbf{r})\phi(\mathbf{r}') > \tag{2.48}$$

in a Ginzburg-Landau type field theory with a fluctuating order-parameter field ϕ. The Ginzburg-Landau Hamiltonian H_0 for the Gaussian field theory is given by

$$H_0\ =\ \frac{1}{2}\int d\mathbf{r}\left((\nabla_{\mathbf{r}}\phi(\mathbf{r}))^2 + t\phi^2(\mathbf{r})\right)\ . \tag{2.49}$$

For later use I introduce the Gaussian susceptibility

$$\chi^{[0]}(t;\mathbf{r})\ =\ \int d\mathbf{r}'\, G_S(t;\mathbf{r},\mathbf{r}')\ . \tag{2.50}$$

It satisfies the equation

$$(-\Delta_{\mathbf{r}} + t)\chi^{[0]}(t;\mathbf{r})\ =\ 1 \tag{2.51}$$

and the Dirichlet boundary condition $\chi^{[0]}(t;\mathbf{r}) \to 0$ for $\mathbf{r}$ approaching the

particle surface. Far away from the particle the susceptibility reaches its bulk limit

$$\lim_{r\to\infty} \chi^{[0]}(t;\mathbf{r}) \;=\; \frac{1}{t}\,. \tag{2.52}$$

The equations (2.46) and (2.51) can be generalized in an obvious way to the case where an external potential is present. The differential equation for the susceptibility for example then takes the form

$$\left(-\Delta_{\mathbf{r}} + t + \mathcal{V}(\mathbf{r})\right) \chi^{[\mathcal{V}]}(t;\mathbf{r}) \;=\; 1\;. \tag{2.53}$$

From $\chi^{[\mathcal{V}]}(t;\mathbf{r})$ one can calculate the end density and the monomer density via the inverse Laplace transforms

$$\mathcal{E}(\mathbf{r}) \;\;=\;\; \mathrm{e}^{\mathcal{S}}\,\mathcal{L}^{-1}\,\chi^{[\mathcal{V}]}(t;\mathbf{r}) \;\equiv\; \mathrm{e}^{\mathcal{S}} \int_\gamma \frac{dt}{2\pi i} \mathrm{e}^{Lt} \chi^{[\mathcal{V}]}(t;\mathbf{r})\,, \tag{2.54}$$

$$\mathcal{M}(\mathbf{r}) \;\;=\;\; \frac{1}{L}\mathrm{e}^{\mathcal{S}} \int_\gamma \frac{dt}{2\pi i} \mathrm{e}^{Lt} \left(\chi^{[\mathcal{V}]}(t;\mathbf{r})\right)^2\,, \tag{2.55}$$

where the integration path γ is parallel to the imaginary axis and to the right of all singularities of the integrand.

There are several advantages of introducing the Laplace transform of the partition function. In fact for the explicit calculation of the solution of the closed system of Eqs. (2.20)-(2.23) which is explained in more detail in Appendix C one solves Eq. (2.53) which in contrast to the diffusion-like partial differential equation (2.20) with L and $\mathbf{r}$ derivatives is a differential equation with only $\mathbf{r}$ derivatives and then uses the inverse Laplace transform of Eqs. (2.54) and (2.55) to get $\mathcal{E}(\mathbf{r})$ and $\mathcal{M}(\mathbf{r})$. Another advantage is that one

can use tools of the field theory like the small radius expansion [34, 35] to get results for the polymer problem. The small radius expansion resembles the short distance expansion and will be the topic of the next subsection. Also the derivation of the density-pressure identity in Appendix A uses the polymer-magnet analogy.

2.6 Small radius expansion

For a spherical particle with a radius R which is small compared to the characteristic polymer lengths $\mathcal{R}_x$, ξ, and to the distance from the surface $r_\perp - R$ one can replace the Boltzmann weight e^{-H_S} that describes the presence of the particle in the corresponding field theory by a series of point operators [34]

$$\frac{\mathrm{e}^{-H_S}}{< \mathrm{e}^{-H_S} >_{\mathrm{bulk}}} = 1 + \sum_j A_j O_j(\mathbf{r} = 0) \ . \tag{2.56}$$

Here A_j are non-fluctuating amplitudes and O_j are fluctuating operators. Since the particle enforces a Dirichlet boundary condition which does not break the $\phi \to -\phi$ symmetry, the leading operator O is the energy density $\sim \phi^2$, corresponding to the monomer density in the polymer system. For a thin generalized cylinder embedded in a polymer solution this reasoning leads in mean-field approximation to a reduction factor in the Boltzmann weight for chain configurations with the form

$$W_{\mathrm{cyl}}[\mathbf{r}_{P,j}] \ \to \ 1 \ - \ A_{\mathrm{id}}(d_\perp)\, R^{d_\perp - 2}\, \mathcal{R}_x^2 \int d\mathbf{r}_{\|}\, \Theta(\mathbf{r}_\perp = 0, \mathbf{r}_{\|}) \ . \tag{2.57}$$

Here

$$\Theta(\mathbf{r}) \;=\; \Theta(\mathbf{r}_\perp, \mathbf{r}_\parallel) \;=\; \sum_{m=1}^{\mathcal{N}} \frac{1}{N} \sum_{j=0}^{N} \delta^{d_\perp}(\mathbf{r}_{\perp;j}^{(m)} - \mathbf{r}_\perp) \delta^{d_\parallel}(\mathbf{r}_{\parallel;j}^{(m)} - \mathbf{r}_\parallel) \tag{2.58}$$

is the configuration dependent density of chains at the point $\mathbf{r}$ and $A_{\rm id}(d_\perp = 3)$ equals [22, 29, 7] 2π. The free energy cost per unit axis length is then simply given by the unperturbed average of the perturbation in Eq. (2.57), i.e. by Eq. (1.5). For the bulk normalized monomer density one gets

$$\begin{aligned} \mathcal{M}(r_\perp) \;&=\; \langle \Theta(\mathbf{r}_\perp, \mathbf{r}_\parallel) \rangle \,/\, n \\ &\to\; 1 \,-\, 2\pi R \mathcal{R}_x^2 \int d\mathbf{r}'_\parallel \, \langle \Theta(\mathbf{r}_\perp, \mathbf{r}_\parallel) \, \Theta(0, \mathbf{r}'_\parallel) \rangle_{c,\,\rm bulk} \,/\, n \\ &=\; 1 \,-\, 2\pi R \mathcal{R}_x^2 \int \frac{d^3p}{(2\pi)^3} \, \mathrm{e}^{i\,\mathbf{p}\,\mathbf{r}_\perp} \frac{D(p^2 L)}{1 \,+\, \mathcal{S} D(p^2 L)} \quad . \end{aligned} \tag{2.59}$$

In the last step the tree expression of the bulk density correlation function [18] has been inserted. The subscript c on the average in the second line stands for cumulant and D is the Debye function

$$D(x) \;=\; 2\,(\mathrm{e}^{-x} - 1 + x)/x^2 \quad . \tag{2.60}$$

2.7 Small curvature expansion

For the opposite limit of very large particle radius R, where large means large compared to the polymer size $\mathcal{R}_x$, one expects [36, 7] a small-curvature expansion of the Helfrich type

$$F = V\,\Pi + \int dS\,[\sigma + \kappa K_m + ...] \tag{2.61}$$

for the free energy of immersion F. Here

$$K_m = \frac{1}{2}\sum_{i=1}^{d-1}\frac{1}{R_i} \tag{2.62}$$

is proportional to the local mean surface-curvature where R_i are the principal radii of curvature. The coefficients σ and κ, which denote the surface tension and the coefficient of spontaneous curvature, respectively, are independent of the shape of the weakly curved surface.

For the generalized cylinder Eq. (2.61) reduces to

$$\frac{F}{V_{\|}} = V_{\perp}\Pi + S_{\perp}\left[\sigma + \frac{d_{\perp}-1}{2}\,\frac{\kappa}{R} + ...\right] \quad , \tag{2.63}$$

which is an expansion in powers of $1/R$. In the limit $1/R \to 0$ where the generalized cylinder becomes a planar wall one finds from a comparison with the mean-field expression in Eq. (2.38) the form

$$\sigma = nk_BT\int_0^{\infty} dz\left(1 - \mathcal{M}_{\rm pw}(z) + \frac{\mathcal{S}}{2}\left[1 - \mathcal{M}_{\rm pw}^2(z)\right]\right) \tag{2.64}$$

of the surface tension σ, where z denotes the distance from the planar surface.

Besides the expansion for the free energy cost there is an expansion in powers of $1/R$ also for the density profile. In the dilute and semi-dilute limit one can derive analytical expressions for the next to leading order contributions, i.e. the corrections for the well known planar wall functions. These will be presented in Secs. 3.1.4 and 3.2.2 below.

Chapter 3

Mean-field results

In this chapter I will present some mean-field results for the situation of a generalized cylinder embedded in a solution of free non-adsorbing polymers in $d = 4 - \epsilon$ dimensions. Choosing a generalized cylinder as in Eq. (2.44) the mean-field results become quantitative for a cylinder in $d \nearrow 4$ and give at least qualitative estimates for an embedded sphere in $d = 3$. Here the meaning of the quantity $\mathcal{S}$ derives from the length ratio $\xi_D/\mathcal{R}_x$ in Eq. (2.17). Moreover the mean-field results serve as an input for the renormalized tree approximation which leads to semi-quantitative results for a sphere in three dimensions and will be discussed in Chapter 4. For the generalized cylinder the mean-field partition function $Z^{[\mathcal{V}]}(L', \mathbf{r}) \equiv Z^{[\mathcal{V}]}(L', \mathbf{r}_\parallel, \mathbf{r}_\perp)$ in Eq. (2.19) *factors* into two functions $Z_\parallel^{[\mathcal{V}]}(L', \mathbf{r}_\parallel) = 1$ and $Z_\perp^{[\mathcal{V}]}(L', r_\perp) = [Z^{[\mathcal{V}]}(L', \mathbf{r})]_{d \to d_\perp\,,\,|\mathbf{r}|=r_\perp}$ where the latter is independent of $\mathbf{r}_\parallel$ and $d_\parallel$. Applying the iteration procedure in Eqs. (2.20) - (2.23) shows that in the mean-field approximation also the functions $\mathcal{V}(\mathbf{r})$ and $\mathcal{M}(\mathbf{r})$, for given R, L, and $\mathcal{S}$, only depend on $r_\perp$ and $d_\perp$.

3.1 Density profiles

On using route (2.44) one finds that the scaling function m_d of the density profile

$$\mathcal{M}(\mathbf{r}) = m_d\Big(\frac{r_\perp - R}{\mathcal{R}_x}, \frac{R}{\mathcal{R}_x}, \frac{n}{n^*}\Big) \tag{3.1}$$

to leading order in $d \nearrow 4$ equals the corresponding mean-field scaling function for a sphere in three dimensions. This is due to the independence of the mean-field scaling function of $\mathbf{r}_\parallel$ and $d_\parallel$. Examples of density profiles are shown in Figs. 3.1 and 3.2. In Fig. 3.1 the size ratio ρ is kept fixed to

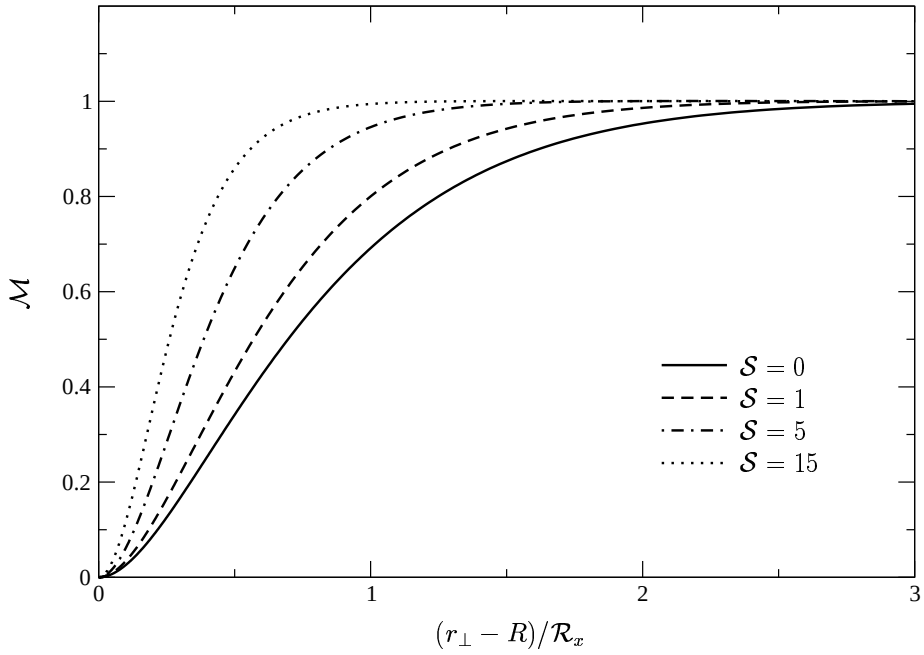

Figure 3.1: Bulk-normalized density profiles $\mathcal{M}$ for a sphere of size ratio $R/\mathcal{R}_x = 1$ versus the scaled distance $(r_\perp - R)/\mathcal{R}_x$ from the surface for various values of the inter-chain overlap $\mathcal{S}$.

1. Close to the surface the density profile increases quadratically with the distance from the surface which is consistent with the mean-field exponent $1/\nu = 2$, compare Eq. (1.3). The amplitude of the quadratic term increases with increasing inter-chain overlap $\mathcal{S}$ and this steeper increase of the density near the surface leads to a smaller depletion layer. This is consistent with the fact that the thickness of the depletion layer in the semi-dilute limit is of the order of the screening length which is much smaller than the end-to-end distance in the dilute limit.

The dependence of the density on the size ratio is shown in Fig. 3.2,

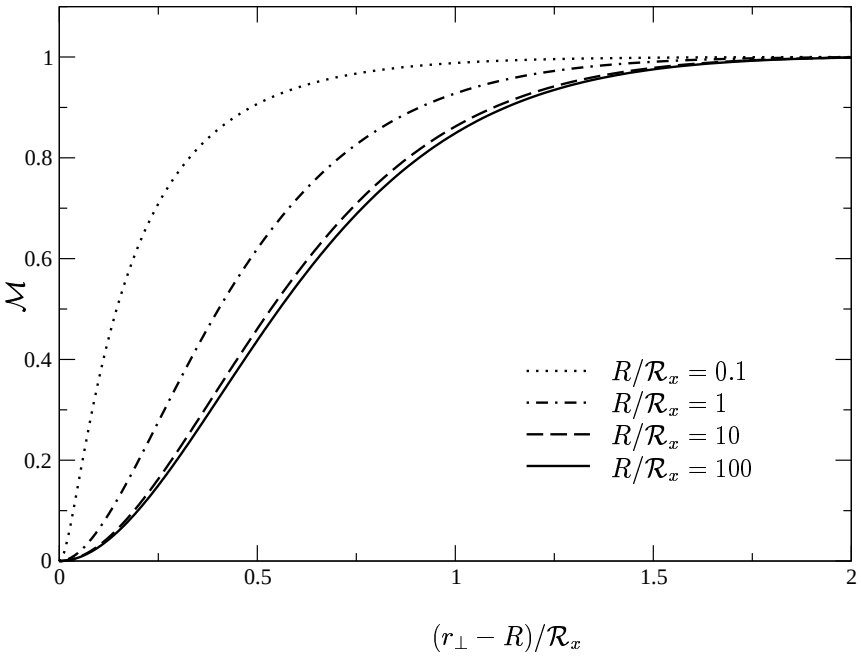

Figure 3.2: Bulk-normalized density profiles $\mathcal{M}$ for finite overlap $\mathcal{S} = 1$ versus the scaled distance $(r_\perp - R)/\mathcal{R}_x$ from the wall for various values of the size ratio ρ.

where $\mathcal{S}$ is constant. The decrease of the size ratio leads to a smaller depletion zone due to the fact that a long chain can coil around a small sphere so that the loss of entropy is smaller. For distances $R \ll r_\perp \ll \mathcal{R}_x, \xi$ away from the surface of a thin cylinder or a small sphere one gets an analytical expression for the density profile. In this limit the Debye function in the small radius expansion in Eq. (2.59) can be expanded for large argument. Thus the density profile of a thin cylinder in four dimensions in this region is given by

$$\begin{aligned} \mathcal{M}(r_\perp) &\rightarrow 1 - 2\pi R \mathcal{R}_x^2 \int \frac{d^3p}{(2\pi)^3} \, \mathrm{e}^{i\,\mathbf{p}\,\mathbf{r}_\perp} \frac{2}{p^2 L} \\ &= 1 - 2R/r_\perp \quad , \end{aligned} \tag{3.2}$$

independent of the overlap, consistent with Eq. (1.4).

3.1.1 Point of Inflection

A good measure for the thickness of the depletion layer is the position of the point of inflection in the density profiles. Fig. 3.3 shows the scaled distance $\xi_I/\mathcal{R}_x = ((r_\perp)_I - R)/\mathcal{R}_x$ of the point of inflection from the surface of the cylinder versus the size ratio $\rho = R/\mathcal{R}_x$ for various values of the overlap $\mathcal{S}$. For $R \ll \mathcal{R}_x$ all the curves merge to approach the overlap-independent value $\xi_I \rightarrow R/2$, corresponding to the point of inflection in Eq. (1.4). In the opposite limit $R \gg \mathcal{R}_x$ the point of inflection reaches the planar wall value $\xi_I^{(\mathrm{pw})}$ which should be of the order of the bulk density correlation length ξ_D that is defined as the square root of the second moment of the bulk density correlation function and that in mean-field approximation is given by Eq.

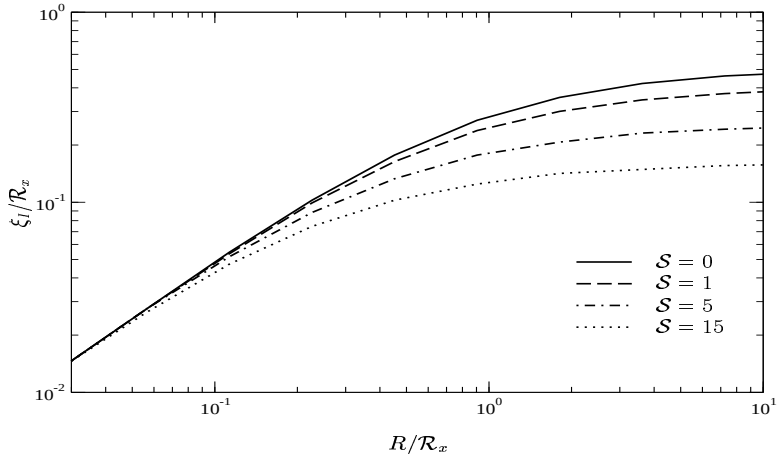

Figure 3.3: Scaled distance $\xi_I/\mathcal{R}_x$ of the point of inflection of the density profile from the surface of a cylinder versus the size ratio $\rho = R/\mathcal{R}_x$, for various values of the inter-chain overlap $\mathcal{S}$.

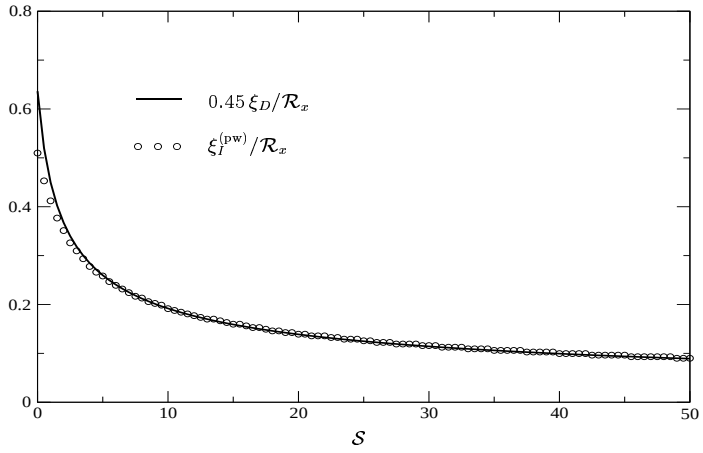

Figure 3.4: Scaled distance $\xi_I^{(\mathrm{pw})}/\mathcal{R}_x$ from the planar wall of the point of inflection of the density profile versus the inter-chain overlap $\mathcal{S}$ (circles). The overlap-dependence of the bulk density correlation length ξ_D with an adjusted prefactor is shown for comparison (full line).

(2.17). In Fig. 3.4 it is shown that the overlap dependence of the point of inflection in the density profile for the planar wall agrees very well indeed with that of the bulk density correlation length.

3.1.2 Non-monotonic behavior

Looking at the density profiles at a finite value of the inter-chain overlap $\mathcal{S}$ on a finer scale, one finds that the bulk value 1 is approached in a *non-monotonic* oscillatory way. Similar behavior was found for the density profile in presence of a planar wall by van der Gucht et al. [38] using a lattice-walk

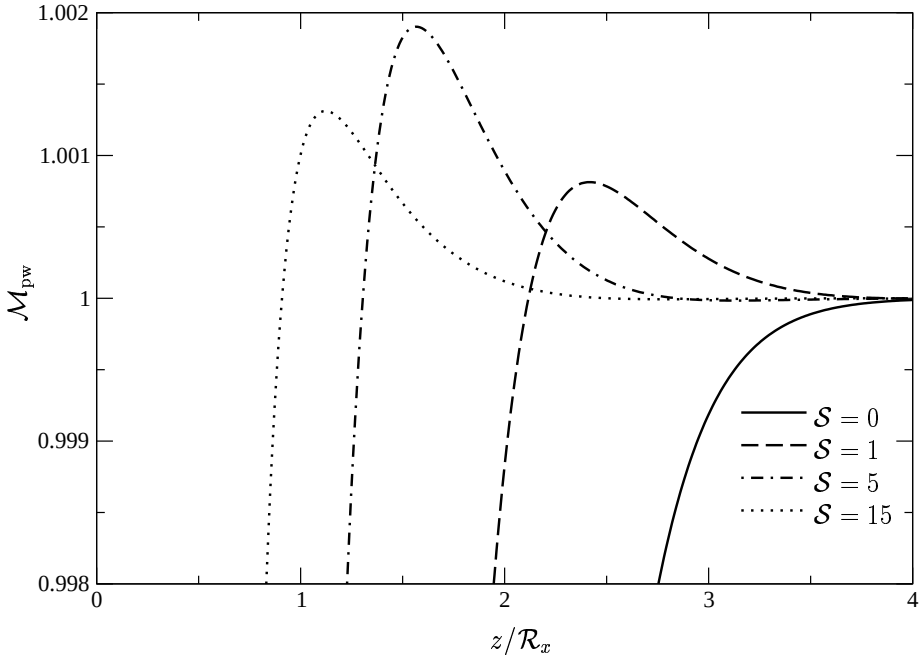

Figure 3.5: Non-monotonic behavior of the density profiles near a planar wall. Note the enlarged scale of the vertical axis.

model for polymers and by Bolhuis et al. [15] with computer simulations for polymers in a good solvent. The mean-field theory yields this non-monotonic behavior for arbitrary values of the size ratio $\rho = R/\mathcal{R}_x$. Fig. 3.5 shows the density profile near a planar wall where the effect is most pronounced for different values of the overlap and with an enlarged scale on the vertical axis. The scaled distance $z_{\max}/\mathcal{R}_x$ of the first maximum from the wall decreases monotonically for increasing overlap as is shown in Fig. 3.6. However the decrease is much slower than that of either $\xi_I^{\mathrm{pw}}/\mathcal{R}_x$ or $\xi_D/\mathcal{R}_x$. This is also in qualitative agreement with the behavior reported in Refs. [38, 15]. It is interesting that the position of the first maximum does not depend on the size ratio. Thus Fig. 3.6 applies for arbitrary size ratio if $z_{\max}$ is replaced by $(r_\perp)_{\max} - R$.

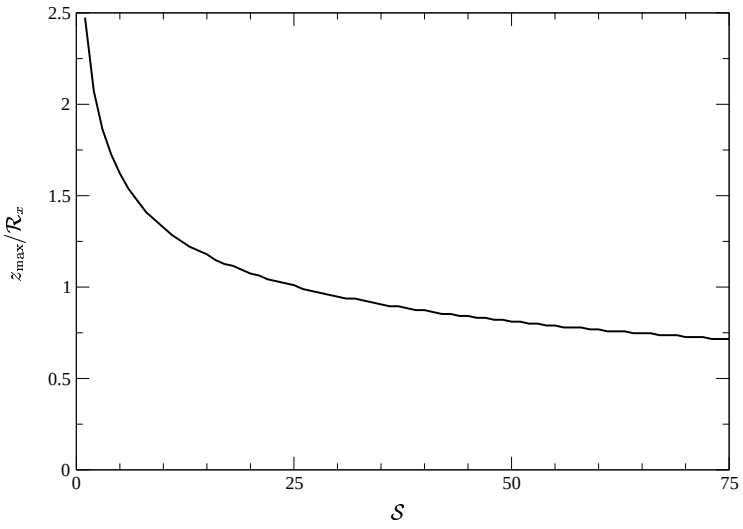

Figure 3.6: Scaled distance $z_{\max}/\mathcal{R}_x$ of the maximum of the density profile from the planar wall versus the inter-chain overlap $\mathcal{S}$.

In contrast to the position, the height of the first maximum depends apart

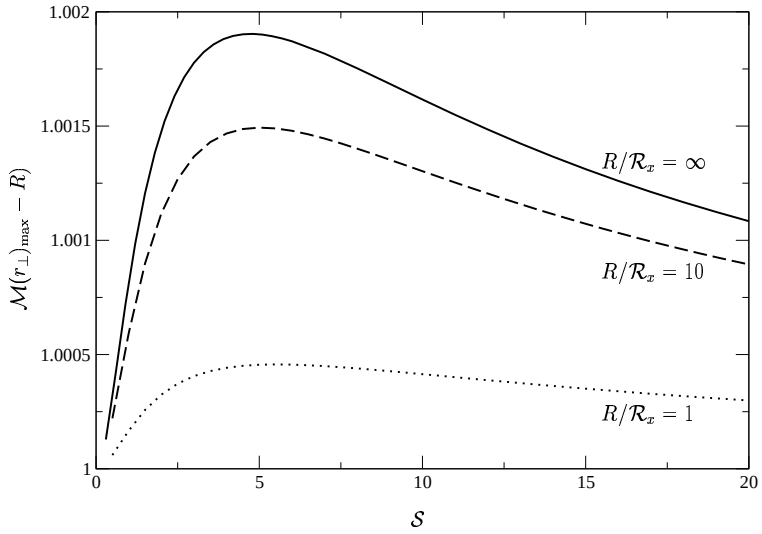

Figure 3.7: Height of the maximum in the density profile near a cylindrical rod versus the inter-chain overlap $\mathcal{S}$, for various values of the size ratio $\rho = R/\mathcal{R}_x$.

from the inter-chain overlap also on the size ratio. Fig. 3.7 indicates that for a given ρ the height shows a maximum at $\mathcal{S} \approx 5$, independent of the value of ρ. Additionally one can see that the height decreases with decreasing ρ but it persists down to very small values of ρ. For this case the maximum can be explained via the small radius expansion in Eq. (2.59) as a minimum in the bulk density correlation function. Fig. 3.8 shows the density profile for a size ratio $\rho = 0.01$ obtained by the numerical method described in Sec. 2.2 (circles) in comparison to the density profile calculated from Eq. (2.59) which is shown by the full line.

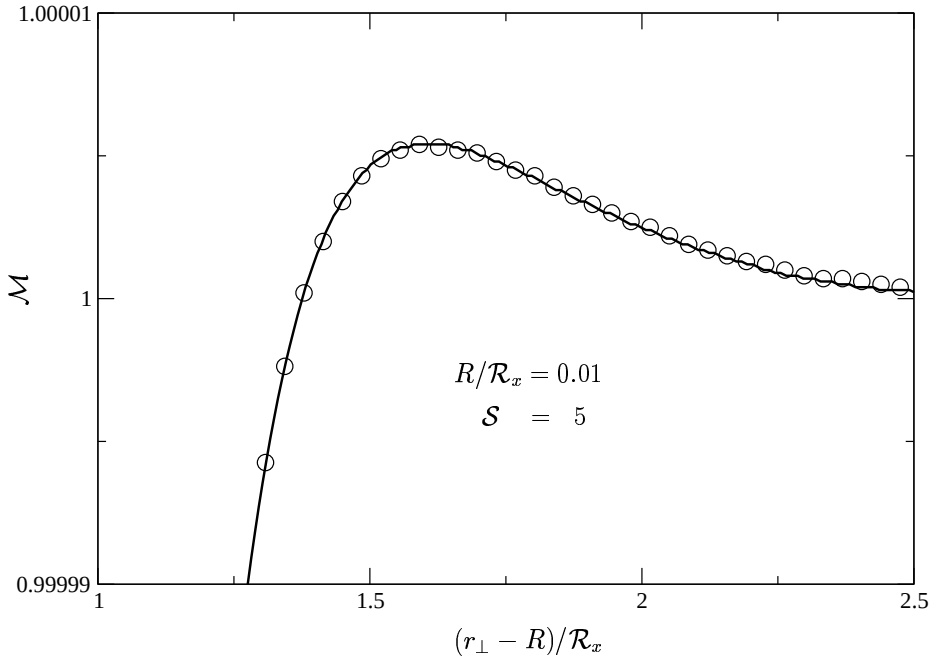

Figure 3.8: Density profile with a maximum for a cylinder with $R \ll \mathcal{R}_x$ (circles). The maximum is well reproduced (full line) by the minimum in the bulk density correlation function on using the small radius expansion (see Eqs. (2.59) and (2.60)).

3.1.3 Small overlap

In order to derive an expansion for the density profile in powers of the inter-chain overlap $\mathcal{S}$ it is convenient to use the grand canonical ensemble. The density profile of free non-adsorbing polymers is given by

$$\begin{aligned} n\,\mathcal{M}(r_\perp) &= \langle \Theta(\mathbf{r}) \rangle \\ &= \frac{1}{L} \sum_{\mathcal{N}=1}^{\infty} \frac{\zeta^{\mathcal{N}}}{\mathcal{N}!} \Big(- \frac{\delta}{\delta \mathcal{W}(\mathbf{r})}\, \mathcal{Z}_c^{(\mathcal{N})[\mathcal{W}]} \Big)_{\mathcal{W}=0} \quad . \end{aligned} \tag{3.3}$$

Here $\mathcal{Z}_c^{(\mathcal{N})}$ is the connected part of the partition function of $\mathcal{N}$ chains with monomer-monomer interaction in the tree approximation. From Eqs. (2.32) and (2.34) it follows that the chain fugacity is given in terms of the chain density by

$$\zeta = n\,\mathrm{e}^{\mathcal{S}} \ . \tag{3.4}$$

Since $\mathcal{S}$ is proportional to n the expansion of the density profile up to first order in $\mathcal{S}$ is given by

$$\mathcal{M}(r_\perp) = \frac{1}{L}\left[(1+\mathcal{S})\Big(-\frac{\delta}{\delta\mathcal{W}(\mathbf{r})}\,\mathcal{Z}_c^{(1)[\mathcal{W}]}\Big) + \mathcal{S}\frac{1}{2bN^2}\Big(-\frac{\delta}{\delta\mathcal{W}(\mathbf{r})}\,\mathcal{Z}_c^{(2)[\mathcal{W}]}\Big)\right] . \tag{3.5}$$

While the first term on the right hand side of Eq. (3.5) is the monomer density of ideal chains multiplied by $(1+\mathcal{S})$ [19], the second term follows from

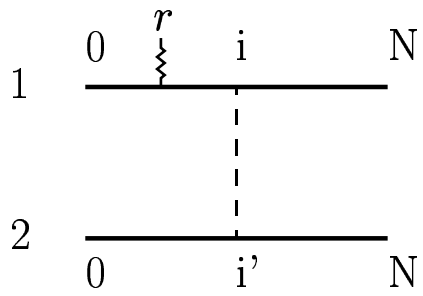

Figure 3.9: One of the four diagrams contributing to $\mathcal{Z}_c^{(2)}$. The other three diagrams emerge by placing the **r**-insertion on the three other possible positions.

the diagrammatic representation in Fig. 3.9. Since the three other diagrams with the $\mathbf{r}$-insertion to the right of position i in line 1 or to the left and right of position i' in line 2, respectively, yield exactly the same contribution, $\frac{\delta}{\delta \mathcal{W}(\mathbf{r})} \mathcal{Z}_c^{(2)[\mathcal{W}]}$ is given by four times the diagram in Fig. 3.9. This yields

$$\begin{aligned}
\mathcal{M}^{[1]}(\mathbf{r}) &\equiv \frac{l^4}{2bL^3}\Big(\frac{\delta}{\delta \mathcal{W}(\mathbf{r})}\, \mathcal{Z}_c^{(2)[\mathcal{W}]}\Big) \\
&= \frac{2}{L^2} \int d\mathbf{r}_i^{(1)} d\mathbf{r}_{i'}^{(2)} \frac{1}{L} \int_0^L dL' Z^{[0]}(L-L';\mathbf{r}_{i'}^{(2)}) Z^{[0]}(L';\mathbf{r}_{i'}^{(2)}) \delta^d(\mathbf{r}_i^{(1)} - \mathbf{r}_{i'}^{(2)}) \cdot \\
&\quad \cdot \int_0^L dL_1 Z^{[0]}(L-L_1;\mathbf{r}_i^{(1)}) \int_0^{L_1} dL_2 Z^{[0]}(L_1-L_2;\mathbf{r}_i^{(1)},\mathbf{r}) Z^{[0]}(L_2;\mathbf{r}) \\
&= \frac{2}{L^2} \int d\mathbf{r}_i^{(1)} \mathcal{M}^{[0]}(\mathbf{r}_i^{(1)}) \cdot \\
&\quad \cdot \int_0^L dL_1 Z^{[0]}(L-L_1;\mathbf{r}_i^{(1)}) \int_0^{L_1} dL_2 Z^{[0]}(L_1-L_2;\mathbf{r}_i^{(1)},\mathbf{r}) Z^{[0]}(L_2;\mathbf{r}).
\end{aligned} \tag{3.6}$$

Thus one has the expansion

$$\mathcal{M}(\mathbf{r}) = \mathcal{M}^{[0]}(\mathbf{r}) + \mathcal{S}\ \Big[\mathcal{M}^{[0]}(\mathbf{r}) - \mathcal{M}^{[1]}(\mathbf{r})\Big] \tag{3.7}$$

with $\mathcal{M}^{[0]}(\mathbf{r})$ given by Eq. (1.6). $\mathcal{M}^{[1]}$ satisfies the identity

$$\begin{aligned}
&\int_{r_\perp > R} d\mathbf{r}_\perp \ \Big\{\mathcal{M}^{[1]}(\mathbf{r}) - \Big[\mathcal{M}^{[0]}(\mathbf{r})\Big]^2\Big\} \\
&= \int_{r_\perp > R} d\mathbf{r}_\perp \ \Big\{\mathcal{M}^{[0]}(\mathbf{r}) \frac{2}{L^2} \int_0^L dL_1 Z^{[0]}(L-L_1;\mathbf{r})\, L_1\, Z^{[0]}(L_1;\mathbf{r}) - \Big[\mathcal{M}^{[0]}(\mathbf{r})\Big]^2\Big\} \\
&= \int_{r_\perp > R} d\mathbf{r}_\perp \ \Big\{\mathcal{M}^{[0]}(\mathbf{r}) \frac{1}{L^2} \int_0^L dL_1 (2L_1 - L)\, Z^{[0]}(L-L_1;\mathbf{r})\, Z^{[0]}(L_1;\mathbf{r})\Big\} \\
&= 0\,.
\end{aligned} \tag{3.8}$$

Here Eq. (2.36) was used in the first step and Eq. (2.23) in the second step. The last line follows from introducing in the second contribution of $2L_1 - L = L_1 - (L - L_1)$ the variable $L - L_1$ instead of L_1 as the integration variable.

3.1.4 Semi-dilute limit

To derive the mean-field density profile for a generalized cylinder of large radius R in the semi-dilute limit $\mathcal{S} \to \infty$ one can use the 'ground-state dominance' [16] to see that the L'-dependence in

$$Z_{L'}(\mathbf{r}) \;\to\; \mathrm{e}^{-L'\mathcal{S}/L}\,\psi(\mathbf{r}) \tag{3.9}$$

factors, i.e. ψ is independent of L', and Eq. (2.23) leads to

$$\mathcal{M}(\mathbf{r}) \;=\; \psi^2(\mathbf{r}) \quad . \tag{3.10}$$

Substituting (3.9) into the diffusion-type equation (2.20) and using Eqs. (2.13) and (3.10) yields the differential equation for ψ

$$\frac{L}{\mathcal{S}}\,\Delta_{\mathbf{r}}\,\psi(\mathbf{r}) \;=\; -\psi(\mathbf{r}) \;+\; \psi^3(\mathbf{r}) \quad , \tag{3.11}$$

where the characteristic length $\sqrt{L/\mathcal{S}}$ in Eq. (3.11) is proportional to the screening length ξ defined in Eq. (2.16). ψ has to fulfill the boundary condition that it vanishes at the particle surface and the normalization condition that it reaches its bulk value 1 far away from the particle. The solution of

Eq. (3.11) for the case of a planar wall is given by [16]

$$\psi_{\rm pw}(x) \;=\; \tanh x \quad , \tag{3.12}$$

with

$$x \;=\; \frac{r_\perp - R}{2\xi} \quad . \tag{3.13}$$

For a generalized cylinder of large radius $R \gg \xi$ one has the expansion

$$\psi(\mathbf{r}) \;=\; \psi_{\rm pw}(x) \;+\; \delta\psi(x) \tag{3.14}$$

with $\delta\psi = O(\frac{\xi}{R})$. Inserting this expansion into Eq. (3.11) leads to the linear inhomogeneous equation

$$\left(\frac{d^2}{dx^2} \;+\; 2 \;-\; 6\psi_{\rm pw}^2 \right) \delta\psi(x) \;=\; -\,\frac{2\xi}{R}\,(d_\perp - 1)\,\frac{d}{dx}\psi_{\rm pw} \tag{3.15}$$

for $\delta\psi$. Since $\psi_{\rm pw}$ fulfills already the boundary conditions for ψ, $\delta\psi(x)$ has to vanish in both limits $x \to 0$ and $x \to \infty$. The solution of Eq. (3.15) showing this behavior is given by

$$\delta\psi(x) \;=\; \frac{2\xi}{R}\,(d_\perp - 1)\,\Psi(x) \quad , \tag{3.16}$$

where

$$\Psi(x) \;=\; \frac{1}{6}\left[\frac{3}{2}\frac{x}{\cosh^2 x} \;+\; \frac{2}{\cosh^2 x} \;+\; \frac{3}{2}\tanh x \;-\; \frac{3}{2} \;-\; \frac{1}{2}{\rm e}^{-2x}\right] \quad . \tag{3.17}$$

Thus the density profile around a generalized cylinder of large radius with $d_\perp = 3$ is given by

$$\mathcal{M}(\mathbf{r}) \;=\; \tanh^2\!\left(\frac{r_\perp - R}{2\xi}\right) + 8\frac{\xi}{R}\tanh\!\left(\frac{r_\perp - R}{2\xi}\right)\Psi\!\left(\frac{r_\perp - R}{2\xi}\right) + O((\xi/R)^2). \tag{3.18}$$

Close to the surface one can expand Eq. (3.18) in powers of $x = (r_\perp - R)/(2\xi)$. This yields

$$\mathcal{M} \rightarrow x^2 \left[1 + \frac{\xi}{R}\frac{8}{3}(d_\perp - 1)\right] \quad . \tag{3.19}$$

For the limit of small particle radius ($R \ll \xi$) one has the small radius expansion in Eq.(2.59). In the semi-dilute limit $\xi \ll \mathcal{R}_x$ the interesting region is $R \ll r_\perp, \xi \ll \mathcal{R}_x$. In this case an expansion of the Debye function in Eq. (2.59) for large argument yields

$$\begin{aligned} \mathcal{M}(r_\perp) &\rightarrow 1 - 2\pi R \mathcal{R}_x^2 \int \frac{d^3p}{(2\pi)^3} \mathrm{e}^{i\,\mathbf{p}\,\mathbf{r}_\perp} \frac{2/L}{p^2 + \xi^{-2}} \\ &= 1 - 2\frac{R}{r_\perp}\mathrm{e}^{-r_\perp/\xi} \quad . \end{aligned} \tag{3.20}$$

For $r_\perp \ll \xi$, this result reduces to the overlap independent result in Eq. (3.2). Fig. 3.10 shows the mean field density profile around a thin cylinder for large overlap near four dimensions. It provides a qualitative estimate for the density profile around a small sphere ($\rho = 0.01$) in a semi-dilute solution in three dimensions. The value $\mathcal{S} = 25$ that leads to the simple relation $R : \xi : \mathcal{R}_x = 1 : 10 : 100$ seems to be large enough to lead to a behavior as expected in the semi-dilute limit. For comparison the limiting values of Eqs. (1.4) and (3.20) close to the surface and far away from the surface are also shown.

In both limits of either large or small radius one can see explicitly the expected scaling behavior in the semi-dilute limit

$$\mathcal{M}(r_\perp) = \tilde{m}\,(\frac{r_\perp}{R}\,,\,\frac{R}{\xi}) \tag{3.21}$$

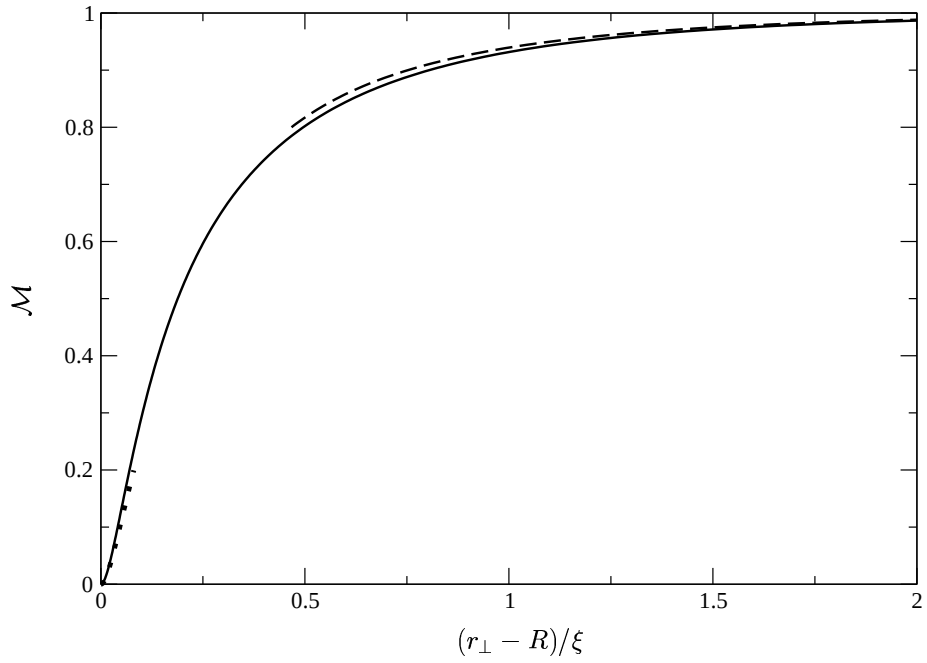

Figure 3.10: Density profile around a thin gen. cylinder in a semi-dilute solution. The full curve shows numerical data for $\rho = 0.01$ and $\mathcal{S} = 25$ which interpolate smoothly between the limiting behaviors (1.4) and (3.20) which are also shown.

which follows directly from Eq. (3.11).

3.1.5 Density of chain ends

The density of chain ends $\mathcal{E}(\mathbf{r})$ is given by Eq. (2.24). In contrast to the segment density $\mathcal{M}(\mathbf{r})$ it increases linearly close to the surface. Fig. 3.11 shows examples of end densities near a planar wall as a function of the

scaled distance from the wall for various values of the inter-chain overlap $\mathcal{S}$. Also the end density profile is non-monotonic for finite values of $\mathcal{S}$ as can be seen in the inset, where the scale of the vertical axis is enlarged. The first maximum is even more than fifty percent larger than for the monomer density in Fig. 3.5.

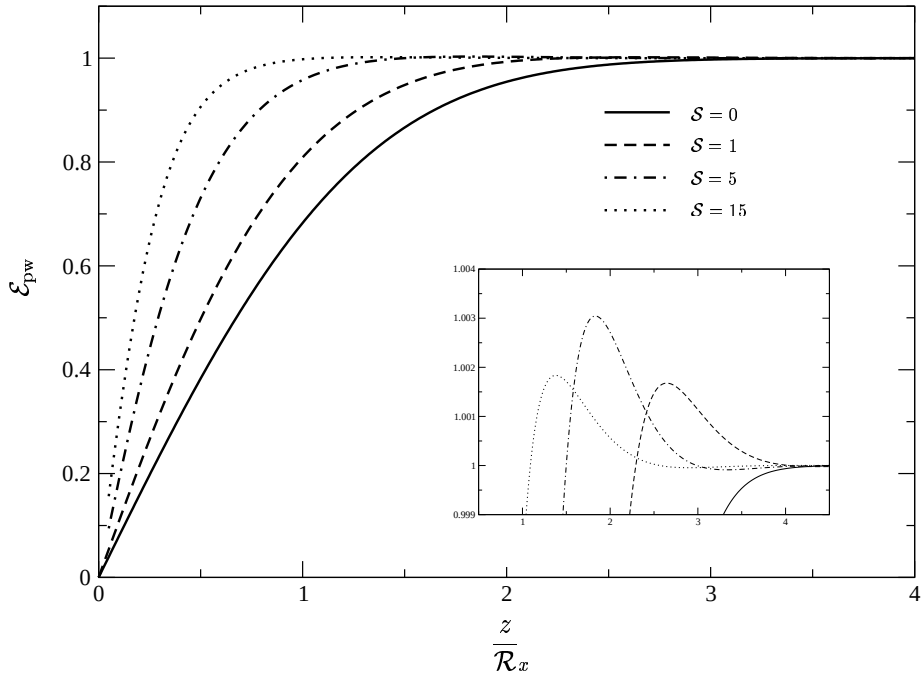

Figure 3.11: Bulk-normalized density of chain ends $\mathcal{E}_{\rm pw}$ near a planar wall versus the scaled distance $z/\mathcal{R}_x$ from the surface for various values of the inter-chain overlap $\mathcal{S}$. The inset shows the same figure with an enlarged scale of the vertical axis.

3.2 Free energy cost

Determining the free energy cost for immersing an infinitely long cylinder from Eq. (2.38) would lead to a divergence. Therefore one has to consider a generalized cylinder with an "axis" of large but finite extent or 'volume'

$$V_{\|} \;=\; v(\lambda/2, d_{\|}) \tag{3.22}$$

which is characterized by a large radius $\lambda/2$. Here

$$v(\lambda/2, d) \equiv \Omega_d \int_0^{\lambda/2} d\, r\, r^{d-1} \;=\; (\lambda/2)^d\, \pi^{d/2}\, [\Gamma(1+d/2)]^{-1} \tag{3.23}$$

is the volume of a sphere with radius $\lambda/2$, and $\Omega_d = 2\pi^{d/2}/\Gamma(d/2)$ is the surface area of a sphere with radius 1, in d dimensions. In the cases of interest one finds

$$V_{\|} \;=\; \lambda\,,\, 1 \quad \text{for} \quad d_{\|} \;=\; 1\,,\, 0 \quad . \tag{3.24}$$

3.2.1 Full scaling function

Now one can calculate the free energy cost per unit axis volume from Eq. (2.38) by replacing V by the cross-sectional volume $V_{\perp} = v(R, d_{\perp})$ and the integration $\int d\mathbf{r}$ by an integration $\int d\mathbf{r}_{\perp}$ over that part of the 'plane' $r_{\|} = 0$ perpendicular to the axis which is outside the particle:

$$F \;\to\; F/V_{\|} \;:\; V \;\to\; V_{\perp}\;;\; \int d\mathbf{r} \;\to\; \int d\mathbf{r}_{\perp}\;,\; r_{\perp} > R \quad . \tag{3.25}$$

Making λ so large that end effects can be neglected the independence of the mean-field profile $\mathcal{M}(\mathbf{r})$ on $d_\parallel$ is transmitted via Eqs. (2.38), (3.25) to the free energy cost per unit axis volume. Thus in the mean-field approximation $F/V_\parallel$ only depends on $d_\perp$ and is independent of $d_\parallel$ [22, 7]. For the case of the special choice of $d_\perp$ and $d_\parallel$ in Eqs. (2.44) one finds again that the scaling function f_d given by

$$\frac{F}{k_B T V_\parallel} = n \mathcal{R}_x^3 f_d\Big(\frac{R}{\mathcal{R}_x}, \frac{n}{n^*}\Big) \quad , \tag{3.26}$$

in leading order $d \nearrow 4$ equals the corresponding mean-field scaling function for a sphere in three dimensions. Here the prefactor follows from dimensional reasons. One should note that the scaling forms for the density profile and the free energy cost given by Eqs. (3.1) and (3.26) also hold for $d < 4$, provided the leading order expressions for $\mathcal{R}_x$ from (2.15) and for n^* from (2.42) are replaced by $\mathcal{R}_{\rm EE}(d)/\sqrt{d}$, with $\mathcal{R}_{\rm EE}(d)$ the end-to-end distance of an isolated self-avoiding chain, and by the reciprocal virial coefficient $(A_2(d))^{-1}$ of self- and mutually avoiding chains in $d < 4$. However, the scaling functions m and f for $d < 4$ are different from the mean-field scaling functions. Fig. 3.12 shows numerical results for the scaling function f_4 versus the size ratio $\rho = R/\mathcal{R}_x$, for various values of the overlap variable $\mathcal{S} = n/n^*$. Note the limits $f_4 \to 2\pi\rho$ for small size ratio independent of $\mathcal{S}$ as predicted by the small radius expansion in Sec. 2.6 and $f_4 = \frac{4\pi}{3}\rho^3(1+\mathcal{S}/2)$ for large size ratio as predicted by the small curvature expansion in Sec. 2.7.

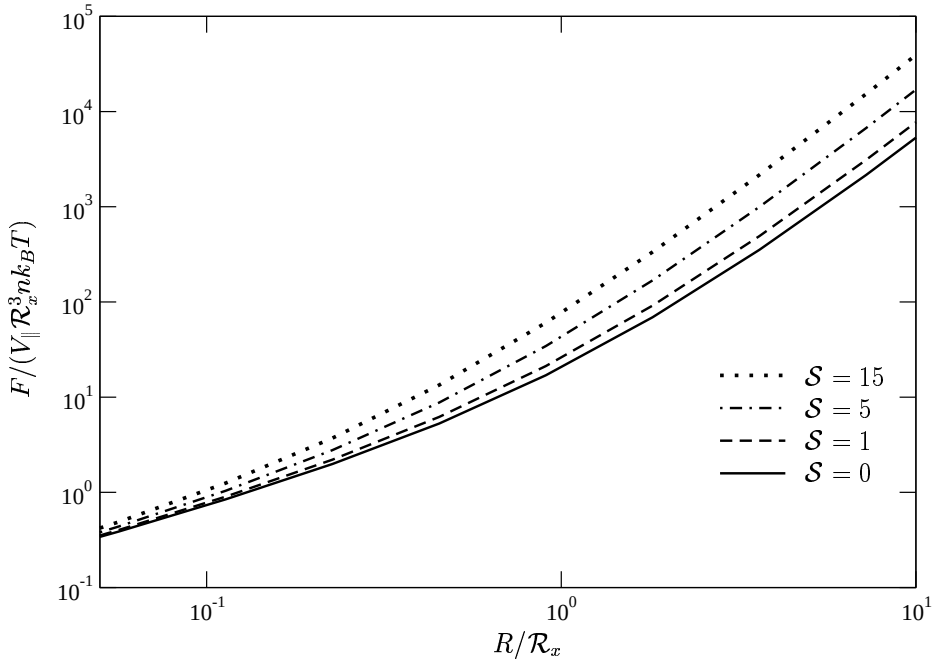

Figure 3.12: Scaled solvation free energy $F/(V_\parallel \mathcal{R}_x^3 n k_B T)$ versus size ratio $\rho = R/\mathcal{R}_x$ for various values of the inter-chain overlap $\mathcal{S}$. Shown is the scaling function f_4 (Eq. (3.26)) for a cylinder of infinite length $V_\parallel = \lambda \to \infty$ in $d = 4$ dimensions. This also furnishes a qualitative estimate of the corresponding scaling function f_3 for a sphere ($V_\parallel = 1$) in $d = 3$ dimensions.

3.2.2 Small overlap and large particle radius

The leading $\mathcal{S}$-dependence for small overlap can be obtained from the small overlap expansion for the density profile in Eq. (3.7). Since $\mathcal{M}^{[0]}$ and $\mathcal{M}^{[1]}$ satisfy the identity (3.8) the free energy is given by

$$\begin{aligned} \frac{F/V_\parallel}{k_B T} &= n\left\{V_\perp + \int_{r_\perp > R} d\mathbf{r}_\perp \, \left[1 - \mathcal{M}^{[0]}(\mathbf{r})\right]\right\} \\ &\quad + \frac{\mathcal{S}}{2} n \left\{V_\perp + \int_{r_\perp > R} d\mathbf{r}_\perp \, \left[1 - \mathcal{M}^{[0]}(\mathbf{r})\right]^2\right\} + O(\mathcal{S}^2) \; . \quad (3.27) \end{aligned}$$

In the rest of this subsection I consider only the case of large particle radius $R \gg \mathcal{R}_x$, where one can obtain an analytical expression for the first order contribution. The density profile around a generalized cylinder with $d_\perp = 3$ for ideal chains in the dilute limit is given by Eq. (1.6). Expanding the prefactors of the iterated error functions in powers of $(r_\perp - R)/R$ leads to

$$\mathcal{M}^{[0]}(\mathbf{r}) \approx \mathcal{M}^{[0]}_{\rm pw}(r_\perp - R) + \frac{r_\perp - R}{R}\,\delta\mathcal{M}^{[0]}(r_\perp - R) \quad , \tag{3.28}$$

with

$$\begin{aligned} \mathcal{M}^{[0]}_{\rm pw}(r_\perp - R) &= 1 - 8\,\mathrm{i}^2\mathrm{erfc}(y) + 4\,\mathrm{i}^2\mathrm{erfc}(2y) \quad , \\ \delta\mathcal{M}^{[0]}(r_\perp - R) &= 8\,\mathrm{i}^2\mathrm{erfc}(y) - 8\,\mathrm{i}^2\mathrm{erfc}(2y) \end{aligned} \tag{3.29}$$

and y given by Eq. (1.7). Inserting these equations into Eq. (3.27) one obtains for the integral in the first order contribution in the overlap

$$\begin{aligned} &\int_{r_\perp > R} d\mathbf{r}_\perp \, \left[1 - \mathcal{M}^{[0]}(\mathbf{r})\right]^2 \\ &= 4\pi \int_0^\infty dz\,(R+z)^2 \left\{ \left[1 - \mathcal{M}^{[0]}_{\rm pw}(z)\right]^2 - 2\frac{z}{R}\delta\mathcal{M}^{[0]}(z) + 2\frac{z}{R}\delta\mathcal{M}^{[0]}(z)\mathcal{M}^{[0]}_{\rm pw}(z) \right\} \\ &= 4\pi R^2 \int_0^\infty dz \left[8\,\mathrm{i}^2\mathrm{erfc}(z/(\sqrt{2}\mathcal{R}_x)) - 4\,\mathrm{i}^2\mathrm{erfc}(\sqrt{2}z/\mathcal{R}_x)\right]^2 \\ &\quad + 8\pi R \int_0^\infty dz\, z \left[32\,\mathrm{i}^2\mathrm{erfc}(z/(\sqrt{2}\mathcal{R}_x))\,\mathrm{i}^2\mathrm{erfc}(\sqrt{2}z/\mathcal{R}_x) - 16\,[\mathrm{i}^2\mathrm{erfc}(\sqrt{2}z/\mathcal{R}_x)]^2\right] \\ &= 8\pi\, R^2\, \mathcal{R}_x \sqrt{\frac{2}{\pi}}\,\lambda_1 + 8\pi\, R\, \mathcal{R}_x^2\,\lambda_2\,, \end{aligned} \tag{3.30}$$

where the abbreviations

$$\lambda_1 = \frac{5\sqrt{5}}{3} - \frac{12\sqrt{2}}{5} = 0.333 \quad , \tag{3.31}$$

$$\lambda_2 = \frac{1}{8}\Big[19 - \frac{1}{\pi}\Big(17 + \frac{75}{2}\arctan(2)\Big)\Big] = 0.047 \tag{3.32}$$

were used. Substituting Eq. (3.30) into Eq. (3.27) one gets

$$\begin{aligned}\frac{F/V_{\|}}{4\pi n R^3 k_B T} &= \left\{\frac{1}{3} + \sqrt{\frac{2}{\pi}}\rho^{-1} + \frac{1}{2}\rho^{-2}\right\} \\ &\quad + \mathcal{S}\left\{\frac{1}{6} + \sqrt{\frac{2}{\pi}}\lambda_1\rho^{-1} + \lambda_2\rho^{-2} + O(\rho^{-3})\right\} \\ &\quad + O(\mathcal{S}^2).\end{aligned} \tag{3.33}$$

3.2.3 Semi-dilute limit

There is no analytical mean-field expression for the free energy cost to immerse a spherical or cylindrical particle with arbitrary radius into a semi-dilute polymer solution. Thus I have calculated the free energy cost from Eq. (2.38) up to $\mathcal{S} = 64$ to get at least an approximation. For $\mathcal{S} \to \infty$ Eq. (2.38) reduces to

$$\begin{aligned}\frac{F}{k_B T V_{\|}} &= n\frac{\mathcal{S}}{2}V_{\perp} + n\frac{\mathcal{S}}{2}\int d\mathbf{r}_{\perp}\,[1 - \mathcal{M}^2(\mathbf{r})] \\ &\equiv 2\pi n R \mathcal{R}_x^2 \tilde{f}(R/\xi)\end{aligned} \tag{3.34}$$

For small particle radius $R \ll \xi$, i.e. small argument, the function $\tilde{f}$ has to approach 1 according to Eq. (1.5). In the opposite limit $R \gg \xi$ one can use

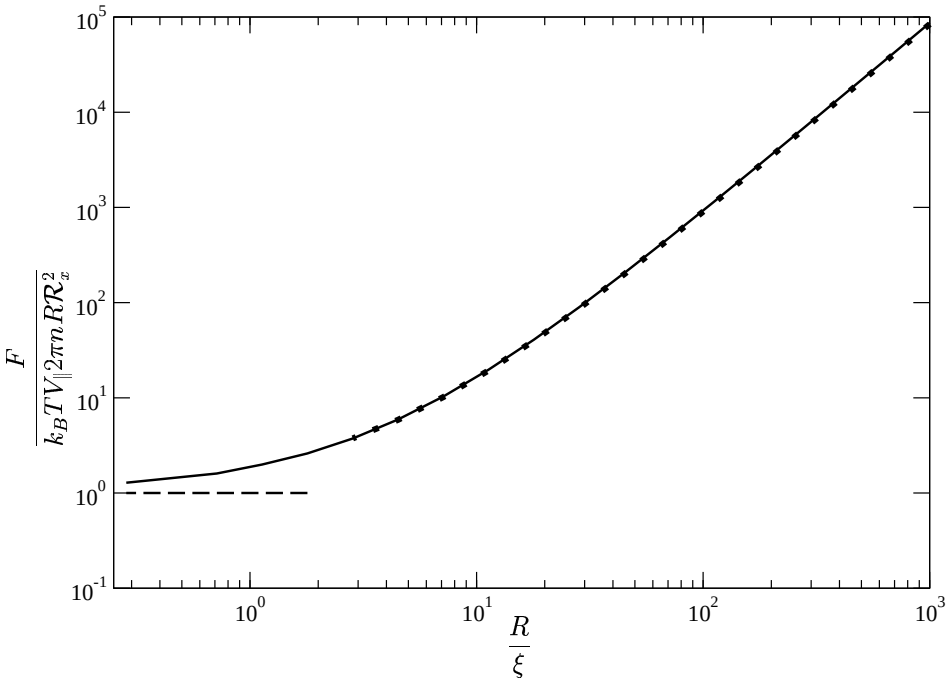

Figure 3.13: Scaling function $\tilde{f} = F/(2\pi V_\parallel R\mathcal{R}_x^2 n k_B T)$ of the solvation free energy in the semi-dilute limit versus the ratio R/ξ. The dots show the large particle limit from Eq. (3.36), the dashed line the small particle limit from Eq. (1.5).

the small curvature expansion for the density profile from Eq. (3.18) and the definition of the screening length ξ from Eq. (2.16) to find

$$\begin{aligned} \tilde{f} \quad \rightarrow \quad & \frac{1}{12}\frac{R^2}{\xi^2} + 2\frac{R}{\xi}\int_0^\infty dy[1-\tanh^4(y)] \\ & + 2\int_0^\infty dy\{y[1-\tanh^4(y)] - 4\tanh^3(y)\Psi(y)\}\,. \end{aligned} \tag{3.35}$$

Evaluating the integrals yields

$$\tilde{f}(x) \;\to\; \frac{1}{12}x^2 + \frac{2}{3}x + \frac{2}{3}(4\ln 2 - 1) \quad , \quad \text{for } x \to \infty \,. \tag{3.36}$$

Fig. 3.13 shows the numerically obtained mean-field scaling function $\tilde{f} = F/(2\pi V_{\|} R \mathcal{R}_x^2 n k_B T)$. There are only very small corrections in $\tilde{f}$ if $\mathcal{S}$ is changed, so that the assumption to be close to the semi-dilute limit seems reasonable. The limits for small and large particle radius are also shown as the dashed and dotted line, respectively. It is remarkable that the large particle limit describes the function very well for $R \geq \xi$.

3.2.4 Surface tension

The volume term in the small curvature expansion for the free energy in Eq. (2.63) is well understood since the osmotic pressure of a polymer solution is known quantitatively as a function of the chain overlap (see Ref. [18] or Eq. (4.51) below). The depletion effect enters in the next terms in Eq. (2.63). The leading term contains the surface tension σ with a scaling form

$$\frac{\sigma}{k_B T} \;=\; n\,\mathcal{R}_x\, g(\mathcal{S}) \tag{3.37}$$

which follows from Eq. (2.64). In the limit of small overlap one obtains from a comparison of Eqs. (3.33) and (2.63) the expansion

$$\frac{\sigma}{n k_B T} \;=\; \mathcal{R}_x \sqrt{\frac{2}{\pi}} \left[1 + \lambda_1 \mathcal{S} + O(\mathcal{S}^2)\right] \quad . \tag{3.38}$$

In the semi-dilute limit the behavior of the surface tension follows from Eqs.

(3.36), (3.34) and (2.63) as

$$\frac{\sigma}{nk_BT} \quad \rightarrow \quad \mathcal{R}_x \frac{2}{3}\sqrt{\mathcal{S}} \ , \ \text{for } \mathcal{S} \rightarrow \infty \ . \tag{3.39}$$

Fig. 3.14 shows the scaling function $g(\mathcal{S})$ for arbitrary $\mathcal{S}$, which is obtained numerically from Eqs. (2.20)-(2.23) and (2.64). It interpolates smoothly between the limits of Eqs. (3.38) and (3.39).

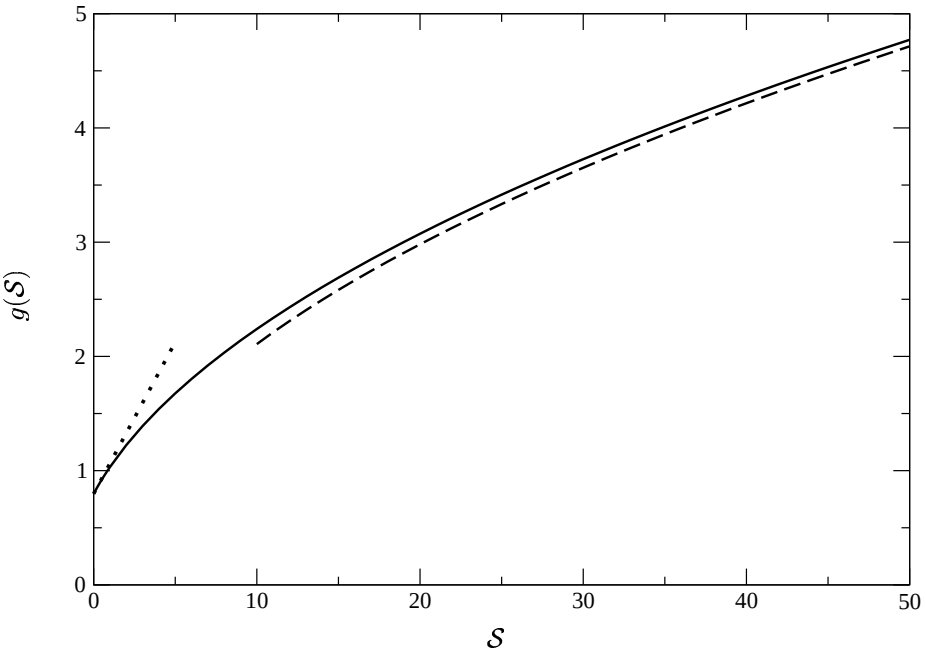

Figure 3.14: Scaling function $g(\mathcal{S})$ of the surface tension $\sigma = k_BTn\mathcal{R}_x g$ in the mean-field approximation (Eq. (3.37)). The dotted and dashed lines show the asymptotic behavior for small and large $\mathcal{S}$, respectively, see Eqs. (3.38) and (3.39).

3.2.5 Coefficient of spontaneous curvature

For the coefficient κ of spontaneous curvature there is no closed formula like Eq. (2.64) for the surface tension. Due to dimensional reasons the scaling form of κ is given by

$$\frac{\kappa}{k_B T} = n \mathcal{R}_x^2 \, h(\mathcal{S}) \quad . \tag{3.40}$$

Like in the case of the surface tension the expansion for small overlap follows

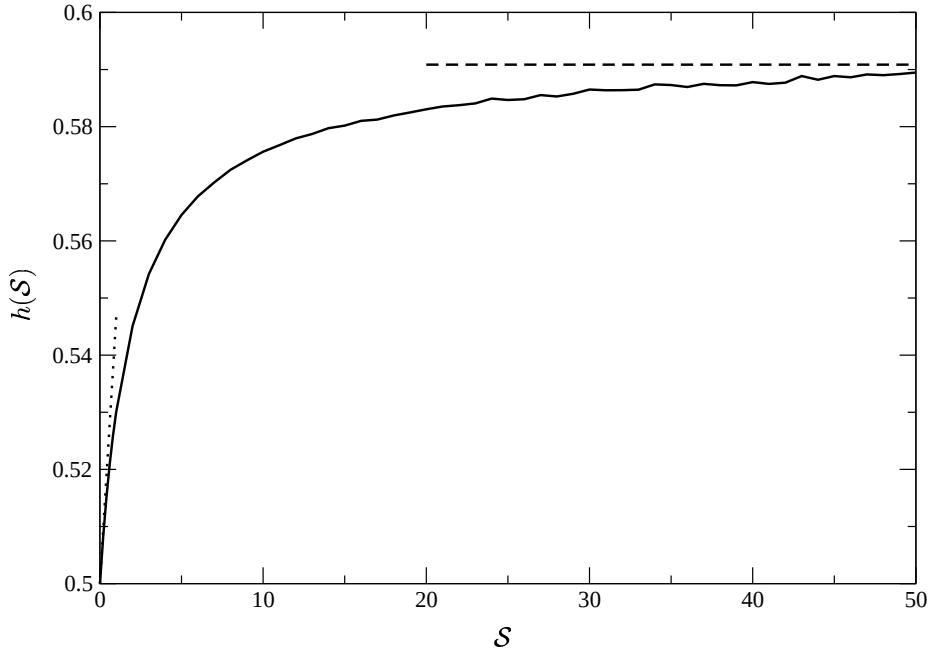

Figure 3.15: Scaling function $h(\mathcal{S})$ of the coefficient $\kappa = k_B T n \mathcal{R}_x^2 h$ of the spontaneous curvature in the mean-field approximation (Eqs. (2.63) and (3.40)). The dotted and dashed lines show the asymptotic behavior for small and large $\mathcal{S}$, respectively, see Eqs. (3.41) and (3.42).

from Eqs. (2.63) and (3.33) as

$$\frac{\kappa}{nk_BT} = \mathcal{R}_x^2\left(\frac{1}{2}+\lambda_2\mathcal{S}+O(\mathcal{S}^2)\right) . \tag{3.41}$$

In the semi-dilute limit Eqs. (2.63), (3.36) and (3.34) give

$$\frac{\kappa}{nk_BT} \to \mathcal{R}_x^2\,\frac{1}{3}\,(4\ln 2-1) \quad , \text{ for } \mathcal{S}\to\infty \ . \tag{3.42}$$

Fig. 3.15 shows the numerically obtained scaling function $h(\mathcal{S})$ for arbitrary $\mathcal{S}$ and the asymptotic expressions for small and large inter-chain overlap.

3.3 Density-pressure identity

The pressure exerted by the polymers onto a given surface element of an embedded mesoscopic particle is proportional to the local monomer density $n\mathcal{R}_x^{1/\nu}\mathcal{M}^{(\mathrm{as})}(\mathbf{r}) = n\mathcal{R}_x^{1/\nu}\mathcal{M}(r_\perp \searrow R)$ near the surface element [27, 28]. Here the limit $(r_\perp \searrow R)$ has to be taken in the scaling regime, which means that the distance from the particle surface is still large compared to microscopic length scales like the segment size l but much smaller than R and $\mathcal{R}_x$. The factor of proportionality involves a universal constant B. In the mean-field approximation one has

$$1/\nu = 2\ ,\ B = 2 \quad . \tag{3.43}$$

For the generalized cylinder the pressure p acts on a surface S with area

$S_\perp V_\parallel$ and with the surface-normal perpendicular to the axis. Thus the identity (1.3) reads

$$\mathcal{M}^{\rm as}(r_\perp) \;=\; 2\Big(\frac{r_\perp - R}{\mathcal{R}_x}\Big)^2 \,\frac{p}{nk_BT} \quad , \tag{3.44}$$

with

$$p = \frac{1}{S_\perp}\,\frac{d}{dR}\,\frac{F}{V_\parallel} \quad . \tag{3.45}$$

Here

$$S_\perp \equiv\; R^{d_\perp - 1}\,\Omega_{d_\perp} \tag{3.46}$$

equals $4\pi R^2$ for the case of a cylinder of type (2.44) in which $d_\perp = 3$. The validity of the density-pressure identity within the mean-field approximation is shown in Appendix A.

Fig. 3.16 shows numerical results for $p/(nk_BT)$ as a function of the size ratio $R/\mathcal{R}_x$ for various values of the overlap $\mathcal{S}$. The pressure increases with increasing $\mathcal{S}$ and decreases with increasing $\rho = R/\mathcal{R}_x$ which is in agreement with the behavior of the density near the surface in Figs. (3.1) and (3.2).

The limiting values for the pressure in the case of small particles ($R \ll \mathcal{R}_x, \xi$) and large particles $R \gg \mathcal{R}_x$ follow via Eq. (3.45) from the limiting values of the free energy cost. Explicitly they are given by

$$\begin{aligned} p \;\;&\to\;\; \frac{1}{4\pi R^2}\,\frac{d}{dR}\left(2\pi\, nk_BT\, R\mathcal{R}_x^2\right) \\ &=\;\; n\,k_BT\,\frac{\mathcal{R}_x^2}{2R^2} \quad , \;\text{for}\;\; R/\mathcal{R}_x \to 0 \end{aligned} \tag{3.47}$$

and

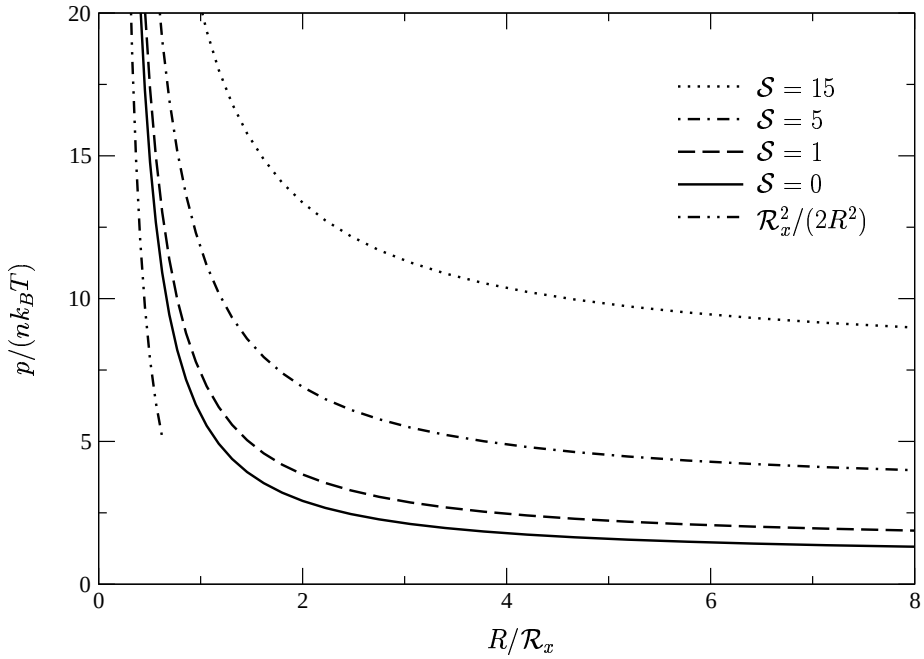

Figure 3.16: Scaled polymer-pressure $p/(nk_BT)$ on the surface of a cylindrical rod in $d = 4$ dimensions as a function of the size ratio $\rho = R/\mathcal{R}_x$ for various values of the overlap $\mathcal{S}$. This result also furnishes a qualitative estimate of the pressure on the surface of a spherical particle in $d = 3$ dimensions.

$$p \;\rightarrow\; \frac{1}{4\pi R^2}\,\frac{d}{dR}\left(\frac{4\pi}{3}R^3\Pi \,+\, 4\pi R^2\left[\sigma \,+\, \frac{\kappa}{R}\right]\right)$$

$$=\quad \Pi \,+\, 2\frac{\sigma}{R} \,+\, \frac{\kappa}{R^2} \quad , \text{ for } \; R/\mathcal{R}_x \rightarrow \infty \;\; . \tag{3.48}$$

Using the last equation, the density pressure identity yields a prediction for the density profile close to the surface of a large particle, given by

$$\begin{aligned}\mathcal{M}(r_\perp \searrow R) &= \mathcal{M}^{(\mathbf{as})}(r_\perp) \\ &= 2\Big(\frac{r_\perp - R}{\mathcal{R}_x}\Big)^2 \Big[1 + \frac{\mathcal{S}}{2} + (d_\perp - 1)\frac{\mathcal{R}_x}{R} g(\mathcal{S}) + \\ &\quad + \frac{(d_\perp - 1)(d_\perp - 2)}{2}\Big(\frac{\mathcal{R}_x}{R}\Big)^2 h(\mathcal{S}) + ...\Big], \qquad (3.49)\end{aligned}$$

where g and h are the scaling functions for the surface tension and the co-

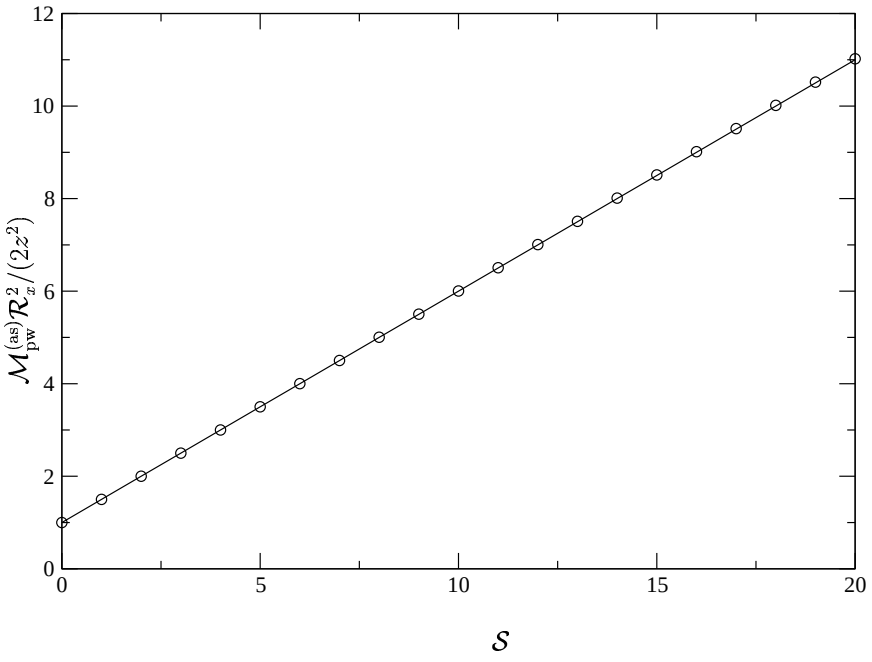

Figure 3.17: Density-pressure identity for a planar wall (see Eq. (3.49) with $r_\perp - R = z$ finite and $R = \infty$). The amplitude $\mathcal{M}^{\rm as}\,\mathcal{R}_x^2\,/\,(2\,z^2)$ of the density profile $\mathcal{M} = \mathcal{M}_{\rm pw}$ (circles) reproduces the scaled osmotic pressure $\Pi/(nk_BT) = 1 + \mathcal{S}/2$ (full line) very well.

efficient of spontaneous curvature introduced in Eqs. (3.37) and (3.40), respectively. Note that in the semi-dilute limit where $\mathcal{S} \to \infty$, this expression reduces to the result in Eq. (3.19). Figs. 3.17 and 3.18 show that the numerically determined profile $\mathcal{M}$ for a cylinder of type (2.44) with $d_\perp = 3$, $d \nearrow 4$ and a large radius R does indeed fulfill the density-pressure identity (3.44).

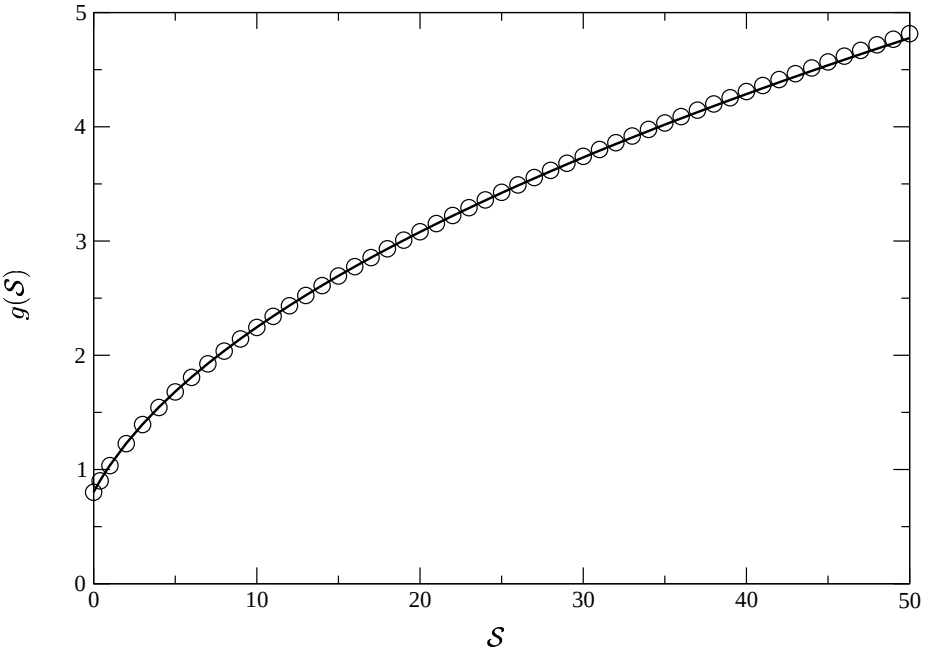

Figure 3.18: Contribution of the surface tension to the density-pressure identity for a weakly curved surface of a cylinder (see Eq. (3.49) with $d_\perp = 3$). The limit $\lim_{R/\mathcal{R}_x \to \infty} \frac{R}{2\mathcal{R}_x}\left[\frac{\mathcal{M}^{(\mathrm{as})}\mathcal{R}_x^2}{2(r_\perp - R)^2} - \left(1 + \frac{\mathcal{S}}{2}\right)\right]$ taken from the density profile near the surface $\mathcal{M}^{(\mathrm{as})}$ is well approximated by the value for $R/\mathcal{R}_x = 100$ (circles) and reproduces the scaling function $g(\mathcal{S})$ of the surface tension (full line).

3.4 Number of missing chains

On inserting a particle into a solution of free non-adsorbing polymers one decreases the number of polymer chains due to the smaller volume accessible for the chains and due to the depletion effect. The decrease $\langle \delta \mathcal{N} \rangle$ of the number $\langle \mathcal{N} \rangle$ of chains in the solution is thus a simple quantity to describe the depletion effect quantitatively. Here I consider the polymers in contact with a large reservoir as described by the grand canonical ensemble with a chain fugacity ζ. The relationship between the chain fugacity ζ and the bulk density n is given in Eq. (2.32) and leads to

$$\begin{aligned} \langle -\delta \mathcal{N} \rangle / V_{\|} &= \langle \mathcal{N}|_{\text{without particle}} - \mathcal{N}|_{\text{with particle}} \rangle / V_{\|} \\ &= \zeta \frac{d}{d\zeta} \frac{F/V_{\|}}{k_B T} \\ &= n \left(V_{\perp} + \int_{r_{\perp}>R} d\mathbf{r}_{\perp} [\, 1 - \mathcal{M}(r_{\perp}) \,] \right) \quad . \end{aligned} \tag{3.50}$$

While the first term dominates for $R \gg \mathcal{R}_x$, one finds in the limit $R \ll \mathcal{R}_x$ from the small radius expansion for the density profile in Eq. (2.59)

$$\begin{aligned} \langle -\delta \mathcal{N} \rangle / V_{\|} &\rightarrow \int_{r_{\perp}>R} d\mathbf{r}_{\perp} [\, 1 - \mathcal{M}(r_{\perp}) \,] \Big) \\ &\rightarrow 2\pi \, R \, \mathcal{R}_x^2 \int_{r_{\perp}>R} d\mathbf{r}_{\perp} \int \frac{d^3p}{(2\pi)^3} \, \mathrm{e}^{i \, \mathbf{p} \, \mathbf{r}_{\perp}} \frac{D(p^2 L)}{1 + \mathcal{S} D(p^2 L)} \\ &= 2\pi \, n \, R \, \mathcal{R}_x^2 \, \frac{1}{1 + \mathcal{S}} \, . \end{aligned} \tag{3.51}$$

In contrast to the free energy cost in Eq. (1.5) and the pressure in Eq.

(3.47), the number of missing chains is not independent of the inter-chain overlap in the small radius limit. Fig. 3.19 shows the numerical results for the scaled number of missing chains. The result shown is for a cylinder in $d = 4$ dimensions with axis length $V_{||} = \lambda$, but it gives also a qualitative estimate for the case of a spherical particle in $d = 3$ in which $V_{||} = 1$.

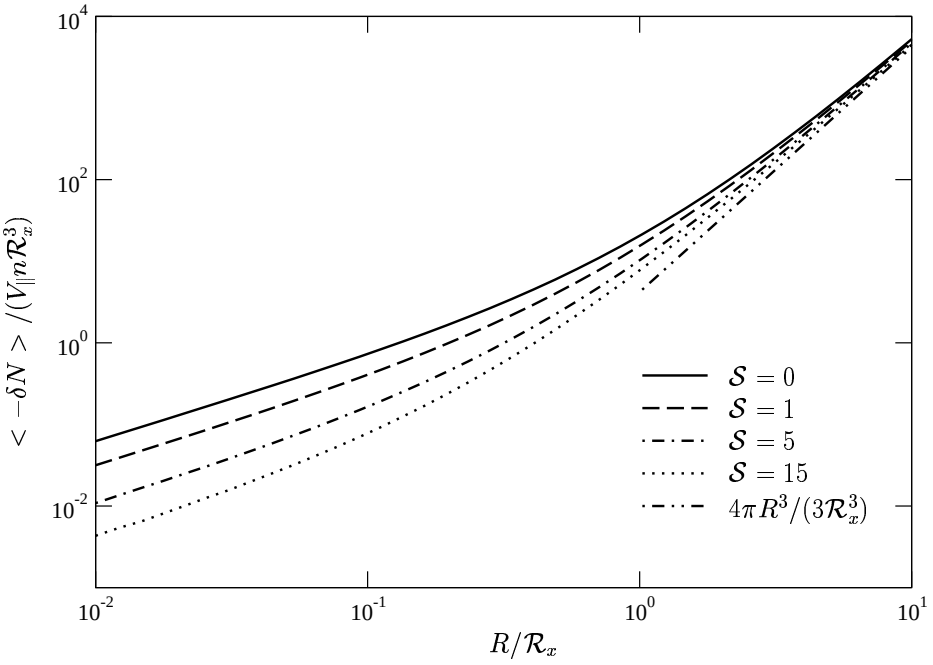

Figure 3.19: Scaled number of missing chains $\langle -\delta\mathcal{N}\rangle/(V_{||} n \mathcal{R}_x^3)$ versus size ratio $\rho = R/\mathcal{R}_x$ for various values of the inter-chain overlap $\mathcal{S}$. Note the crossover from the result $2\pi\rho/(1+\mathcal{S})$ for small ρ (Eq. (3.51)) to the overlap-independent behavior $\frac{4\pi}{3}\rho^3$ for large ρ.

Chapter 4

Renormalized tree approximation in three dimensions

As pointed out before, in three dimensions the mean-field results of Sec. 3 give only *qualitative* dependencies of various scaling functions on the size ratio and the inter-chain overlap. The aim of this section is to obtain semi-*quantitative* results, i.e. scaling functions with the correct power law exponents in three dimensions, by means of the field theoretic renormalization group (R.G.) [18]. In this theory the microstructure (cutoff) dependence of all properly normalized observables, which are infinitely many, can be absorbed into only three renormalization factors that reparameterize the theory. Apart from negligible corrections the renormalized, i.e. reparameterized, observables are independent of the microstructure. The reparameterization involves an arbitrary inverse length scale μ. Varying μ for fixed bare pa-

rameters leads to flow equations for the renormalized observables. These display an infrared stable fixed point for the renormalized excluded volume interaction and can be used to map the "critical" polymer system with L_r large and $n_r L_r$ small onto a "noncritical" one [18, 19] for which the loop expansion makes sense and where mean-field theory applies approximately. There is some freedom in choosing the renormalization factors and the concomitant renormalization scheme. Actually the most convenient version of the field theoretic renormalization group is based on a mass shifted bare theory without cutoff which is finite for $d < 4$ and develops pole terms for $d \to 4$. Here renormalization proceeds by absorbing the pole terms into the renormalization factors.

In this chapter I derive the renormalized tree approximation for the free energy cost of immersing a spherical particle into a solution of non-adsorbing polymer chains with excluded volume interaction in $d = 3$. For simplicity I discuss only the three special cases where the free energy cost depends only on two of the three length scales R, $\mathcal{R}_x$, and ξ in the system. These cases correspond to the left, top, and bottom margin of Fig. 1.1.

4.1 Renormalization of the free energy

As explained above, one has to express the basic variables b, N, n, and R in terms of renormalized variables u_r, L_r, n_r, and R_r. The renormalized variables are introduced via the relations

$$b/l^4 = (4\pi)^{d/2} \mu^\epsilon Z_u u_r / 3 \,, \tag{4.1}$$

$$N l^2 = \mu^{-2} L_r / Z_t \,, \tag{4.2}$$

$$n = \mu^d n_r \ , \tag{4.3}$$

$$R = \mu^{-1} R_r \ , \tag{4.4}$$

where μ, as stated above, is some arbitrary inverse length scale taking care of the spatial dimensions, and Z_u, Z_t are renormalization factors which eliminate the microstructure dependence. These factors are independent of the chain length and can be defined via a Taylor series expansion in powers of u_r.

For the renormalization of the free energy cost for immersing a spherical particle into a solution of polymers with excluded volume interaction it is advantageous to use the grand canonical description. The grand canonical partition function $\mathcal{Z}_G$ in presence of the particle was introduced in Eq. (2.25), and via the linked cluster theorem [18] the grand canonical free energy per $k_B T$ is given by

$$\mathcal{F}_G \ = \ - \ln \left\{ 1 + \sum_{\mathcal{N}=1}^{\infty} \frac{1}{\mathcal{N}!} \zeta^{\mathcal{N}} \, \mathcal{Z}^{(\mathcal{N})} \right\} \ = \ - \sum_{\mathcal{N}=1}^{\infty} \frac{1}{\mathcal{N}!} \zeta^{\mathcal{N}} \, \mathcal{Z}_c^{(\mathcal{N})} \ , \tag{4.5}$$

where again the subscript c stands for the connected part of the partition function $\mathcal{Z}^{(\mathcal{N})}$. Since $\mathcal{Z}_c^{(\mathcal{N})}$ can be viewed essentially as an $\mathcal{N}$-fold inverse Laplace transform of a correlation function of $2\mathcal{N}$ order parameter fields ϕ, the renormalization of $\mathcal{Z}_c^{(\mathcal{N})}$ is given by the relation

$$\mathcal{Z}_c^{(\mathcal{N})} \ = \ \left(\mathrm{e}^{t_c L} Z_\phi Z_t \mu^{-d} \right)^{\mathcal{N}} \mathcal{Z}_{c,r}^{(\mathcal{N})} \, . \tag{4.6}$$

Eq. (4.6) applies for both situations, in presence and in absence of the particle. Here Z_ϕ is another renormalization factor occurring in the renormalization of the order parameter field ϕ. The t_c-shift and the renormalization

factor Z_t arise from the Laplace transform in Eq. (2.45), since the reparameterization of t is given by

$$t - t_c \;=\; \mu^2 Z_t t_r \;. \tag{4.7}$$

The chain fugacity ζ was defined in Eq. (2.26), and if one now defines

$$\zeta_r \;=\; \mu^{-d} \mathrm{e}^{t_c L} Z_\phi Z_t \zeta \;, \tag{4.8}$$

then one has

$$\zeta^{\mathcal{N}} \mathcal{Z}_c^{(\mathcal{N})} \;=\; \zeta_r^{\mathcal{N}} \mathcal{Z}_{c,r}^{(\mathcal{N})} \;, \tag{4.9}$$

and the microstructure dependence is eliminated. In order to obtain the renormalized grand canonical free energy as a function of n_r, L_r, R_r, and u_r, one has to know the relation between ζ_r and n_r. Renormalizing the bulk relation $n = -\zeta \frac{d}{d\zeta} \mathcal{F}_G / \mathcal{U}$ with the same steps as above yields

$$n_r \;=\; \frac{\mu^{-d}}{\mathcal{U}} \sum_{\mathcal{N}=1}^{\infty} \frac{\mathcal{N} \zeta_r^{\mathcal{N}}}{\mathcal{N}!} \mathcal{Z}_{c,r}^{(\mathcal{N})} \;. \tag{4.10}$$

Inverting this relation and substituting the result into Eq. (4.5) one finally arrives at

$$\mathcal{F}_G(n, L, R, b, \mathcal{U}) \;=\; \mathcal{F}_{G,r}(n_r, L_r, R_r, u_r, \mathcal{U}\mu^d) \tag{4.11}$$

with $\mathcal{U}$ the normalization volume. Thus the free energy cost for immersing the particle is simply given by

$$\frac{F}{k_B T} \;=\; \mathcal{F}(n_r, L_r, R_r, u_r) \,, \tag{4.12}$$

where $\mathcal{F} = \mathcal{F}_{G,r} \;-\; \mathcal{F}_{G,r}|_{\text{without particle}}$ in the thermodynamic limit $\mathcal{U} \to \infty$.

In order to derive the renormalization group equation, one has to perform a simultaneous variation $D\mu$, Du_r, DL_r, Dn_r, DR_r of the renormalized quantities, keeping the bare quantities, i.e. the left hand sides of Eqs. (4.1)-(4.4), fixed. Then DF vanishes and one obtains

$$0 = [(Du_r)\partial_{u_r} + (DL_r)\partial_{L_r} + (DR_r)\partial_{R_r} + (Dn_r)\partial_{n_r}]\, \mathcal{F}(n_r, L_r, R_r, u_r)\,. \tag{4.13}$$

Introducing the functions

$$\beta_u(u_r) = \mu\frac{Du_r}{D\mu} \quad , \quad \vartheta_t(u_r) = \frac{\mu}{L_r}\frac{DL_r}{D\mu} \quad , \tag{4.14}$$

the renormalization group equation follows from Eq. (4.13) in the form

$$0 = [\beta_u(u_r)\partial_{u_r} + \vartheta_t(u_r)L_r\partial_{L_r} + R_r\partial_{R_r} - dn_r\partial_{n_r}]\, \mathcal{F}(n_r, L_r, R_r, u_r)\,. \tag{4.15}$$

Changing the inverse length scale $\mu \to \mathrm{e}^{-\lambda}\mu$, Eq. (4.15) implies

$$\mathcal{F}(n_r, L_r, R_r, u_r) = \mathcal{F}(\bar{n}_r(\lambda), \bar{L}_r(\lambda), \bar{R}_r(\lambda), \bar{u}_r(\lambda)) \tag{4.16}$$

with flowing parameters $\bar{u}_r$, $\bar{L}_r$, $\bar{R}_r$, and $\bar{n}_r$ which are determined by the characteristic equations

$$\frac{d}{d\lambda}\bar{u}_r(\lambda) = -\beta_u(\bar{u}_r(\lambda)) \quad , \quad \bar{u}_r(0) = u_r\,, \tag{4.17}$$

$$\frac{d}{d\lambda}\bar{L}_r(\lambda) = -\vartheta_t(\bar{u}_r(\lambda))\bar{L}_r(\lambda) \quad , \quad \bar{L}_r(0) = L_r\,, \tag{4.18}$$

$$\frac{d}{d\lambda}\bar{R}_r(\lambda) = -\bar{R}_r(\lambda) \quad , \quad \bar{R}_r(0) = R_r\,, \tag{4.19}$$

$$\frac{d}{d\lambda}\bar{n}_r(\lambda) = d\bar{n}_r(\lambda) \quad , \quad \bar{n}_r(0) = n_r\,. \tag{4.20}$$

Eqs. (4.16)-(4.20) can be verified by showing that $\frac{d}{d\lambda}\mathcal{F}(\bar{n}_r, \bar{L}_r, \bar{R}_r, \bar{u}_r)$ vanishes due to the validity of Eq. (4.15) with arguments u_r, L_r, R_r, and n_r replaced by $\bar{u}_r$, $\bar{L}_r$, $\bar{R}_r$, and $\bar{n}_r$. The flow equations (4.17)-(4.20) will be used below to map the 'critical' polymer system of interest onto a noncritical one. In the asymptotic critical region, where $L_r \to \infty$, $L_r n_r \to 0$, and $R_r \to \infty$, the mapping parameter λ in Eq. (4.16) tends to infinity. In this case the solutions of the characteristic equations (*characteristics*) are given by

$$u_r \to u_{r,\mathrm{FP}} \,, \tag{4.21}$$

$$L_r \to \bar{L}_r(\lambda) = D_L(u_r)\, L_r\, \mathrm{e}^{-\lambda/\nu} \,, \tag{4.22}$$

$$n_r \to \bar{n}_r(\lambda) = n_r \mathrm{e}^{d\lambda} \,, \tag{4.23}$$

$$R_r \to \bar{R}_r(\lambda) = R_r \mathrm{e}^{-\lambda} \,. \tag{4.24}$$

Here D_L follows from the solution of Eq. (4.18) in the limit $\lambda \to \infty$ which is given by

$$\begin{aligned} \bar{L}_r(\lambda) &= L_r \exp\left\{-\int_0^\lambda d\lambda' \vartheta_t(\bar{u}_r(\lambda'))\right\} \\ &\to \underbrace{\exp\left\{-\int_0^\infty d\lambda' [\vartheta_t(\bar{u}_r(\lambda')) - \vartheta_t(u_{r,FP})]\right\}}_{\equiv D_L} L_r\, \mathrm{e}^{-\lambda/\nu} \,. \end{aligned} \tag{4.25}$$

In the second line $\vartheta_t(u_{r,FP}) = 1/\nu$ was used.

4.2 Polymer length scales

In this section I derive the renormalized tree expression for the typical polymer length scales that are given by the projected end-to-end distance $\mathcal{R}_x$ in the dilute and by the screening length ξ in the semi-dilute limit. The corresponding renormalization group and flow equations hold also for these quantities. The end-to-end distance in a dilute polymer solution is a function of only L_r and u_r. Since $\mathcal{R}_x$ is a renormalized quantity, it follows from dimensional reasons and from Eqs. (4.21), (4.22) that

$$\mathcal{R}_x^2 \;=\; \mu^{-2}\,\mathcal{X}(L_r, u_r) \;=\; \mu^{-2}\,\mathrm{e}^{2\lambda}\,\mathcal{X}(\bar{L}_r,\, u_{r,\mathrm{FP}}) \quad . \tag{4.26}$$

For the noncritical state the function $\mathcal{X}$ can be approximated by its tree or mean-field expression

$$\mathcal{X}(\bar{L}_r, u_{r,\mathrm{FP}}) \;\approx\; \mathcal{X}_{\mathrm{tree}}(\bar{L}_r, u_{r,\mathrm{FP}}) \;=\; 2\bar{L}_r \quad . \tag{4.27}$$

For the screening length in the semi-dilute limit that depends on L_r, u_r, and n_r the R.G. mapping is given by

$$\xi^2 \;=\; \mu^{-2}\,\mathcal{Y}(L_r, n_r, u_r) \;=\; \mu^{-2}\,\mathrm{e}^{2\lambda}\,\mathcal{Y}(\bar{L}_r, \bar{n}_r, u_{r,\mathrm{FP}}) \quad . \tag{4.28}$$

The tree expression that is given by $\xi^2 = L/(2\mathcal{S})$ includes the inter-chain overlap $\mathcal{S}$. This is expressed in renormalized variables via the reparameterization in Eqs. (4.1)-(4.3) as

$$\begin{aligned} \mathcal{S} \;&=\; bN^2 n \;=\; (4\pi)^{d/2}\mu^{\epsilon}\,Z_u\,\frac{u_r}{3}\,\mu^{-4}L_r^2 Z_t^{-2}\,\mu^d n_r \\ &=\; (4\pi)^{d/2}\,\frac{u_r}{3}\,L_r^2\,n_r Z_u\,Z_t^{-2}\,. \end{aligned} \tag{4.29}$$

Thus

$$\bar{\mathcal{S}} = a\,\bar{L_r}^2\,\bar{n_r}\ , \tag{4.30}$$

since in the noncritical region I apply the tree approximation with the Z-factors put equal to 1. In Eq. (4.30) I introduced the abbreviation

$$a = \frac{1}{2}(4\pi)^{3/2}u^* = 8.11 \tag{4.31}$$

with the fixed-point value $u_{r,\mathrm{FP}} = \frac{3}{2}u^*$ and $u^* = 0.364$ in $d = 3$ dimensions, given in Eq. (13.4) of Ref. [18]. Thus the renormalized tree approximation for the screening length in the semi-dilute limit is given by

$$\mathcal{Y}(\bar{L}_r, \bar{n}_r, u_{r,\mathrm{FP}}) \approx \mathcal{Y}_{\mathrm{tree}}(\bar{L}_r, \bar{n}_r, u_{r,\mathrm{FP}}) = \frac{1}{2a\,\bar{L}_r\,\bar{n_r}} \quad . \tag{4.32}$$

4.3 Choice of the noncritical manifold

Now the question arises how one should choose the value of λ and thus the noncritical manifold. The idea is that $\mu^{-1}\mathrm{e}^{\lambda}$ should be of the order of the smallest of the three mesoscopic length scales $\mathcal{R}_x$, ξ, and R in the system. Actually the manifold is chosen so that [18, 39]

$$\frac{\rho_0}{\bar{L}_r} + \zeta_0\,a\,\bar{n}_r\,\bar{L}_r + \frac{R_0}{\bar{R}_r^2} = 1 \quad , \tag{4.33}$$

where ρ_0, ζ_0, and R_0 are constants of order 1. This relation smoothly interpolates between the different limits where one of the length scales $\mathcal{R}_x$,

ξ, and R is much smaller than the others. In this case the value λ has to be chosen in such a way that the smallest of the renormalized length scales $\bar{L}_r$, $1/(a\bar{L}_r\bar{n}_r)$, and $\bar{R}_r$ of the system is of order 1. For example in a dilute polymer solution without particle one has $\bar{L}_r = \rho_0$. Thus Eq. (4.22) leads to $\mathrm{e}^{2\lambda} = (D_L L_r/\rho_0)^{2\nu}$, and Eqs. (4.26) and (4.27) lead to the relation

$$\frac{1}{2}\,(\mu\mathcal{R}_x)^2 \;=\; \rho_0^{1-2\nu}\,(D_L L_r)^{2\nu} \quad . \tag{4.34}$$

In the semi-dilute limit $\mathcal{S} \to \infty$ without particle λ is chosen such that $a\bar{n}_r\bar{L}_r = 1/\zeta_0$. Here Eqs. (4.22) and (4.23) lead in $d = 3$ dimensions to $\mathrm{e}^{\lambda} = (aD_L L_r n_r \zeta_0)^{-\nu/(3\nu-1)}$. The relation for ξ obtained from Eqs. (4.28) and (4.32) is thus

$$2\,(\mu\xi)^2 \;=\; \zeta_0\,(aD_L L_r n_r \zeta_0)^{-2\nu/(3\nu-1)} \quad . \tag{4.35}$$

Combining Eqs. (4.34) and (4.35), it follows that

$$\begin{aligned} \xi^2 \;&=\; \frac{\zeta_0}{2}\left(\frac{2\rho_0}{(a\rho_0\zeta_0)^{2\nu}}\right)^{1/(3\nu-1)} \left(\mathcal{R}_x^{1/\nu} n\right)^{-2\nu/(3\nu-1)} \\ &=\; \frac{\zeta_0}{2}\left(\frac{\rho_0}{(a\rho_0\zeta_0)^{2\nu}}\right)^{1/(3\nu-1)} \left(\mathcal{R}_g^{1/\nu} n\right)^{-2\nu/(3\nu-1)} , \end{aligned} \tag{4.36}$$

where in the last step the relation between $\mathcal{R}_g$ and $\mathcal{R}_x$ from Eq. (4.44) below was used. Eq. (4.36) relates the screening length in the semi-dilute limit to the monomer density which is proportional to $\mathcal{R}_x^{1/\nu} n$. Inserting the values (4.58), (4.61), (4.31) for ρ_0, ζ_0, a one finds for the universal amplitude $\xi^2 \cdot (\mathcal{R}_g^{1/\nu} n)^{2\nu/(3\nu-1)}$ in the present renormalized tree approximation the value 0.0148. The more precise one loop result 0.0098 which follows from Eqs.

(15.14), (15.15) and (19.32) of Ref. [18] is by only about 34 % smaller. Note that ξ_E^2 in Ref. [18] has to be identified with $3\xi^2$.

In the next sections the renormalized tree approximation for the free energy cost is derived in the special cases where one of the three terms on the left hand side of Eq. (4.33) is much smaller than the two others so that it drops out of the relation.

4.4 Large spheres

In the case that the radius of the imbedded sphere R is much larger than the typical polymer lengths $\mathcal{R}_x$, ξ the relation (4.33) simplifies to

$$\frac{\rho_0}{\bar{L}_r} + \zeta_0\, a\, \bar{n}_r\, \bar{L}_r \;=\; 1 \quad . \tag{4.37}$$

Here the left hand side is basically the inverse square of the dimensionless renormalized density correlation length, see Eq. (2.17), and interpolates between $\bar{L}_r = O(1)$ in the dilute limit and $\bar{L}_r/(a\bar{n}_r\bar{L}_r^2) = \bar{L}_r/\bar{\mathcal{S}} = O(1)$ in the semi-dilute limit, i.e. the length scale is set by the end-to-end distance and the screening length, respectively.

In section 2.7 I presented the Helfrich expansion for large spheres. It includes as leading contributions the osmotic pressure, the surface tension and the coefficient of spontaneous curvature which are all independent of R. From the flow equations (4.16)-(4.24) it follows that

$$\frac{\Pi}{nk_BT} \;=\; 1 + \mathcal{P}(n_r, L_r, u_r) \;=\; 1 + \mathcal{P}(\bar{n}_r, \bar{L}_r, u_{r,\mathrm{FP}}) \quad , \tag{4.38}$$

$$\frac{\sigma}{nk_BT} = \mu^{-1}\,\mathcal{Q}(n_r, L_r, u_r) = \mu^{-1}\,\mathrm{e}^{\lambda}\,\mathcal{Q}(\bar{n}_r, \bar{L}_r, u_{r,\mathrm{FP}}) \quad , \tag{4.39}$$

$$\frac{\kappa}{nk_BT} = \mu^{-2}\,\mathcal{T}(n_r, L_r, u_r) = \mu^{-2}\,\mathrm{e}^{2\lambda}\,\mathcal{T}(\bar{n}_r, \bar{L}_r, u_{r,\mathrm{FP}}) \quad . \tag{4.40}$$

Now one again can approximate the functions $\mathcal{P}$, $\mathcal{Q}$, $\mathcal{T}$ for the noncritical state by their tree-expressions

$$\mathcal{P}(\bar{n}_r, \bar{L}_r, u_{r,\mathrm{FP}}) \approx \mathcal{P}_{\mathrm{tree}}(\bar{n}_r, \bar{L}_r, u_{r,\mathrm{FP}}) = \frac{1}{2} a \bar{L}_r^2 \bar{n}_r \quad , \tag{4.41}$$

$$\mathcal{Q}(\bar{n}_r, \bar{L}_r, u_{r,\mathrm{FP}}) \approx \mathcal{Q}_{\mathbf{tree}}(\bar{n}_r, \bar{L}_r, u_{r,\mathrm{FP}}) = (2\bar{L}_r)^{1/2}\, g(a\bar{L}_r^2 \bar{n}_r) \quad , \tag{4.42}$$

$$\mathcal{T}(\bar{n}_r, \bar{L}_r, u_{r,\mathrm{FP}}) \approx \mathcal{T}_{\mathbf{tree}}(\bar{n}_r, \bar{L}_r, u_{r,\mathrm{FP}}) = 2\bar{L}_r\, h(a\bar{L}_r^2 \bar{n}_r) \quad , \tag{4.43}$$

where the functions g and h are the mean-field scaling functions from Eq. (3.37) and Fig. 3.14 and from Eq. (3.40) and Fig. 3.15. One expects from scaling arguments that the scaling functions $\Pi/(nk_BT)$, $\sigma/(nk_BT\mathcal{R}_x)$, and $\kappa/(nk_BT\mathcal{R}_x^2)$ in $d = 3$ depend only on the geometrical overlap

$$s \equiv n\mathcal{R}_g^3 \approx n(\mathcal{R}_x/\sqrt{2})^3 \equiv s_3^{(x)}/2\sqrt{2} \quad . \tag{4.44}$$

Here it was used that in three dimensions the mean square radius of gyration $\mathcal{R}_g^2 \equiv 3\mathcal{R}_{g,x}^2$ is equal to $\mathcal{R}_x^2/2$, to a very good approximation [17]. To get the scaling functions in the renormalized tree approximation for $d = 3$ one has to express the renormalized inter-chain overlap $\bar{\mathcal{S}}$ in Eq. (4.30) and the quantity $\mu^{-1}\mathrm{e}^{\lambda}\bar{L}_r^{1/2}/\mathcal{R}_x$ from the prefactors in Eqs. (4.38)-(4.40) in terms of the usual geometrical overlap s. For that purpose it is advantageous to use the first term in Eq. (4.37)

$$\frac{\rho_0}{\bar{L}_r} = v \tag{4.45}$$

as an intermediate variable [18] v. Note that λ drops out of the combination

$$(1-v)\,/\,v^{d\nu-1} = a\zeta_0\rho_0^{-d\nu+1} n_r (D_L L_r)^{d\nu} = a\zeta_0\rho_0^{-\frac{d}{2}+1} n(\mathcal{R}_x/\sqrt{2})^d \quad . \tag{4.46}$$

In the last step Eqs. (4.34) and (4.3) have been used. Inserting now $d = 3$ and Eq. (4.44) one finds the relation

$$(1-v)\,/\,v^{3\nu-1} \;=\; a\zeta_0\rho_0^{-1/2} s \tag{4.47}$$

between s and v which can be inverted numerically to yield $v = v(s)$. From Eq. (4.37) and the definition (4.45) of v it follows directly that

$$a\bar{L}_r^2 \bar{n}_r \;=\; \frac{\rho_0}{\zeta_0}\Big(\frac{1}{v} \,-\, 1\Big) \;. \tag{4.48}$$

Together with

$$2\bar{L}_r \;=\; \frac{2\rho_0}{v} \tag{4.49}$$

which follows from Eq. (4.45) one has obtained the functions $\mathcal{P}$, $\mathcal{Q}$, and $\mathcal{T}$ in Eqs. (4.41)-(4.43). For the surface tension in (4.39) and the coefficient of spontaneous curvature in (4.40) one still needs

$$\mu^{-1}\,\mathrm{e}^{\lambda} \;=\; \mu^{-1}\left(v\,\frac{D_L L_r}{\rho_0}\right)^{\nu} \;=\; v^{\nu}\,(2\,\rho_0)^{-1/2}\,\mathcal{R}_x \;, \tag{4.50}$$

where Eqs. (4.45), (4.22) and Eq. (4.34) have been used. Combining now all the results one finally arrives at

$$\frac{\Pi}{nk_BT} \;=\; 1 \,+\, \frac{1}{2}\,\frac{\rho_0}{\zeta_0}\Big(\frac{1}{v} \,-\, 1\Big) \;, \tag{4.51}$$

$$\frac{\sigma}{nk_BT} \;=\; \mathcal{R}_x\, v^{\nu-1/2}\, g\Big(\frac{\rho_0}{\zeta_0}\Big(\frac{1}{v} \,-\, 1\Big)\Big) \;, \tag{4.52}$$

and

$$\frac{\kappa}{nk_BT} = \mathcal{R}_x^2\, v^{2\nu-1}\, h\Big(\frac{\rho_0}{\zeta_0}\Big(\frac{1}{v} - 1\Big)\Big)\,. \tag{4.53}$$

In the case of small and large overlap one can invert Eq. (4.47) analytically to yield

$$\frac{\Pi}{nk_BT} \;\to\; \begin{cases} 1 + \frac{1}{2}a\rho_0^{1/2}s\,, & s \to 0 \\ \frac{1}{2}\frac{\rho_0}{\zeta_0}\Big(\frac{a\zeta_0 s}{\rho_0^{1/2}}\Big)^{1/(3\nu-1)}, & s \to \infty \end{cases} \tag{4.54}$$

for the osmotic pressure,

$$\frac{\sigma}{nk_BT\mathcal{R}_x} \;\to\; \begin{cases} \sqrt{\frac{2}{\pi}}\Big(1 + \Big[a\rho_0^{1/2}\lambda_1 - a\zeta_0\rho_0^{-1/2}\Big(\nu - \frac{1}{2}\Big)\Big]s\Big), & s \to 0 \\ \frac{2}{3}\Big(\frac{\rho_0}{\zeta_0}\Big)^{1/2}\Big(\frac{a\zeta_0 s}{\rho_0^{1/2}}\Big)^{\frac{1-\nu}{3\nu-1}}, & s \to \infty \end{cases} \tag{4.55}$$

for the surface tension, and

$$\frac{\kappa}{nk_BT\mathcal{R}_x^2} \to \begin{cases} \frac{1}{2}(1 + [2a\rho_0^{1/2}\lambda_2 - a\zeta_0\rho_0^{-1/2}(2\nu-1)]s)\,, & s \to 0 \\ \frac{1}{3}(4\ln 2 - 1)\,, & s \to \infty \end{cases} \tag{4.56}$$

for the coefficient of spontaneous curvature. Here the abbreviations λ_1, λ_2 from Eqs. (3.31), (3.32) were used. The exponents $\frac{1}{3\nu-1}$, $\frac{1-\nu}{3\nu-1}$, and $-\frac{2\nu-1}{3\nu-1}$ have the property that Π/k_BT, σ/k_BT, and κ/k_BT in the limit of strong overlap only depend on the monomer density, i.e. only on the combination $n\mathcal{R}_x^{1/\nu}$, and are proportional to ξ^{-3}, ξ^{-2}, and ξ^{-1}, respectively.

The values of the two constants ρ_0 and ζ_0 follow from comparing Eq. (4.54) with known amplitude ratios of the osmotic pressure [18]. For ρ one uses the fact that the interpenetration ratio, defined by

$$\psi^* \;=\; \frac{A_2}{(4\pi)^{3/2}\mathcal{R}_g^3}\;, \tag{4.57}$$

is a universal number, determined experimentally as $\psi^* \approx 0.245$. Here A_2 is the second virial coefficient of the osmotic pressure, see Eq. (2.43). Comparing with the small s behavior of Eq. (4.54) yields

$$\rho_0 \;=\; \frac{(4\pi)^3}{a^2}\,(\psi^*)^2 \;=\; 1.81\;\;. \tag{4.58}$$

The other constant ζ_0 follows from another known universal ratio given by [18]

$$\mathcal{A}_{\infty/2} \;=\; (\lim_{s\to\infty} s^{-1}[\tilde{\mathcal{P}}(s)]^{3\nu-1})/(\lim_{s\to 0} s^{-1}\tilde{\mathcal{P}}(s)) \;\approx\; 1.098\;\;, \tag{4.59}$$

where $\tilde{\mathcal{P}}(s) = -1 + \Pi/(nk_BT)$ is a scaling function of the osmotic pressure. Taking the limits from Eq. (4.54) one gets

$$\frac{a\,2^{1-3\nu}\,\rho_0^{3\nu-3/2}\,\zeta_0^{2-3\nu}}{(a/2)\sqrt{\rho_0}} \;=\; 1.098\;\;, \tag{4.60}$$

and thus

$$\zeta_0 \;=\; \frac{\rho_0}{1.098^{1/(3\nu-2)}\,2} \;=\; 1.34\;\;. \tag{4.61}$$

Fig. 4.1 shows the surface tension which follows from Eqs. (4.52) and (4.47). The limiting behavior for small and large overlap is numerically given by

$$\frac{\sigma}{nk_BT\mathcal{R}_x} \;\to\; (0.798[1+2.920\,s]\;,\;(5.034\,s)^{0.539})\;,\;\; s\;\to\;(0\,,\,\infty)\;. \tag{4.62}$$

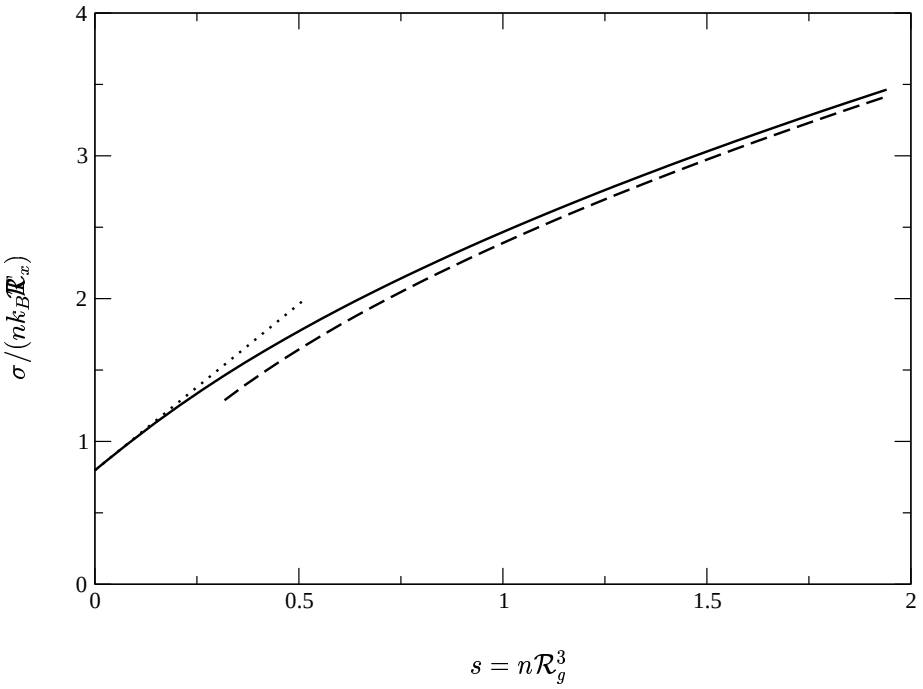

Figure 4.1: Scaling function of the surface tension in the renormalized tree approximation (Eqs. (4.52), (4.47)). The quantity s is the geometrical overlap in Eq. (4.44). The dotted and dashed lines show the asymptotic behavior for small and large s, respectively (compare Eq. (4.62)).

In Eq. (4.62) the leading contribution in the dilute limit equals the result for ideal chains. Actually in an ϵ-expansion one finds a small correction $0.798 \to 0.798\,(1-0.051\epsilon)$ due to monomer-monomer repulsion [7]. The value 5.034 of the universal amplitude in the semi-dilute limit is not too far from the extrapolation 6.203 to three dimensions of the leading contribution $4\sqrt{2}\pi^2\epsilon/9$ in the ϵ-expansion. The leading contribution near four dimensions follows from inserting the fixed point value (2.14) into the mean field expression (3.39) in the semi-dilute limit and using $\mathcal{R}_x = \sqrt{2}\mathcal{R}_g$.

Recently Louis *et al.* [41] used a combination of Monte Carlo simulations and scaling theories to calculate the surface tension. Fig. 4.2 shows a comparison between their result (solid line with open squares) and the present result from Fig. 4.1 (dashed line). There is good agreement between both curves. Only for large geometrical overlap there is a slight deviation. But nevertheless in this region the renormalized tree approximation is much closer to the simulation result than the leading contribution of the epsilon-expansion [41].

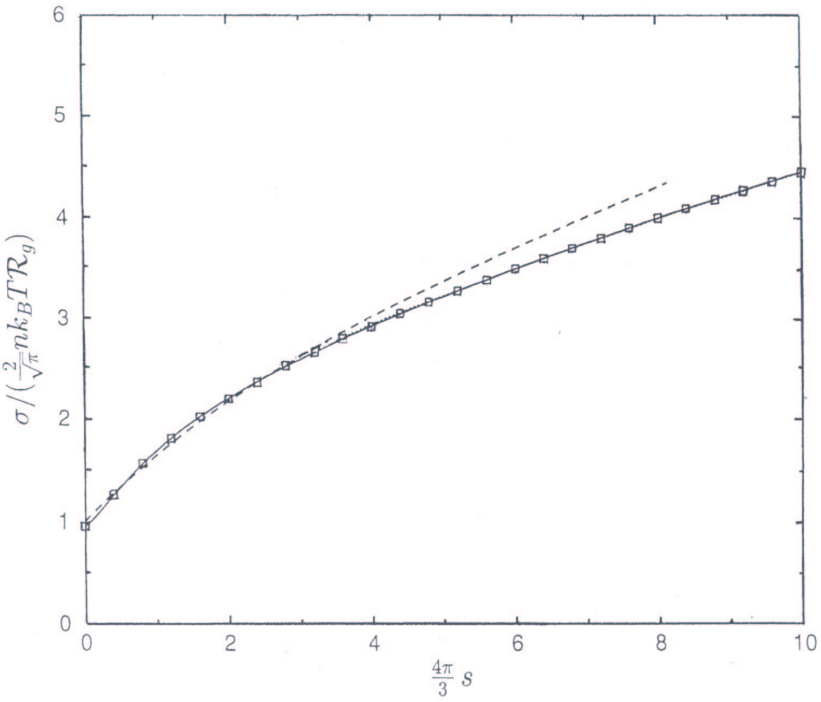

Figure 4.2: The surface tension devided by its value for ideal chains. The dashed line is the present result from the renormalized tree approximation as given by Fig. 4.1, the solid line with open squares is from Ref. [41] where this figure is taken from. Note the differences to Fig. 4.1 in the axes labels.

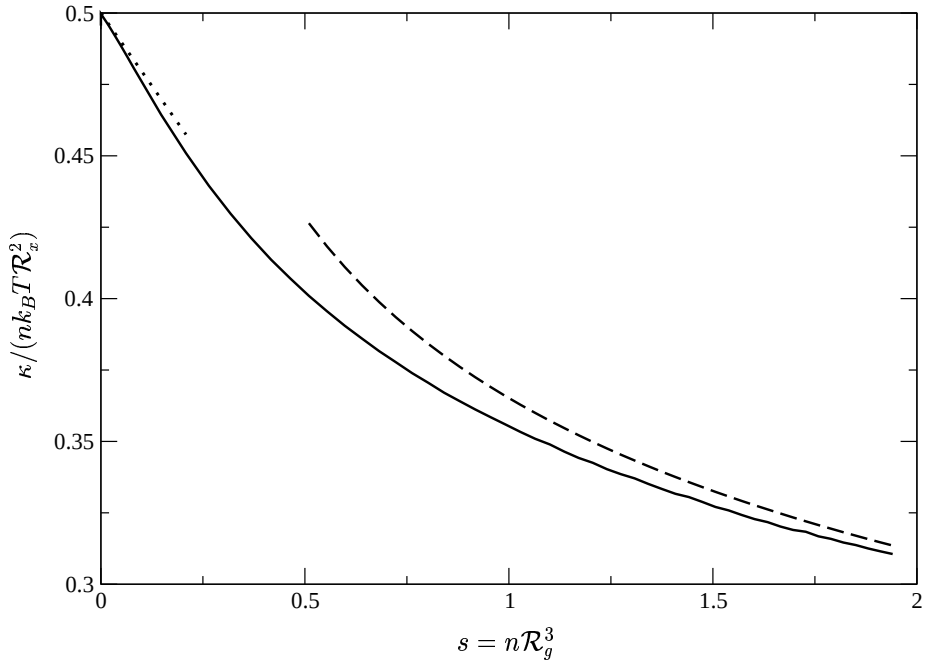

Figure 4.3: Scaling function of the coefficient of spontaneous curvature in the renormalized tree approximation (Eqs. (4.53), (4.47)). The dotted and dashed lines show the asymptotic behavior for small and large geometrical overlap s, respectively (compare Eq. (4.63)).

Fig. 4.3 shows the coefficient of spontaneous curvature which follows from Eqs. (4.53) and (4.47). In this case the limiting behavior for small and large overlap is given by

$$\frac{\kappa}{nk_BT\mathcal{R}_x^2} \to (\,0.5\,[1-0.402\,s\,]\,,\;(\,79.61\,s\,)^{-0.230}) \quad , \quad s \to (0\,,\,\infty)\,. \tag{4.63}$$

The mean-field result (Fig. 3.15) and the result from the renormalized tree approximation (Fig. 4.3) for the coefficient of spontaneous curvature are

qualitatively different. Note that the overlap dependence $s^{-(2\nu-1)/(d\nu-1)}$ for $s \to \infty$ leads to a constant in the mean-field approximation (with $\nu = 1/2$), while it leads to a power law decay in the renormalized tree approximation (with $\nu = 0.588$). Also the small overlap behavior is different since the sign of the linear contribution is different. The value 0.5 for $s = 0$ is an ideal chain result which is corrected in the ϵ-expansion by a factor $1 - 0.131\epsilon$ [7].

4.5 Free energy in the dilute limit

If the polymer solution is dilute, the second term in Eq. (4.33) vanishes, and thus the condition for the uncritical manifold becomes

$$\frac{\rho_0}{\bar{L}_r} + \frac{R_0}{\bar{R}_r^2} = 1 \quad . \tag{4.64}$$

The renormalized expression for the free energy cost $F/(k_BT)$ is given by Eq. (4.12), and the function $\mathcal{F}$ for the noncritical state in Eq. (4.16) can be approximated by the tree result

$$\begin{aligned} \mathcal{F}(\bar{n}_r, \bar{L}_r, \bar{R}_r, u_{r,\mathrm{FP}}) &\approx \mathcal{F}_{\mathrm{tree}}(\bar{n}_r, \bar{L}_r, \bar{R}_r, u_{r,\mathrm{FP}}) \\ &= 2\pi \bar{n}_r \bar{R}_r^3 \left(\frac{2}{3} + 2\sqrt{\frac{2}{\pi}} \sqrt{\frac{2\bar{L}_r}{\bar{R}_r^2}} + \frac{2\bar{L}_r}{\bar{R}_r^2} \right) \quad , \end{aligned} \tag{4.65}$$

compare Eq. (1.8). Since $\bar{n}_r \bar{R}_r^3 = nR^3$, one has only to determine $2\bar{L}_r/\bar{R}_r^2$ as a function of R and $\mathcal{R}_x$. For that purpose I use the same intermediate variable $v = \rho_0/\bar{L}_r$ as in the section before, but now the relation independent of λ is

$$(1-v)/v^{2\nu} \;=\; R_0/R_r^2\,\rho_0^{-2\nu}(D_L L_r)^{2\nu} \;=\; \frac{R_0}{2\rho_0}\,\frac{\mathcal{R}_x^2}{R^2}\,, \tag{4.66}$$

where Eq. (4.34) was used in the last step. From this equation one gets $v = v(\mathcal{R}_x/R)$. The ratio in Eq. (4.65) can be expressed in terms of v as

$$\frac{2\bar{L}_r}{\bar{R}_r^2} \;=\; \frac{2\rho_0}{R_0}\left(\frac{1}{v}-1\right) \tag{4.67}$$

which can be inserted into Eq. (4.65) to yield the full result. In the limit of small spheres which is equivalent with $v \to 0$ an inversion of Eq. (4.66) yields

$$v^{-2\nu} \;\approx\; \frac{R_0}{2\rho_0}\,\frac{\mathcal{R}_x^2}{R^2} \tag{4.68}$$

and thus

$$\frac{F}{k_B T} \longrightarrow 2\pi\left(\frac{2\rho_0}{R_0}\right)^{1-\frac{1}{2\nu}}\; R^{3-\frac{1}{\nu}}\,\mathcal{R}_x^{\frac{1}{\nu}}\,n \tag{4.69}$$

for $R \ll \mathcal{R}_x$. Eq. (4.69) displays the well known power law behavior of the free energy cost for chains with excluded volume interaction. The amplitude can be fitted to the amplitude in Ref. [7] that is calculated within an ϵ-expansion. This leads to

$$A \;=\; 9.82 \;=\; 2\pi\left(\frac{3.62}{R_0}\right)^{0.15}\,, \tag{4.70}$$

where the values $\nu = 0.588$ and $\rho_0 = 1.81$ have been inserted. Calculating R_0 from this condition, one finds

$$R_0 = 0.18\,. \tag{4.71}$$

In the opposite limit of large spheres, i.e. $v \to 1$, it is interesting to consider the leading and the next to leading order term in an expansion in powers of $\mathcal{R}_x/R$. Setting

$$x^2 = \frac{R_0}{2\rho_0}\frac{\mathcal{R}_x^2}{R^2} \quad , \quad y^2 = \frac{R_0}{2\rho_0}\frac{2\bar{L}_r}{\bar{R}_r^2} \quad , \tag{4.72}$$

Eqs. (4.66) and (4.67) lead to

$$x \;=\; y(1+y^2)^{\nu-1/2} \;\approx\; y + (\nu - 1/2)y^3 + O(y^5) \tag{4.73}$$

which yields

$$y \;\approx\; x - (\nu - 1/2)x^3 + O(x^5) \tag{4.74}$$

or reexpressed in the original variables

$$\sqrt{\frac{2\bar{L}_r}{\bar{R}_r^2}} \;=\; \frac{\mathcal{R}_x}{R}\left(1 - (\nu - 1/2)\frac{R_0}{2\rho_0}\frac{\mathcal{R}_x^2}{R^2}\right) + O\left((\mathcal{R}_x/R)^5\right) \quad . \tag{4.75}$$

Substituting this result into Eq. (4.65), one finds for the free energy cost in the dilute limit

$$\frac{F}{k_B T} \longrightarrow 4\pi n R^3 \left(\frac{1}{3} + \sqrt{\frac{2}{\pi}}\frac{\mathcal{R}_x}{R} + \frac{1}{2}\frac{\mathcal{R}_x^2}{R^2} - \sqrt{\frac{2}{\pi}}(\nu - 1/2)\frac{R_0}{2\rho_0}\frac{\mathcal{R}_x^3}{R^3} + ...\right) \tag{4.76}$$

for $R \gg \mathcal{R}_x$. While the first three terms in Eq. (4.76) reproduce just the mean-field expressions and could have been calculated also from the results in Sec. 4.5 in the limit $s \to 0$, the R.G. flow generates another term in the free energy that is independent of R and corresponds to a combination of bending rigidities. This behavior should be compared with the ϵ-expansion results in Ref. [7]. The corrections from the ϵ-expansion for the second and

third term are given in the previous section and are of the order of a few percent. The bending rigidity term that occurs only for chains with excluded volume interaction is given by [7]

$$\frac{\tilde{\kappa}}{k_B T} \approx -0.0141\,\epsilon\, n\, \mathcal{R}_x^3 \tag{4.77}$$

in the ϵ-expansion. In three dimensions, where ϵ is equal to 1, this has to be compared with the last term of Eq. (4.76). Note that both contributions have the same sign. They would be equal for a value $R_0 = 0.73$. This value is four times larger than the value in Eq. (4.71), estimated from the fit to the small sphere amplitude. Since the parameter R_0 determines the region where R becomes the shortest length scale in the system, one should calculate it in the small sphere limit. Therefore I choose R_0 from the small sphere fit in Eq. (4.71).

Fig. 4.4 shows the scaling function for the free energy cost in the dilute limit, obtained in renormalized tree approximation. Note that this scaling function is defined in a different way than the one in Fig. 3.12 and that it is shown as a function of $1/\rho$. The limits for small and large particles are represented very well.

4.6 Free energy in the semi-dilute limit

In contrast to the dilute limit, there is no analytical mean-field result for the free energy cost in the semi-dilute limit. To proceed I have numerically calculated the free energy up to $\mathcal{S} = 64$, where the ratio $\mathcal{R}_x/\xi$ in mean-field

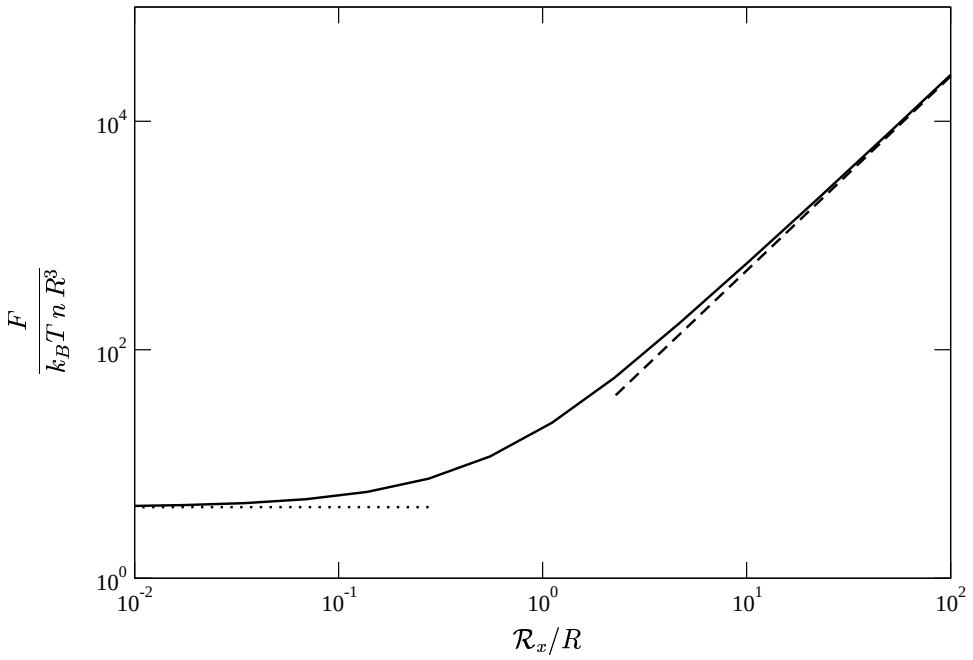

Figure 4.4: Scaling function for the free energy cost to immerse a spherical particle into a dilute polymer solution in the renormalized tree approximation versus the inverse size ratio $1/\rho$. The dotted and dashed line give the limits of large and small particles.

approximation is equal to 16. Thus one is at least in a region where $\mathcal{R}_x \gg \xi$ holds approximately. Right in the semi-dilute limit the noncritical manifold is chosen such that

$$\zeta_0\, a\, \bar{n}_r\, \bar{L}_r \;+\; \frac{R_0}{\bar{R}_r^2} \;=\; 1\;, \tag{4.78}$$

compare Eq. (4.33). The free energy cost in the noncritical state can be approximated by the tree expression which is given by

$$\begin{aligned} \mathcal{F}(\bar{n}_r, \bar{L}_r, \bar{R}_r, u_{r,\mathrm{FP}}) &\approx \mathcal{F}_{\mathrm{tree}}(\bar{n}_r, \bar{L}_r, \bar{R}_r, u_{r,\mathrm{FP}}) \\ &= 4\pi \bar{n}_r \bar{R}_r \bar{L}_r \, \tilde{f}(\bar{R}_r \sqrt{2a\bar{n}_r \bar{L}_r}) \end{aligned} \tag{4.79}$$

with the numerically obtained scaling function $\tilde{f}$, compare Eq. (3.34) and Fig. 3.13. Like in the two sections before an intermediate variable is introduced. This time I choose

$$w = \frac{R_0}{\bar{R}_r^2} \ . \tag{4.80}$$

The combination

$$\frac{(1-w)^{2\nu}}{w^{3\nu-1}} = (a\zeta_0 n_r D_L L_r)^{2\nu} \left(\frac{R_r^2}{R_0}\right)^{3\nu-1} = \left(\frac{\zeta_0}{2R_0}\frac{R^2}{\xi^2}\right)^{3\nu-1} \tag{4.81}$$

is independent of λ and yields $w = w(R/\xi)$. In the last step Eq. (4.35) was used. The combinations of renormalized variables that occur in Eq. (4.79) follow from Eqs. (4.78) and (4.80) as

$$\bar{n}_r \bar{R}_r \bar{L}_r = \frac{\sqrt{R_0}}{a\zeta_0} \frac{1-w}{\sqrt{w}} \tag{4.82}$$

and

$$\bar{R}_r \sqrt{2a\bar{n}_r \bar{L}_r} = \sqrt{\frac{2R_0}{\zeta_0}\left(\frac{1}{w} - 1\right)} \ . \tag{4.83}$$

In the limit of small spheres $R \ll \xi$ which is equivalent with $w \to 1$ the scaling function $\tilde{f}$ reaches the value 1, see Fig. 3.13, and thus the free energy cost is given by the prefactor in Eq. (4.79) with the result

$$\begin{aligned} \frac{F}{k_B T} &\rightarrow 4\pi \bar{n}_r \bar{R}_r \bar{L}_r \approx 4\pi \frac{\sqrt{R_0}}{a\zeta_0}(1-w) \\ &\approx 4\pi \frac{\sqrt{R_0}}{a\zeta_0}\left(\frac{\zeta_0}{2R_0}\right)^{(3\nu-1)/(2\nu)}\left(\frac{R}{\xi}\right)^{3-1/\nu} , \end{aligned} \tag{4.84}$$

where Eq. (4.81) has been used in the last step. In previous works, see e.g. Ref. [7], it was pointed out that the free energy cost for small spheres should be independent of the overlap and only a function of the bulk monomer density $nN \sim n\mathcal{R}_x^{1/\nu}$. At first sight the right hand side does not look like the result for the dilute limit given by Eq. (4.69). Nevertheless both expressions are the same. Substituting Eq. (4.36) into Eq. (4.84) one gets the same overlap independent result (4.69) as in the dilute limit.

For large spheres $R \gg \xi$, w goes to zero and the argument (4.83) of the scaling function equals R/ξ. The prefactor (4.82) in this limit is given by

$$4\pi \bar{n}_r \bar{R}_r \bar{L}_r = 4\pi \frac{1}{a\sqrt{2\zeta_0}} \frac{R}{\xi} . \tag{4.85}$$

Since the mean-field scaling function is for large arguments given by $\tilde{f}(x) \approx \frac{1}{12}x^2$, compare Eq. (3.36), one obtains for the large sphere limit the expression

$$\frac{F}{k_B T} \rightarrow \frac{\pi}{3a\sqrt{2\zeta_0}} \frac{R^3}{\xi^3} \tag{4.86}$$

which is consistent with the small curvature expansion in Eq. (2.61) and the semi-dilute limit of the osmotic pressure from Eq. (4.54), if Eq. (4.36) is used. The scaling function for the free energy cost in the semi-dilute limit is shown in Fig. 4.5. In contrast to Figs. 3.12 and 4.4 there is no trivial

n-dependence, i.e. no prefactor proportional to n. The free energy depends on the monomer density only via the screening length ξ.

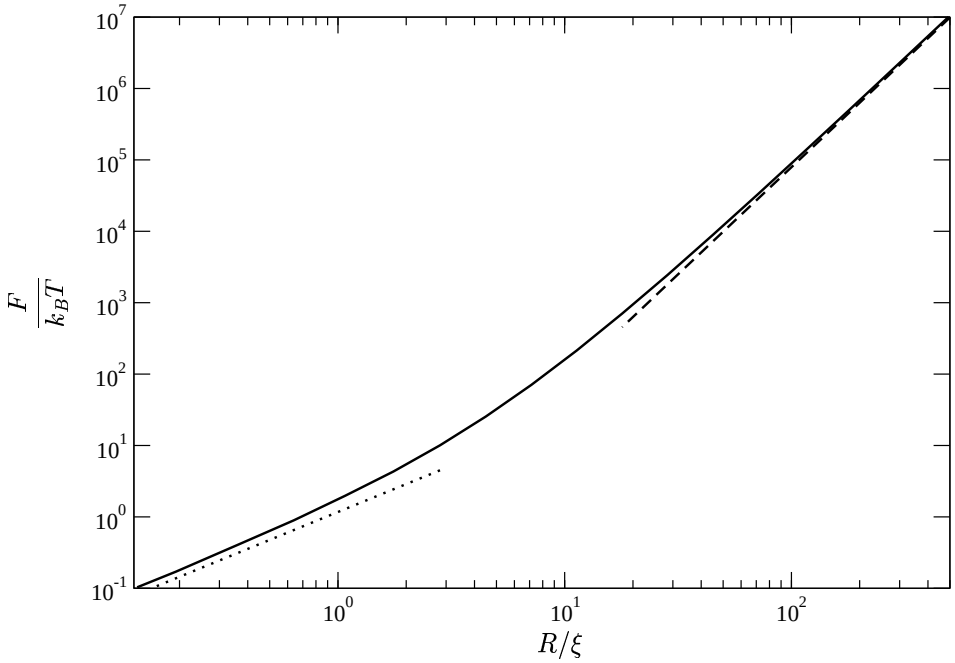

Figure 4.5: The free energy cost to immerse a spherical particle into a semi-dilute polymer solution in the renormalized tree approximation versus R/ξ. The dotted and dashed line give the limits of small and large particles, respectively.

Chapter 5

Ellipsoidal particle

The aim of this chapter is to study ellipsoids as an example of anisotropic particles. For simplicity only ellipsoids of revolution are considered which arise by rotating an ellipse around its major or minor axis. Again one has to solve the differential equation for the 'susceptibility' χ which is the Laplace transform of the end density, compare section 2.5, but now for the outer space $\mathcal{U}_E$ of the ellipsoid. Because of the lower symmetry even the mean-field problem is not an effective one-dimensional one. Therefore it is much more complicated than the problem of the generalized cylinder, and only ideal chains are considered. Nevertheless this is the first step towards an understanding of anisotropic particles in a dilute polymer solution. The boundary value problem that has to be solved takes the form

$$\begin{cases} (-\Delta + t)\,\chi(t;\mathbf{r}) &= 1 \quad , \text{ for } \quad \mathbf{r} \in \mathcal{U}_E \\ \chi(t;\mathbf{r_S}) &= 0 \quad , \text{ for every surface point } \mathbf{r}_S \quad , \end{cases} \tag{5.1}$$

where for simplicity I omitted the superscript [0]. The best way to handle

this problem mathematically is to introduce spheroidal coordinates and to calculate the quantities of interest from the Green's function of the wave equation. It is possible to check the results in special cases, where the shape of the ellipsoid is close to a sphere, a cylinder, or a plate. For small particles an anisotropic version of the 'small-radius expansion' is tested and found to work.

5.1 Spheroidal coordinates

The prolate and oblate spheroidal coordinates are the appropriate coordinates for an ellipsoid of revolution, where the axis of revolution is the major or minor axis, respectively, of the two-dimensional ellipse. The introduction of the coordinates follows Ref. [45].

The relation between the prolate spheroidal coordinates, shown in Fig. 5.1, and the Cartesian coordinates is given by

$$x = \frac{f}{2}\,[(1-\eta^2)(\xi^2-1)]^{\frac{1}{2}}\,\cos\phi,\quad y = \frac{f}{2}[(1-\eta^2)(\xi^2-1)]^{\frac{1}{2}}\,\sin\phi,\quad z = \frac{f}{2}\,\eta\,\xi \tag{5.2}$$

with

$$-1 \le \eta \le 1,\quad 1 \le \xi < \infty,\quad 0 \le \phi \le 2\pi\,. \tag{5.3}$$

Here the z-axis is taken as the axis of revolution. The surface $\xi = constant > 1$ is an elongated (prolate) ellipsoid of revolution with the major and minor axis lengths

$$2a \;=\; f\,\xi,\quad 2b \;=\; f\,\sqrt{\xi^2-1}\,. \tag{5.4}$$

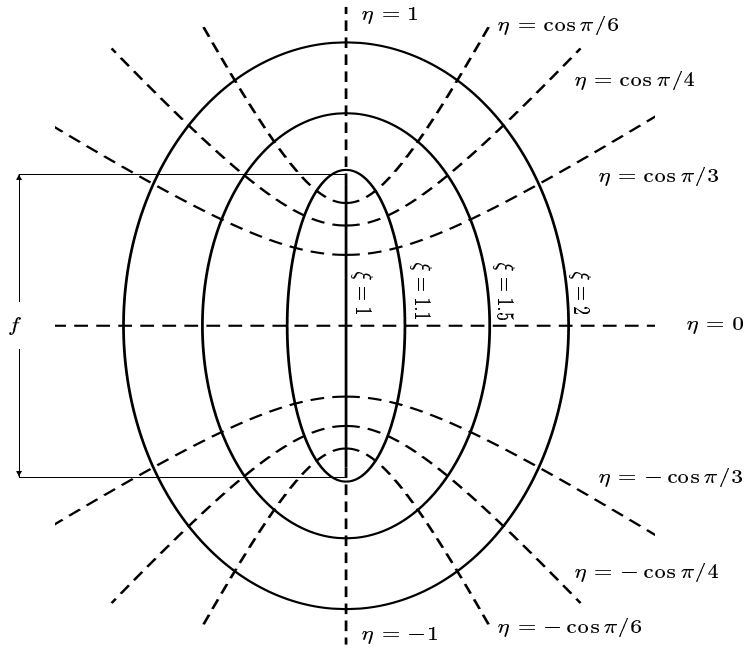

Figure 5.1: The prolate spheroidal coordinates. The vertical axis is the axis of revolution.

The degenerate surface $\xi = 1$ is an infinitely thin needle which extends along the z-axis from $z = -f/2$ to $z = f/2$. The surface $|\eta| = constant < 1$ is a hyperboloid of revolution. The cases $\eta = 0$ and $|\eta| = 1$ yield the xy-plane and the part of the z-axis with $|z| > f/2$, respectively. ϕ denotes the azimuthal angle, and because of the cylindrical symmetry $\chi(t; \mathbf{r})$ should not depend on ϕ. The oblate spheroidal coordinates, illustrated in Fig. 5.2, are related to the cartesian coordinates by

$$x = \frac{f}{2}\left[(1-\eta^2)(\xi^2+1)\right]^{\frac{1}{2}} \cos\phi, \quad y = \frac{f}{2}\left[(1-\eta^2)(\xi^2+1)\right]^{\frac{1}{2}} \sin\phi, \quad z = \frac{f}{2}\,\eta\,\xi \tag{5.5}$$

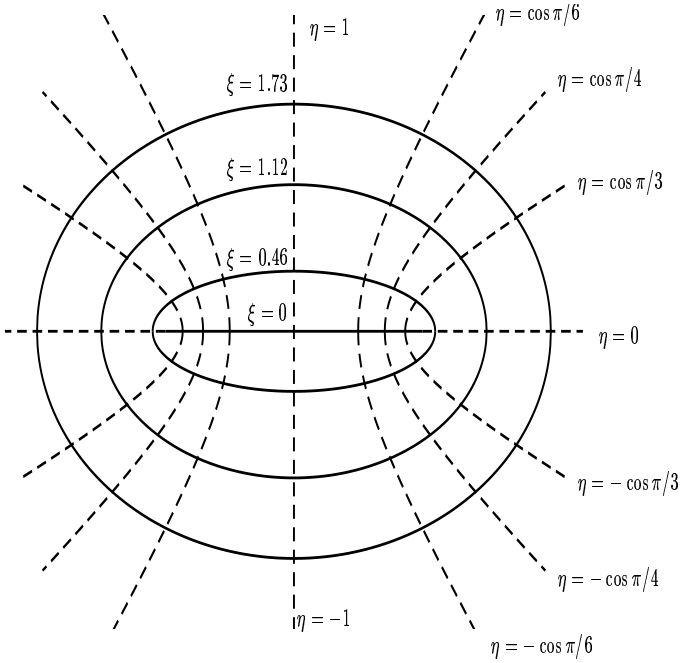

Figure 5.2: The oblate spheroidal coordinates. Again the vertical axis is the axis of revolution.

with

$$-1 \leq \eta \leq 1, \;\; 0 \leq \xi < \infty, \;\; 0 \leq \phi \leq 2\pi \; , \tag{5.6}$$

and again the z-axis is the axis of revolution. Here the surface $\xi = constant > 0$ is a flattened (oblate) ellipsoid of revolution with major and minor axis

$$2a \; = \; f\sqrt{\xi^2+1}, \quad 2b \; = \; f\,\xi \, . \tag{5.7}$$

The limiting case $\xi = 0$ represents a circular disk in the xy-plane of radius $a = f/2$ while the surface $|\eta| = 1$ is the z-axis.

Both the prolate and oblate spheroidal coordinate systems are systems of orthogonal curvilinear coordinates and in each case the coordinates η, ξ, ϕ form a right-handed system.

There are some limits where the ellipsoid reduces to a geometry of higher symmetry. First of all in the limit $f \to 0$ with $R = \frac{f}{2}\xi$ kept fixed the ellipsoid becomes a sphere with radius R. For an elongated ellipsoid of revolution the case $b = \frac{f}{2}\sqrt{\xi^2 - 1}$ fixed and $f \to \infty$ describes a cylinder of infinite length with radius b. For the flattened ellipsoid the case $b = \frac{f}{2}\xi$ fixed and $f \to \infty$ leads to a plate of thickness $2b$. As mentioned above, in the prolate case the limit $\xi \searrow 1$ with arbitrary f leads to a 'needle' of length f placed on the z-axis, while the case $\xi \searrow 0$ with arbitrary f in the oblate case gives a circular disk of radius $f/2$ in the xy-plane.

5.2 The differential equation

In both the prolate and oblate spheroidal coordinates is the wave equation

$$(\Delta + k^2)\,\psi \;=\; 0 \tag{5.8}$$

separable. Thus solutions to Eq. (5.8) may be obtained in the form of the so called Lamé products [45]

$$\psi_{m;n} \;=\; S_{m;n}(c,\eta) R_{m;n}(c,\xi) \exp(\pm i m \phi) \tag{5.9}$$

for the prolate case and

$$\psi_{m;n} \;=\; S_{m;n}(-ic,\eta) R_{m;n}(-ic,i\xi) \exp(\pm i m \phi) \tag{5.10}$$

for the oblate case, where

$$c = \frac{1}{2} f k \,. \tag{5.11}$$

Due to the cylindrical symmetry of χ only solutions independent of ϕ are of interest, which means that only Lamé products with $m = 0$ can contribute. Then the differential equations for the angle function $S_n := S_{0;n}$ and the radial function $R_n := R_{0;n}$ are given by

$$\frac{d}{d\eta}\left[(1-\eta^2)\frac{d}{d\eta}S_n(c,\eta)\right] + \left[\lambda_n - c^2\eta^2\right] S_n(c,\eta) = 0 \tag{5.12}$$

and

$$\frac{d}{d\xi}\left[(\xi^2-1)\frac{d}{d\xi}R_n(c,\eta)\right] - \left[\lambda_n - c^2\xi^2\right] R_n(c,\eta) = 0\,. \tag{5.13}$$

The separation constants $\lambda_n := \lambda_{0;n}$ are the same in both equations and depend only on c. The equations for the oblate case can be obtained by the transformation

$$\xi \to i\xi, \quad , \quad c \to -ic \quad , \tag{5.14}$$

compare Eq. (5.10). Thus I derive the solution only for prolate ellipsoids. The solution for the oblate case follows then by the transformation in Eq. (5.14). For each of the two differential equations (5.12) and (5.13) there exist two independent solutions called the angle or radial functions of the first and second kind. Here we need only angle functions of the first kind because the functions of the second kind diverge in the outer space of the ellipsoid at $\eta = \pm 1$. The angle functions of the first kind can be represented by an infinite sum over Legendre polynomials

$$S_n(c,\eta) = \sum_{r=0,1}^{\infty}{}' d_r^n(c) P_r(\eta) \quad , \tag{5.15}$$

where here and in the sequel the prime over the summation sign indicates that the summation is over only even values of r if n is even, and over only odd values of r if n is odd. The coefficients d_r^n follow from a recursion formula given in Appendix C, and the c-dependence is a dependence on c^2. Thus they are real also in the oblate case.

For the radial part one requires functions both of the first and of the second kind which can be represented by infinite sums over spherical Bessel or Neumann functions, respectively:

$$R_n^{(1)}(c,\xi) \;=\; \frac{1}{\sum\limits_{r=0,1}^{\infty\ \prime} d_r^n(c)} \sum_{r=0,1}^{\infty\ \prime} i^{r-n} d_r^n(c) j_r(c\xi)\;, \tag{5.16}$$

$$R_n^{(2)}(c,\xi) \;=\; \frac{1}{\sum\limits_{r=0,1}^{\infty\ \prime} d_r^n(c)} \sum_{r=0,1}^{\infty\ \prime} i^{r-n} d_r^n(c) n_r(c\xi)\;. \tag{5.17}$$

An important linear combination of both that will be used to write down the solution in the simplest form is the so called radial function of the third kind, given by

$$R_n^{(3)}(c,\xi) \;=\; R_n^{(1)}(c,\xi) + i\, R_n^{(2)}(c,\xi). \tag{5.18}$$

From this set of functions one can construct the Green's function of the wave equation that satisfies

$$(\Delta + k^2)\, G(\mathbf{r},\mathbf{r}') \;=\; -\delta(\mathbf{r}-\mathbf{r}') \tag{5.19}$$

and the boundary condition

$$G(\mathbf{r},\mathbf{r}') \;=\; \mathbf{0} \;\text{ for }\; \xi \;=\; \xi_{\mathbf{0}} \;\text{ or }\; \xi' \;=\; \xi_{\mathbf{0}} \;\;, \tag{5.20}$$

i.e. for $\mathbf{r}$ or $\mathbf{r}'$ on the surface of the ellipsoidal particle with major axis $2a_0$ and minor axis $2b_0$. It is given by [45]

$$G(\eta,\xi,\phi;\eta',\xi',\phi') = \frac{ik}{2\pi}\sum_{m=0}^{\infty}\sum_{n=m}^{\infty}\frac{1}{N_{m;n}(c)}\mathrm{e}^{im(\phi-\phi')}S_{m;n}(c,\eta)S_{m;n}(c,\eta')\cdot$$

$$\cdot\begin{cases} R^{(1)}_{m;n}(c,\xi)R^{(3)}_{m;n}(c,\xi') - \dfrac{R^{(1)}_{m;n}(c,\xi_0)}{R^{(3)}_{m;n}(c,\xi_0)}R^{(3)}_{m;n}(c,\xi)R^{(3)}_{m;n}(c,\xi'), & \xi<\xi' \\ R^{(1)}_{m;n}(c,\xi')R^{(3)}_{m;n}(c,\xi) - \dfrac{R^{(1)}_{m;n}(c,\xi_0)}{R^{(3)}_{m;n}(c,\xi_0)}R^{(3)}_{m;n}(c,\xi)R^{(3)}_{m;n}(c,\xi'), & \xi>\xi' \;, \end{cases} \tag{5.21}$$

where

$$N_{m;n}(c) \;=\; 2\sum_{r=0,1}^{\infty}{}'\frac{(r+2m)!(d_r^{m;n})^2}{(2r+2m+1)r!} \tag{5.22}$$

is a normalization factor.

5.3 End density

From the Green's function, given by Eq.(5.21), one can directly calculate the solution of Eq. (5.1) by setting $k \to i\sqrt{t}$ and integrating the function G with respect to the unprimed variables. This leads to

$$\begin{aligned}\chi(t;\mathbf{r}') &= \int d\mathbf{r} G(\mathbf{r},\mathbf{r}')|_{\mathbf{k}=\mathbf{i}\sqrt{\mathbf{t}}} \\ &= \int_0^{2\pi} d\phi \int_{-1}^{1} d\eta \int_{\xi_0}^{\infty} d\xi f^3(\xi^2-\eta^2) G(\eta,\xi,\phi;\eta',\xi',\phi') \\ &= \frac{1}{t}\left\{1 - \sum_{l=0}^{\infty} \frac{2d_0^{2l}(i\sqrt{t}f)}{N_{2l}(i\sqrt{t}f)} S_{2l}(i\sqrt{t}f,\eta) \frac{R_{2l}^{(3)}(i\sqrt{t}f,\xi)}{R_{2l}^{(3)}(i\sqrt{t}f,\xi_0)}\right\}. \quad (5.23)\end{aligned}$$

After the integration there remain only terms with $m = 0$ and even values of n. These are independent of ϕ and even in η in agreement with the symmetry requirements of χ. In the limit $r \to \infty$ which corresponds to $\xi \to \infty$ the function χ reaches its $\mathbf{r}$-independent bulk value $1/t$ because $R_{2l}^{(3)}(i\sqrt{t}f,\xi)$ vanishes exponentially, compare Eq. (C.10). Details of the integration can be found in Appendix C.

By inverting the Laplace transform one gets the end density [1]

$$\mathcal{E}(\mathbf{r}) = \frac{1}{2\pi i}\int_\gamma dt\, e^{Lt}\chi(t;\mathbf{r}) \ . \quad (5.24)$$

Results for the end density as a function of the distance r from the center of the ellipsoid in the prolate and oblate case for various values of η are shown in Figs. 5.3 and 5.4. The major and minor halfaxes have been chosen as $a_0 = 2\sqrt{L} \equiv 2\mathcal{R}_g$ and $b_0 = \sqrt{L} \equiv \mathcal{R}_g$ with $\mathcal{R}_g$ the radius of gyration of the polymer. As expected the depletion zone increases with decreasing curvature. However, the different end density profiles do not cross, and thus the end density at a certain distance $r > a_0$ from the ellipsoid is an increasing (decreasing) function of η in the prolate (oblate) case if one varies η from zero to one. For small ellipsoids this can be seen directly from the small ellipsoid

[1] Compare Eq. (2.54) for $\mathcal{S} = 0$.

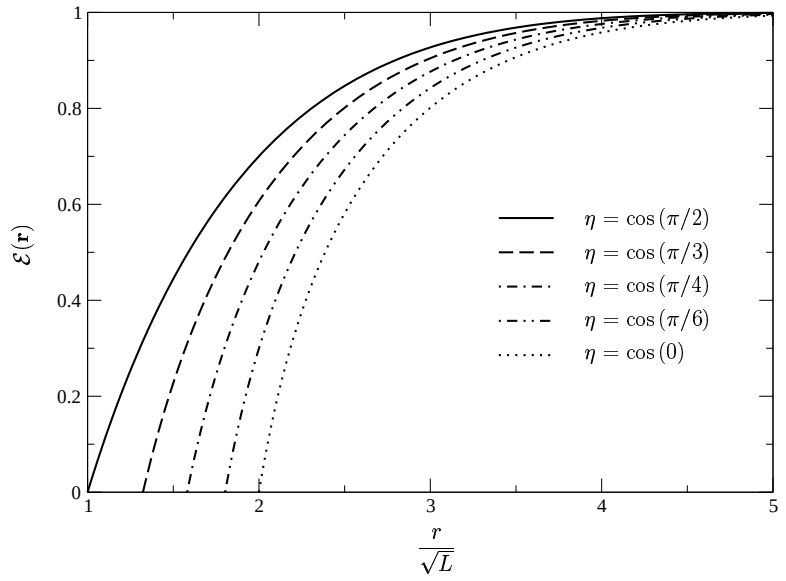

Figure 5.3: Density of chain ends versus the scaled distance from the center of a prolate ellipsoid. The halfaxes are given by $a_0 = 2\sqrt{L}$ and $b_0 = \sqrt{L}$.

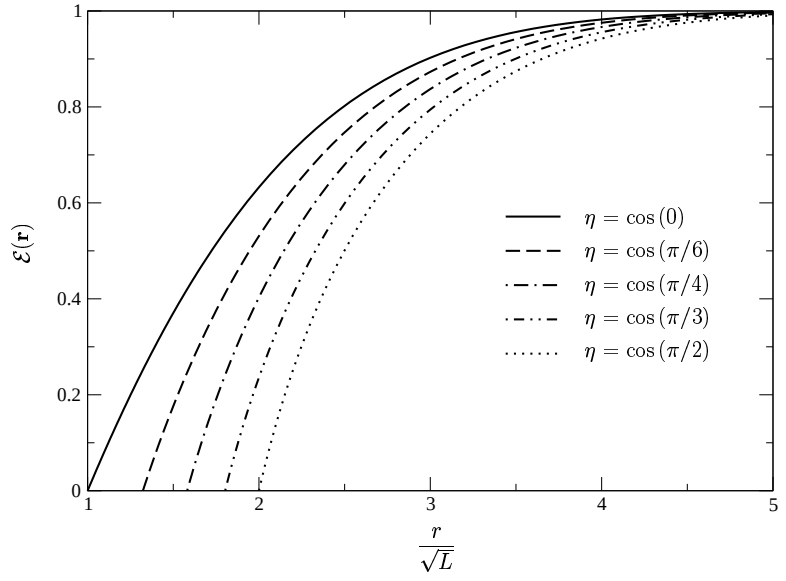

Figure 5.4: Density of chain ends versus the scaled distance from the center of an oblate ellipsoid. Again the halfaxes are given by $a_0 = 2\sqrt{L}$ and $b_0 = \sqrt{L}$.

expansion which is discussed in Sec. 5.4 below. Note that the depletion near the oblate ellipsoid is larger than near the prolate ellipsoid. This can be understood, since for given major and minor axis the volume and the surface area of an oblate ellipsoid are larger than those of a prolate ellipsoid.

In Figs. 5.3 and 5.4 the length of the major and minor axis of the ellipsoid were kept fixed, while the 'angle' η was varied. Now one is also interested in analyzing the dependence of the end density on the interfocal distance f. In order to compare with known results from an embedded sphere, cylinder or plate, I consider only the end density along (perpendicular to) the z-axis in the oblate (prolate) case. The length of the minor axis is fixed to $2b_0 = \mathcal{R}_g$ and the interfocal distance f varies from small to large values.

In the limit $f \searrow 0$ the sum in Eq. (5.23) reduces to a single term because the coefficients d_0^{2l} in this case equal the Kronecker-delta δ_{0l}, see Appendix C for details. Also the sums in the definition of the angular function S_n and the radial functions $R_n^{(i)}$ reduce to the first terms with $r = 0$, while the normalization factor N_{2l} becomes 2. Therefore one obtains in the sphere-limit

$$\begin{aligned}
\chi(t;\mathbf{r}) &\rightarrow \frac{1}{t}\left\{1 - \frac{j_0(i\sqrt{t}f\xi) + in_0(i\sqrt{t}f\xi)}{j_0(i\sqrt{t}f\xi_0) + in_0(i\sqrt{t}f\xi_0)}\right\} \\
&= \frac{1}{t}\left\{1 - \frac{\xi_0}{\xi}\frac{\sinh(\sqrt{t}f\xi) - \cosh(\sqrt{t}f\xi)}{\sinh(\sqrt{t}f\xi_0) - \cosh(\sqrt{t}f\xi_0)}\right\} \\
&\rightarrow \frac{1}{t}\left\{1 - \frac{b_0}{r}\mathrm{e}^{-\sqrt{t}(r-b_0)}\right\} \qquad (5.25)
\end{aligned}$$

which indeed is the well known expression for a sphere of radius b_0 imbedded in a solution of ideal chains [22, 7].

The limit of an infinitely long cylinder results from a prolate ellipsoid

by fixing the length of the short halfaxis b_0 and letting f go to infinity. It follows from Eq.(1) in chapter 3.91 of Ref. [46] that the corresponding limit of the radial function is apart from some prefactor a Hankel function of order zero, independent of the index $2l$, and therefore it can be taken out of the summation to yield

$$\begin{aligned}
\chi(t;\mathbf{r}) &\rightarrow \frac{1}{t}\left\{1-\sqrt{\frac{\xi_0}{\xi}}\frac{H_0^{(1)}(i\sqrt{t}f\sqrt{\xi^2-1})}{H_0^{(1)}(i\sqrt{t}f\sqrt{\xi_0^2-1})}\right\}\sum_{l=0}^{\infty}\frac{2d_0^{2l}}{N_{2l}}(-1)^l S_{2l}(i\sqrt{t}f,0) \\
&\rightarrow \frac{1}{t}\left\{1-\frac{K_0(\sqrt{t}\rho)}{K_0(\sqrt{t}b_0)}\right\}\sum_{l=0}^{\infty}\frac{2d_0^{2l}}{N_{2l}}(-1)^l S_{2l}(i\sqrt{t}f,0) \\
&= \frac{1}{t}\left\{1-\frac{K_0(\sqrt{t}\rho)}{K_0(\sqrt{t}b_0)}\right\} \quad . \qquad (5.26)
\end{aligned}$$

Here $\rho=\sqrt{x^2+y^2}$ is the distance from the z-axis. In the last step of Eq. (5.26) the relation

$$\sum_{l=0}^{\infty}\frac{2d_0^{2l}(i\sqrt{t}f)}{N_{2l}(i\sqrt{t}f)}S_{2l}(i\sqrt{t}f,\eta)=1 \qquad (5.27)$$

for arbitrary η was used that follows from Eq. (5.3.9) of reference [45] [2]. The last line in Eq. (5.26) is indeed the result for a solution of ideal chains around a cylinder of radius b_0 in three dimensions [22, 7].

In the oblate case the limit $f\rightarrow\infty$ with fixed $b_0=\frac{f}{2}\xi_0$ leads to a plate, bounded by the two planar walls $z=\pm b_0$. In this case the radial function becomes an exponential function, compare Eq. (7) in chapter 3.91 of Ref. [46], which again can be taken out of the sum. As expected, the limit is the well known result of the susceptibility in the presence of a planar wall. For

[2] To derive the relation in Eq. (5.26) one has to take the limit $c\xi\rightarrow\infty$ in Eq. (5.3.9) of reference [45].

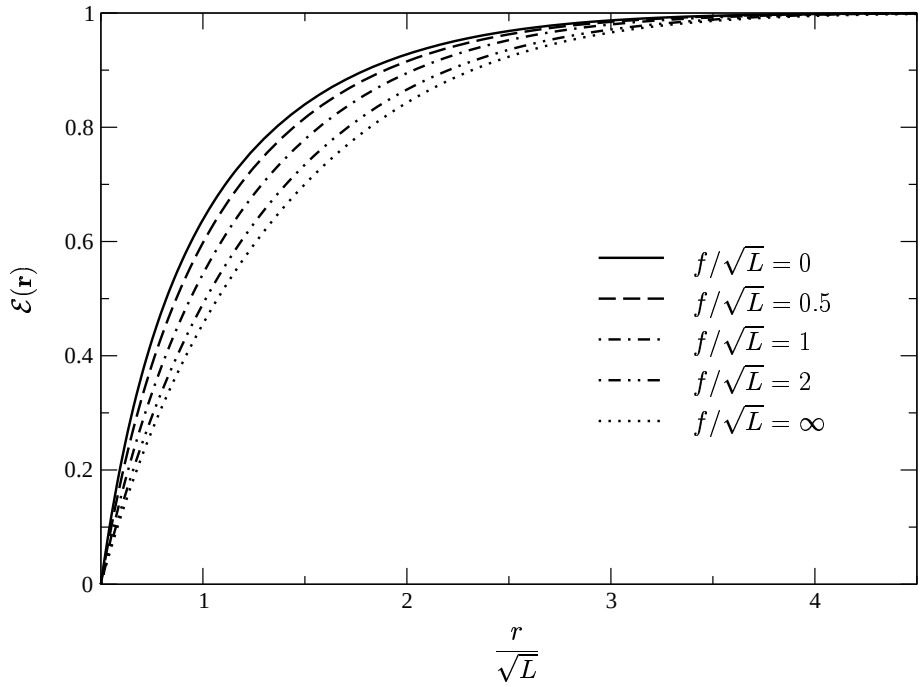

Figure 5.5: Density of chain ends near a prolate ellipsoid versus the scaled interfocal distance. The minor axis is given by $2b_0 = \sqrt{L}$ and the major axis by $2a_0 = \sqrt{L}\sqrt{1+(f^2/L)}$. The values $f/\sqrt{L} = 0$ and $f/\sqrt{L} = \infty$ give the results for a sphere and an infinitely long cylinder, respectively.

example for $z \geq b_0$

$$\begin{aligned}
\chi(t;\mathbf{r}) &\rightarrow \frac{1}{t}\left\{1 - \sqrt{\frac{1+\xi_0^2}{1+\xi^2}}\mathrm{e}^{-\sqrt{t}f(\xi-\xi_0)}\right\}\sum_{l=0}^{\infty}\frac{2d_0^{2l}}{N_{2l}}(-1)^l S_{2l}(i\sqrt{t}f,1) \\
&\rightarrow \frac{1}{t}\left\{1-\mathrm{e}^{-\sqrt{t}\zeta}\right\}\sum_{l=0}^{\infty}\frac{2d_0^{2l}}{N_{2l}}(-1)^l S_{2l}(i\sqrt{t}f,1) \\
&= \frac{1}{t}\left\{1-\mathrm{e}^{-\sqrt{t}\zeta}\right\}\,, \qquad (5.28)
\end{aligned}$$

where $\zeta = z - b_0$ is the distance from the wall at $z = b_0$.

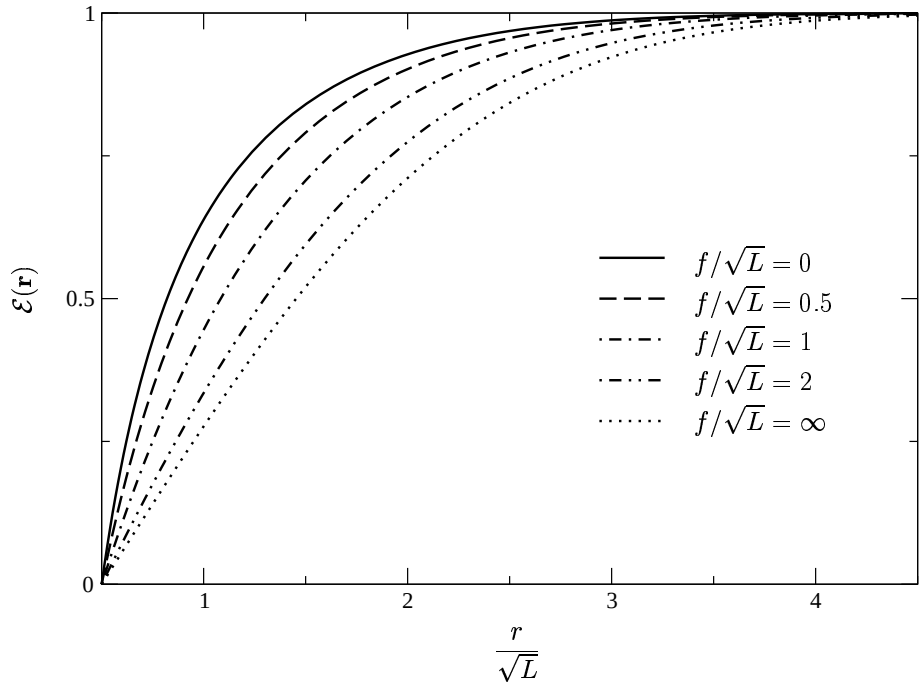

Figure 5.6: Density of chain ends near an oblate ellipsoid versus the scaled interfocal distance. The minor axis is given by $2b_0 = \sqrt{L}$ and the major axis by $2a_0 = \sqrt{L}\sqrt{1 + f^2/L}$. The values $f/\sqrt{L} = 0$ and $f/\sqrt{L} = \infty$ give the results for a sphere and a plate, respectively.

Figures 5.5 and 5.6 show how the end densities for different ellipses interpolate between the different limits. The limits also serve as a check of the numerical accuracy.

5.4 Small ellipsoids

In this section I discuss two different methods to get simple analytical expressions for the density of chain ends. The method in the first subsection

is an extension of the small radius expansion, introduced in Sec. 2.6. This method works well if the axes of the ellipsoid are small compared to the polymer length $\mathcal{R}_g$ and to the distance r from the center of the ellipsoid. In the second subsection I show results for the limit $L \to \infty$ which should be applicable if the condition $a_0, b_0, r \ll \mathcal{R}_g$ holds.

5.4.1 Operator expansion

In the case of an ellipsoid the anisotropy has to be taken into account. Thus the series of the right hand side of Eq. (2.56) now includes also anisotropic operators. The leading anisotropic operators are given by $(\partial_z \phi)^2$ and $\phi(\partial_z^2 \phi)$. The susceptibility $\chi(t; \mathbf{r})$ in the leading isotropic order is given by

$$\begin{aligned} \chi_{\rm iso}(t;\mathbf{r}) &\to \int d\mathbf{r}' < \phi(\mathbf{r})\phi(\mathbf{r}') \left[1 + A_1 \phi^2(0)\right] >_{\rm b} \\ &= \frac{1}{t}\left[1 + 2A_1 G_{S,{\rm b}}(t;\mathbf{r},0)\right] \\ &= \frac{1}{t}\left[1 + 2A_1 \frac{{\rm e}^{-r\sqrt{t}}}{4\pi r}\right] , \end{aligned} \tag{5.29}$$

where the bulk expressions for χ and G_S were inserted. The amplitude A_1 depends only on the size and shape of the ellipsoid and is therefore a function of f and ξ_0. It can be obtained by expanding the Green's function in Eq. (5.21) for $r, r' \gg f$ and by comparing with the operator expansion. This yields

$$A_{1,{\rm prol}} = -\frac{2\,\pi\, f}{Q_0(\xi_0)} \quad , \quad A_{1,{\rm obl}} = \frac{2\,\pi\, i\, f}{Q_0(i\,\xi_0)} \tag{5.30}$$

in the prolate and oblate case, respectively, where

$$Q_0(x) = \frac{1}{2}\ln\frac{x+1}{x-1} \tag{5.31}$$

is a Legendre function of the second kind. The leading anisotropic contribution is

$$\chi_{\rm ani}(t;\mathbf{r}) \to \int d\mathbf{r}' < \phi(\mathbf{r})\phi(\mathbf{r}')\left[A_2(\partial_z\phi(0))^2 + A_3\phi(\partial_z^2\phi(0))\right] >_{\rm b} \quad . \tag{5.32}$$

Using Wick's theorem and Eqs. (2.47), (2.48), (2.50) the first addend becomes

$$\begin{aligned} 2A_2\partial_z < \int d\mathbf{r}'\phi(\mathbf{r}')\phi(0) >_{\rm b} \partial_z < \phi(\mathbf{r})\phi(0) >_{\rm b} \\ = A_2(\partial_z G_S(t;\mathbf{r},0))(\partial_z\frac{1}{t}) = 0 \, . \end{aligned} \tag{5.33}$$

The second addend includes two terms, namely

$$\begin{aligned} A_3(\partial_z^2 < \int d\mathbf{r}'\phi(\mathbf{r}')\phi(0) >_{\rm b}) < \phi(\mathbf{r})\phi(0) >_{\rm b} \\ = A_3 G_S(t;\mathbf{r},0)(\partial_z^2\frac{1}{t}) = 0 \end{aligned} \tag{5.34}$$

and

$$\begin{aligned} A_3 < \int d\mathbf{r}'\phi(\mathbf{r}')\phi(0) >_{\rm b} (\partial_z^2 < \phi(\mathbf{r})\phi(0) >_{\rm b}) = A_3(\partial_z^2 G_S(t;\mathbf{r},0))\frac{1}{t} \\ = A_3\frac{{\rm e}^{-r\sqrt{t}}}{4\pi r^3}\cos^2\vartheta\left(r^2 + 3\frac{r}{\sqrt{t}} + \frac{1}{t}\right) \quad , \end{aligned} \tag{5.35}$$

where ϑ denotes the angle between the vector $\mathbf{r}$ and the z-axis, and all isotropic contributions were neglected. The amplitude A_3 follows from the same expansion as A_1 and is given by

$$A_{3,\mathrm{prol}} = -\frac{2\pi f^3}{3Q_0(\xi_0)} \quad , \quad A_{3,\mathrm{obl}} = -\frac{2\,\pi\,i\,f^3}{3Q_0(i\,\xi_0)} \quad . \tag{5.36}$$

Applying the inverse Laplace transform to χ_{iso} and χ_{ani} yields the small ellipsoid result for the end density near a small prolate ellipsoid

$$\begin{aligned} \mathcal{E}_{\mathrm{SE}}^{\mathrm{iso}}(\mathbf{r}) &= 1 - \frac{1}{Q_0(\xi_0)}\frac{f}{r}\mathrm{erfc}(y) \\ \mathcal{E}_{\mathrm{SE}}^{\mathrm{ani}}(\mathbf{r}) &= -\frac{1}{6Q_0(\xi_0)}\frac{f^3}{r^3}\cos^2\vartheta\left[(2y^3+3y)\frac{2\mathrm{e}^{-y^2}}{\sqrt{\pi}} + 3\mathrm{erfc}(y)\right] \end{aligned} \tag{5.37}$$

with $y = \frac{r}{2\sqrt{L}}$. Here it can be seen directly that for a fixed value of r the end density is a decreasing function of $\cos\vartheta$.

Figure 5.7 shows a comparison of the analytical small ellipsoid expression (circles) with the full numerical result from Eq. (5.23) (full line) for the leading anisotropic contribution $\mathcal{E}_{\mathrm{SE}}^{\mathrm{ani}}(\mathbf{r}) = \mathcal{E}_{\mathrm{SE}}(\vartheta = \pi/2, \mathbf{r}) - \mathcal{E}_{\mathrm{SE}}(\vartheta = 0, \mathbf{r})$. There is a good agreement between the two curves as long as the distance from the surface is not too small.

5.4.2 Infinitely long chains

In the limit of infinitely long chains the end density follows directly from the Laplace equation

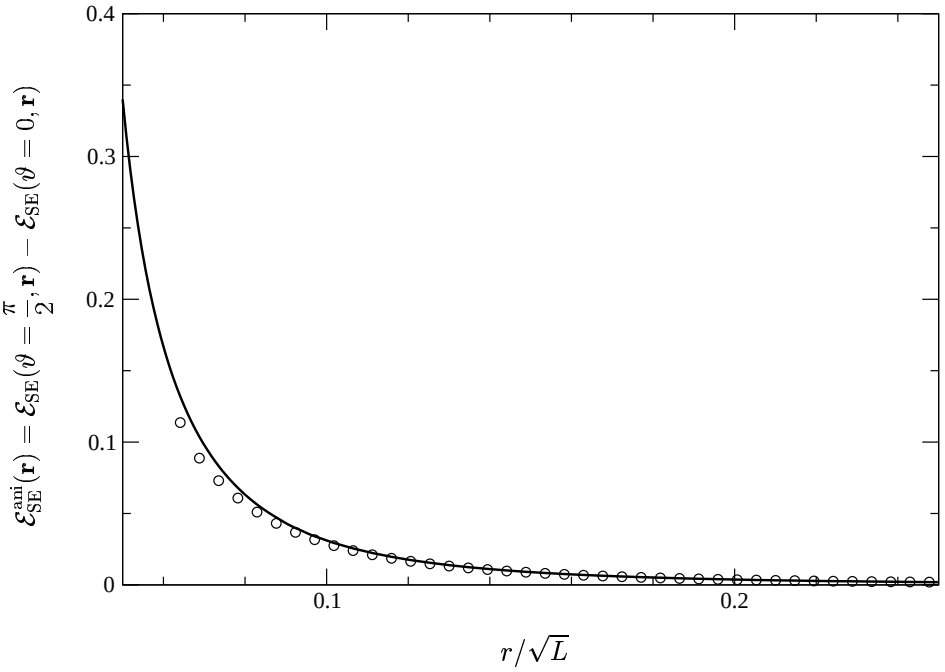

Figure 5.7: Leading anisotropic contribution to the density of chain ends near a small prolate ellipsoid with $a_0/\sqrt{L} = 0.05$, $b_0/\sqrt{L} = 0.03$ versus the scaled distance from the center (full line). This is compared with the small ellipsoid expression of Eq. (5.37) (circles).

$$-\triangle \mathcal{E}_\infty(\mathbf{r}) \; = \; 0 \tag{5.38}$$

with the boundary conditions

$$\mathcal{E}_\infty(\mathbf{r} \to \mathbf{r}_S) \; = \; 0 \;\; , \;\; \mathcal{E}_\infty(\mathbf{r} \to \infty) \; = \; 1 \;\; . \tag{5.39}$$

Here $\mathbf{r}_S$ denotes again a point on the surface. The solution of the Laplace equation with these boundary conditions is given by

$$\mathcal{E}_\infty(\mathbf{r}) = 1 - \frac{Q_0(\xi)}{Q_0(\xi_0)} \quad , \quad \mathcal{E}_\infty(\mathbf{r}) = 1 - \frac{Q_0(i\xi)}{Q_0(i\xi_0)} \tag{5.40}$$

for the prolate and oblate case, respectively, where Q_0 is the Legendre function, defined in Eq. (5.31). As an example I want to study the case of a small circular disk. As mentioned above, this is obtained in the limit $\xi_0 \to 0$ from an oblate ellipsoid. In the case $r, f \ll \mathcal{R}_g$, where the radius $R = f/2$ of the disk and the distance from the disk are much smaller than the polymer length, the limit $L \to \infty$ should be applicable. Then the density of chain ends perpendicular to and in the plane of the *s*mall *c*ircular *d*isk are given by

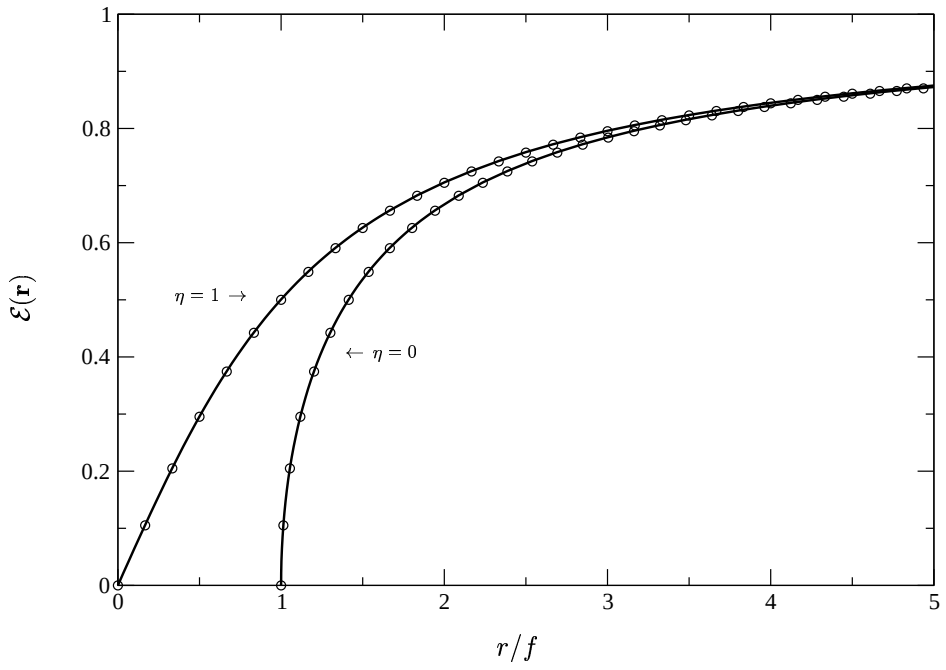

Figure 5.8: Density of chain ends near a small circular disk for $f/\sqrt{L} = 0.01$ (full line). Note that the distance from the center is scaled with the diameter f of the disk. The circles give the analytical expression from Eq. (5.41).

$$\mathcal{E}_{\rm scd}(\mathbf{r}) = \frac{2}{\pi}\begin{cases} \arctan\left(\frac{r}{f}\right) & , \eta = 1 \\ \arctan\sqrt{\left(\frac{r}{f}\right)^2 - 1} & , \eta = 0 \ . \end{cases} \tag{5.41}$$

Fig. 5.8 shows the excellent agreement of the numerically obtained density of chain ends with this prediction in the case $f/\sqrt{L} = 0.01$.

5.5 Free energy cost

The free energy cost for immersing an ellipsoidal particle in a solution of ideal polymers depends of course on the volume of the particle but also on the shape that means on the eccentricity $e = f/(2a) = \sqrt{1-(b/a)^2}$. In order to study the dependence on the latter, I keep the volume of the ellipsoid fixed and calculate the free energy cost as a function of the eccentricity. Fig. 5.9 shows the results for both a prolate and an oblate ellipsoid of a volume $V = (4\pi/3)\mathcal{R}_g^3$. It is remarkable that the free energy cost is very close to that of a sphere with radius $R = \mathcal{R}_g$ as long as the eccentricity is smaller than 0.8. For ellipsoids with $e \to 1$ which is equivalent with $b/a \to 0$ the free energy diverges. This is due to the fact that the surface area of the ellipsoid becomes infinitely large. Since for a plate the depletion layer is larger than for a cylinder, the free energy cost of immersing an oblate ellipsoid (full line) is larger than that for a prolate ellipsoid (dots) of the same volume.

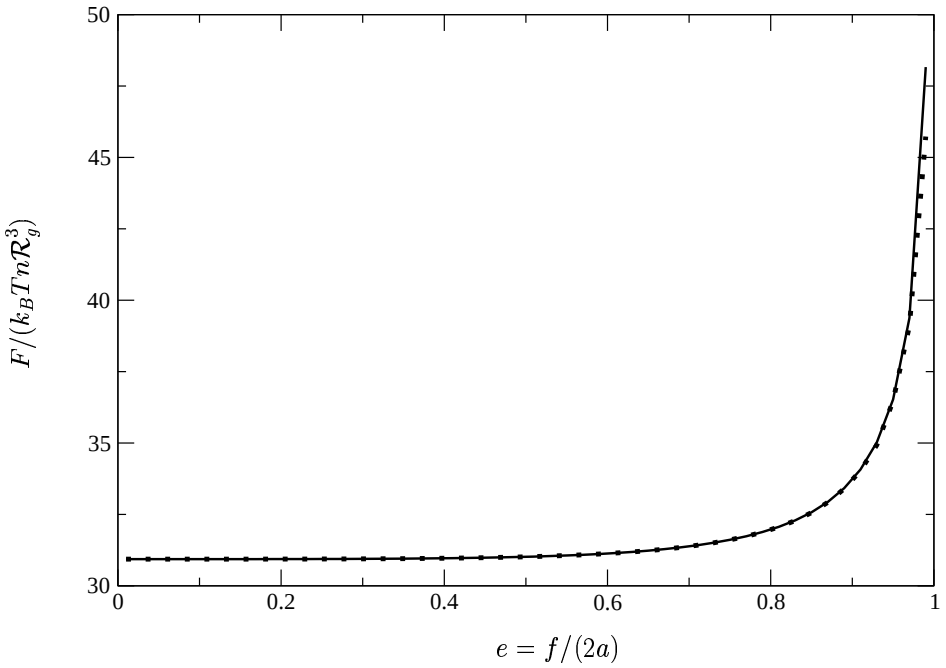

Figure 5.9: Free energy cost for immersing an ellipsoidal particle with the volume $V = (4\pi/3)\mathcal{R}_g^3$ into a solution of ideal polymer chains versus the eccentricity of the ellipsoid. The full line is for an oblate ellipsoid, the dotted line for a prolate one.

Chapter 6

Center of mass distribution of a polymer chain near a planar wall

In the previous sections different density profiles were given for various geometries and for different values of the inter-chain overlap. Besides the density of all the chain segments $\mathcal{M}$ and the density of chain ends $\mathcal{E}$, the density of the center of mass of a polymer chain is also of great interest. However, this is much harder to evaluate, and it has been pointed out by Bolhuis, Louis, Hansen, and Meijer [15] that even for *ideal*, random walk like polymers and the simplest boundary of a planar wall no analytic expression was yet available for the center of mass density profile. In this chapter I show that this gap can be filled and that one can analytically calculate the bulk-normalized center of mass density profile of free ideal polymer chains in a half space bounded by a hard planar wall.

To derive the profile I consider a single ideal chain of N segments in the halfspace bounded by a planar wall at $z = 0$. Then the bulk normalized center of mass density profile is given by

$$\mathcal{C}_{\rm pw}(\mathbf{r}) = \mathcal{C}_{\rm pw}(z) = \int_0^\infty dz_0 ... \int_0^\infty dz_N \prod_{j=1}^{N} P(z_j, z_{j-1}) \delta(z_{\rm cm} - z) \,. \qquad (6.1)$$

Here

$$P(z_A, z_B) = (4\pi l^2)^{-\frac{1}{2}} \exp\left\{ -\frac{1}{4l^2}(z_A - z_B)^2 \right\} \,, \qquad (6.2)$$

and $z_{\rm cm} = \sum_{j=0}^{N} z_j/N$ is the component perpendicular to the wall of the *c*enter of *m*ass of the chain with z_j the distance from the wall of segment j. It is advantageous to introduce a Laplace transform

$$\begin{aligned} \tau(q, L) &\equiv \frac{1}{\sqrt{L}} \int_0^\infty dz \, {\rm e}^{-\,q\,L\,z} \, \mathcal{C}_{\rm pw}(z) \\ &= \frac{1}{\sqrt{L}} \int_0^\infty dz_0 \int_0^\infty dz_N \, {\rm e}^{-l^2\,q\,\frac{z_N + z_0}{2}} \, \tilde{\mathcal{Z}}_{L,l}^{[W]}(z_0, z_N) \end{aligned} \qquad (6.3)$$

with respect to the distance z. Here

$$\begin{aligned} \tilde{\mathcal{Z}}_{L,l}^{[W]}(z_0, z_N) &= \int_0^\infty dz_1 ... \int_0^\infty dz_{N-1} \prod_{j=1}^{N} P(z_j, z_{j-1}) \cdot \\ &\quad \cdot \exp\left\{ -l^2 \sum_{j=1}^{N} W\left(\frac{z_j + z_{j-1}}{2} \right) \right\} \end{aligned} \qquad (6.4)$$

is the partition function for an ideal chain in the external potential W as defined in Sec. 2.1. In the present case $W(z) = qz$ has the structure of a gravitational field with a strength proportional to the Laplace conjugate q. The continuous chain limit $l \to 0$ leads to the representation

$$\tau(q,L) \;=\; \frac{1}{\sqrt{L}} \int_0^\infty dz_0 \int_0^\infty dz_N \, Z^{[W]}(L; z_0, z_N) \tag{6.5}$$

with the continuous chain partition function $Z^{[W]}(L; z', z)$ that satisfies the differential equation (compare Sec. 2.2)

$$\left(\frac{\partial}{\partial L'} - \frac{\partial^2}{\partial z^2} + qz \right) Z^{[W]}(L', z', z) \;=\; 0 \;, \tag{6.6}$$

with the 'initial condition'

$$Z^{[W]}(L' = 0, z', z) \;=\; \delta(z' - z) \tag{6.7}$$

and the boundary condition

$$Z^{[W]}(L', z', z) \;=\; 0 \quad , \quad \text{for} \;\; z = 0 \;\; \text{or} \;\; z' = 0 \;. \tag{6.8}$$

Since the chain is trapped by the hard wall and the gravitational field, this problem has only bound states, and the solution of Eq. (6.6) is given by

$$Z^{[W]}(L', z', z) \;=\; \sum_n \mathrm{e}^{-LE_n} \, \psi_n(z') \, \psi_n(z) \;, \tag{6.9}$$

where the discrete set of eigenfunctions ψ_n and eigenvalues E_n satisfies

$$(\partial_{\tilde{z}}^2 \;-\; q\tilde{z} \;+\; E_n) \, \psi_n(\tilde{z}) \;=\; 0 \quad , \quad \psi_n(0) \;=\; 0 \tag{6.10}$$

and the orthonormality condition that $\int_0^\infty d\tilde{z} \, \psi_n(\tilde{z}) \, \psi_m(\tilde{z})$ equals one for $n = m$ and zero otherwise. The solution of (6.10) is given by [30]

$$\psi_n(z) \;=\; \mathrm{const}_n \cdot \mathrm{Ai}(q^{1/3} z - |a_n|) \;, \tag{6.11}$$

where a_n denotes the n'th zero of the Airy function Ai. The eigenvalues are given by $E_n = q^{2/3}|a_n|$, and the constant follows from the orthonormality condition as

$$\text{const}_n = \frac{q^{1/6}}{\sqrt{\int_0^\infty dx\, \text{Ai}^2(x - |a_n|)}} = \frac{q^{1/6}}{\text{Ai}'(a_n)} \quad . \tag{6.12}$$

In the last step the differential equation for the Airy function was used, and the prime in Ai$'$ denotes a derivative. Inserting ψ_n into Eq. (6.9) and the resulting $Z^{[\mathcal{W}]}$ into Eq. (6.5) yields the result

$$\tau(q,L) \equiv \int_0^\infty d\zeta\, \mathrm{e}^{-Q\zeta}\, \mathcal{C}_{\text{pw}}(z) = Q^{-1/3} \sum_n \mathrm{e}^{-Q^{2/3}|a_n|}\, B_n\, |a_n| \;, \tag{6.13}$$

where $Q = qL^{\frac{3}{2}}$ and $\zeta = z/\sqrt{L} = z/\mathcal{R}_g$. The coefficients B_n are given by

$$B_n = \left[\int_{a_n}^\infty dY\, \text{Ai}(Y)\right]^2 \Big/ \left\{|a_n|\, [\text{Ai}'(a_n)]^2\right\} \quad . \tag{6.14}$$

Inverting the Laplace transform in Eq. (6.13) leads to

$$\begin{aligned}
\mathcal{C}_{\text{pw}}(z) &= \mathcal{L}^{-1}\left\{\tau(q,L)\right\} = \mathcal{L}^{-1}\left\{\sum_{n=1,2,..}^{\infty} B_n\, |a_n|\, Q^{-1/3}\, \mathrm{e}^{-Q^{2/3}|a_n|}\right\} \\
&= \mathcal{L}^{-1}\left\{\sum_{n=1,2,..}^{\infty} B_n \left(-\frac{3}{2}\frac{d}{dQ}\mathrm{e}^{-Q^{2/3}|a_n|}\right)\right\} \\
&= \frac{3}{2}\, z \sum_{n=1,2,..}^{\infty} B_n\, \mathcal{L}^{-1}\left\{\mathrm{e}^{-Q^{2/3}|a_n|}\right\} \quad .
\end{aligned} \tag{6.15}$$

The inverse Laplace transform in the last line can be found in Reference [44] and is given by

$$\mathcal{L}^{-1}\left\{ \mathrm{e}^{-Q^{2/3}|a_n|} \right\} = \sqrt{\frac{3}{\pi}}\, z^{-1}\, G^{3,0}_{2,3}\left(\frac{4}{27}\frac{|a_n|^3}{z^2} \,\middle|\, \begin{matrix} 0, & 1/2 \\ 0, & 1/3, \quad 2/3 \end{matrix} \right) , \qquad (6.16)$$

where G is Meijer's G-function. In Appendix D it is shown that this G-function can be converted into modified Bessel functions, yielding

$$\mathcal{C}_{\mathrm{pw}}(z) = \frac{3\sqrt{3}}{2\pi} \sum_{n=1,2,..}^{\infty} B_n\, X_n\, \mathrm{e}^{-X_n} \left[K_{1/3}(X_n) + K_{2/3}(X_n) \right] \qquad (6.17)$$

with the distance z from the wall contained in

$$X_n = \frac{2}{27}\, |a_n|^3 \,/\, \zeta^2. \qquad (6.18)$$

As expected, $\mathcal{C}_{\mathrm{pw}}(z)$ only depends on the ratio $\zeta = z/R_g$.

For $z/R_g \gg 1$ the main contribution to the sum in (6.17) comes from $n \gg 1$. In this case one has [30]

$$B_n \to 2/(3n) \;\text{ and }\; X_n \to \frac{1}{6}(\pi n/\zeta)^2 \,, \qquad (6.19)$$

and the sum can be replaced by an integral. Performing the integration, one finds that $\mathcal{C}_{\mathrm{pw}}(z)$ approaches 1, as expected.

For $z/R_g \ll 1$ the first term in the sum in (6.17) dominates and

$$\begin{aligned} \mathcal{C}_{\mathrm{pw}}(z) &\to \frac{1}{\sqrt{\pi}}\, B_1\, |a_1|^{3/2}\, \frac{1}{\zeta} \exp\!\left(-\frac{4}{27}\frac{|a_1|^3}{\zeta^2} \right) \\ &\to 2.85\, \frac{1}{\zeta} \exp(-1.89\,/\,\zeta^2) \quad . \end{aligned} \qquad (6.20)$$

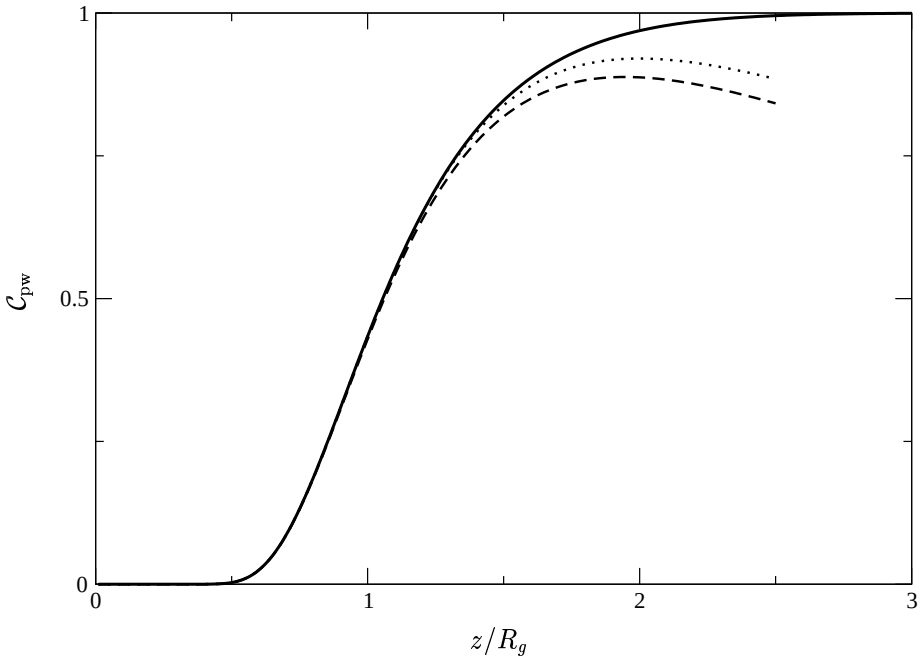

Figure 6.1: Normalized center of mass density profile for ideal polymer chains near a hard wall as given by Eq. (6.17) (full line). The dotted line shows the contribution from the 'ground state' $n = 1$ in (6.17) and the line of dashes shows the asymptotic expression given in Eq. (6.20).

The behavior of the center of mass density profile (6.17) for arbitrary z/R_g is shown as the full line in Fig. 6.1. The good agreement with the corresponding simulation result in Ref. [15] shows that the simulation indeed probes the universal scaling region.

For $\zeta \to 0$ the center of mass density profile Eq. (6.20) drops to zero much more rapidly than profiles for the monomer density or the density of the chain endpoints as can be seen in Fig. 6.2. These display power laws [15, 19] proportional to ζ^2 or ζ rather than the exponential behavior

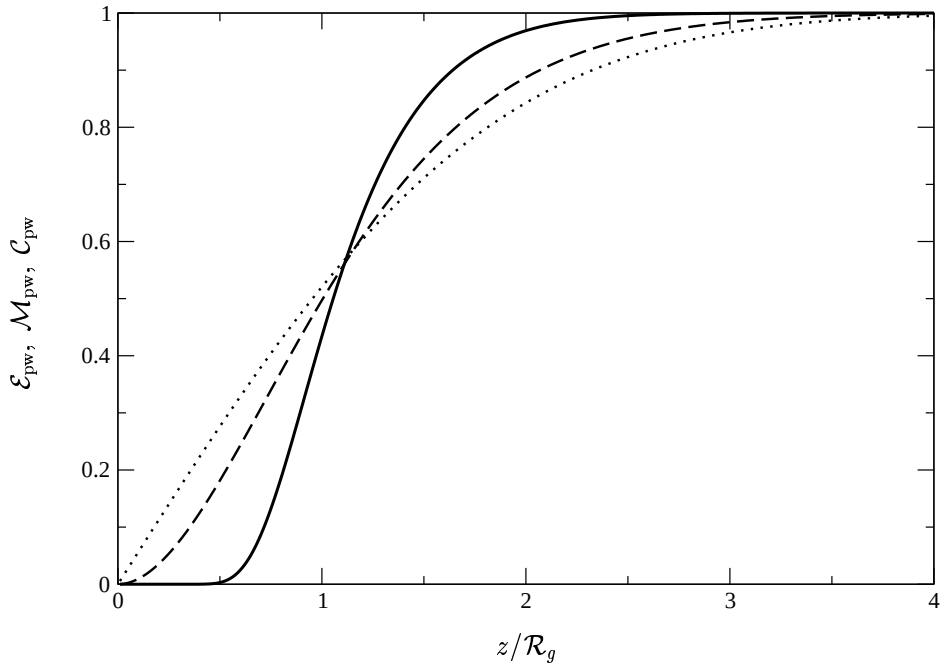

Figure 6.2: Comparison between the profiles of the normalized center of mass density (full line), the density of chain ends (dotted line) and the segment density (dashed line) for ideal polymer chains near a hard wall. Note that the area between the different curves and the axis $y = 1$ is always the same.

in (6.20). For $\zeta \ll 1$ the corresponding repulsive free energy of interaction $\delta F_{\rm cm}(z) = -k_B T \ln[\mathcal{C}_{\rm pw}(z)]$ between the polymer center of mass and the wall is of the power law type $\propto \zeta^{-2}$, while the interaction between a fixed end $\delta F_{\rm end}$ or a fixed midpoint $\delta F_{\rm mid}$ of the polymer and the wall is of the much softer logarithmic type $\propto \ln(1/\zeta)$. The qualitative difference in entropy loss is obvious, since fixing the center of mass close to the wall restricts the polymer configurations much more than fixing an end point or averaging over all segments. For $z_{\rm cm} = 0$ for example only configurations with $z_j = 0$ for all

j can contribute.

Note the close similarity of Eq. (6.20) with the ratio $8\pi^{-2}\exp(-\pi^2 R_g^2/D^2)$ of the partition function of a chain between *two* walls a small distance D apart and averaged over the position of its fixed end to the partition function with fixed end in the bulk [1]. This is consistent with the expectation that chain configurations contributing to a center of mass distance $z \ll R_g$ from a single wall resemble the configurations of a chain trapped between two walls with a distance D of the order of z [1]. Guided by this analogy one would expect for a single chain with excluded volume interactions between monomers [40] that the exponential behavior in the center of mass distribution $\rho(z)/\rho_{\text{bulk}}$ for $z/R_g \ll 1$ is of the form $\exp(-\text{const}/\zeta^{1/\nu})$ with ν the Flory exponent.

What can also be seen in Fig. 6.2 is that the center of mass density profile reaches its bulk value much faster than the other density profiles. This is clear from a formal point of view, since the polymer induced surface tension of the wall which essentially is the integral over the polymer density must not depend on the special choice of the density. Integrating out the last degree of freedom should always yield the same value independent of whether this last degree of freedom is the position of one chain end, any chain segment or the center of mass. In fact one finds for ideal chains the relation

$$\begin{aligned} \int_0^\infty dz\,(1-\mathcal{M}_{\text{pw}}(z)) &= \int_0^\infty dz\,(1-\mathcal{E}_{\text{pw}}(z)) \\ &= \int_0^\infty dz\,(1-\mathcal{C}_{\text{pw}}(z)) = \frac{2}{\sqrt{\pi}}\mathcal{R}_g \end{aligned} \qquad (6.21)$$

and the surface tension is given by $(2/\sqrt{\pi})\,p\mathcal{R}_g$. Here $p = nk_BT$ is the pressure of ideal chains in the dilute solution.

[1] The exponential contributions coincide if $D = 2.3z$.

Chapter 7

Conclusions

In this thesis I have studied the solvation free energy and the polymer density depletion profile of a single mesoscopic colloidal particle immersed in a solution of free non-adsorbing polymer chains. For cylindrical and spherical particles the main goal was to give a global description valid for *arbitrary* values of the particle to polymer size ratio $\rho = R/\mathcal{R}_x$ and of the interchain overlap. It is interesting to see how the qualitatively different behavior evolves in the limits of small and large size ratio and of a dilute and a semidilute polymer solution. For ellipsoidal particles with an axis of rotational symmetry only a dilute solution of ideal polymers was considered. This is a first step towards an understanding of anisotropic colloids in dilute polymer solutions. Since the length of the axes of the ellipsoid was also arbitrary one can study in particular the solvation free energy and the depletion profiles of a thin needle or a circular disk.

Many of the results have been obtained within a mean-field description of the polymer solution, see Eqs. (2.20)-(2.23) and (2.38). While this is quan-

titatively correct only near four dimensions, most of the qualitative features persist down to three dimensions. The mean-field approximation is a consistent theory, which obeys exact relationships such as the density-pressure relation (see Eqs. (1.3) and (3.44)) and identities which follow from the small radius expansion (see Sec. 2.6). The mean-field results from Chapter 3 obtained for a cylindrical particle in four dimensions can be used to describe the qualitative features of a spherical particle in three dimensions. More quantitative results in three dimensions were obtained for the free energy cost to immerse the spherical particle into the polymer solution by means of a 'renormalized tree approximation' (see Ch. 4).

Here I summarize briefly the main results. In the first section of Ch. 3 I calculated scaling functions for the density profile $\mathcal{M}$. Close to the surface the density increases quadratically in accordance with the density-pressure relation in mean-field approximation, see Eq. (3.44). Far away from the surface the profile reaches its bulk value 1. In between it shows a point of inflection. The scaled distance $\xi_I/\mathcal{R}_x$ of the point of inflection from the surface increases with increasing size ratio and decreases with increasing overlap. For $R \gg \mathcal{R}_x$ this decrease with increasing overlap is comparable with the decrease of the density correlation length ξ_D. In the opposite limit of small radius $R \ll \mathcal{R}_x, \xi_D$ the scaled distance is of the order of $R/\mathcal{R}_x$, i.e. independent of the overlap.

For finite values of the inter-chain overlap $\mathcal{S}$ there is a *maximum* in the density profile $\mathcal{M}$ (see Fig. 3.7). This maximum persists down to small size ratio $R \ll \mathcal{R}_x$, where it can be explained via the small radius expansion as a minimum in the bulk density correlation function. The scaled distance of the maximum from the surface is independent of the size ratio and a

decreasing function of the overlap. In the dilute and the semi-dilute limit the maximum vanishes. For small particle radius the density in a semi-dilute solution crosses over from the overlap independent power law behavior for $R, r_\perp \ll \xi$ given in Eq. (1.4) to an exponential decay towards the bulk value for $R \ll r_\perp, \xi$, see Eq. (3.20).

Besides the scaling functions for the density profiles also the mean-field scaling functions for the free energy of immersion of a particle and for the pressure which the polymers exert on the particle were calculated. The numerical mean-field results interpolate smoothly between the analytical results for small and large size ratio ρ. For increasing ρ the pressure decreases, due to an entropically driven decrease in the polymer density near a particle of increasing size. The results for small ρ are independent of the inter-chain overlap $\mathcal{S}$, compare Fig. 3.16. In contrast to that, the scaling function for the decrease of the number of chains $\langle -\delta\mathcal{N} \rangle$ on immersing a particle shows the opposite behavior. It is independent of the overlap for large size ratio, but it depends on $\mathcal{S}$ for particles with small radius, see Eq. (3.51).

The density-pressure identity within the mean-field approximation has been derived in Appendix A and holds for arbitrary size ratio and arbitrary overlap. Thus it can serve as a check of the accuracy of our numerical procedure.

In the Helfrich expansion (2.63) for a weakly curved particle surface the scaling functions for the overlap dependence of the surface tension σ and of the coefficient κ of spontaneous curvature were evaluated both in the mean field and renormalized tree approaches. In the case of σ the mean-field result agrees qualitatively with the renormalized tree result. However, there are qualitative differences in the case of κ. In particular the scaling law

$\kappa/(n\mathcal{R}_x^2) \propto s^{-(2\nu-1)/(d\nu-1)}$ in the semi-dilute limit [which guarantees that κ only depends on the combination $n\mathcal{R}_x^{1/\nu}$ of the segment density] leads to an s-independent behavior in the mean-field approximation (with $\nu = 1/2$) and to a power law decay in the overlap s in the renormalized tree approximation (with $\nu = 0.588$). The renormalized tree result for σ agrees well with the result by Louis *et al.* [41] which was obtained by a combination of simulations and scaling theory.

The renormalized tree approximation was also used to obtain the solvation free energy in the dilute and semi-dilute limit, see Secs. 4.5 and 4.6. The scaling function in the dilute limit depends only on the size ratio $R/\mathcal{R}_x$ and interpolates between the well known limits of large and small size ratio which are determined by the bulk osmotic pressure and by Eq. (4.69), respectively. In the semi-dilute limit the free energy cost per k_BT is a function of the ratio R/ξ and depends on the density only via the screening length ξ. Together with the overlap independent result (4.69) for small particle radius the present renormalized tree results provide a consistent and semi-quantitative description of the free energy cost along the four 'margins' of Fig. 1.1. The scaling functions along the two vertical lines 'large particle radius' and 'small particle radius' and along the two horizontal lines 'dilute solutions' and 'semi-dilute solutions' fit together in the four corners of Fig. 1.1, where they lead to power laws with the correct exponents in three spatial dimensions.

For the case of an ellipsoidal particle immersed in a dilute solution of ideal chains I calculated in Ch. 5 the density of chain ends. The depletion layer around the particle increases with decreasing curvature. Near an oblate particle the depletion is larger than near a prolate particle with the same

major and minor axes. Varying the interfocal distance and keeping the small axis fixed, the ellipsoid interpolates smoothly between a sphere and a cylinder (prolate ellipsoid) or a sphere and a plate (oblate ellipsoid), respectively. For small ellipsoids one can derive analytical expressions for the end density from an anisotropic version of the small radius expansion [34, 35] and from the infinitely long chain limit. Both predictions are in good agreement with the numerical results.

In order to study the effect of anisotropy for the free energy cost for immersing an ellipsoidal particle into a dilute solution of ideal polymer chains, I calculated the scaling function of the free energy cost as a function of the eccentricity for fixed volume. It turned out that the free energy cost increases monotonically with increasing eccentricity. The increase is slightly larger for oblate ellipsoids than for prolate ones.

In Ch. 6 I derived analytically the center of mass density profile $\mathcal{C}_{\mathrm{pw}}$ for a dilute solution of ideal chains in presence of a wall. $\mathcal{C}_{\mathrm{pw}}$ shows qualitative differences to the monomer or end density. Very close to the wall the monomer or end density drop to zero with a power law, while the center of mass density vanishes exponentially. The much larger entropy loss is obvious, since fixing the center of mass close to the wall restricts the polymer configurations much more than fixing e.g. an endpoint.

Appendix A

Derivation of the density-pressure identity

A.1 Pressure on a sphere from a single ideal chain

For simplicity I consider first the case of a single spherical particle immersed in a solution of ideal polymers. All properties follow from the correlation function $G_S(t;\mathbf{r}_A,\mathbf{r}_B)$ of the corresponding Ginzburg-Landau model defined in Eq. (2.45) of Section 2.5. Consider now a particle with a surface S' which deviates slightly from the spherical surface S. S' is obtained by shifting each surface point $\mathbf{r}_S$ of S by a small amount $\eta(\Omega_S)$ towards the center of S. Here Ω_S is the solid angle of the surface point $\mathbf{r}_S$. For the particular cases $\eta(\Omega_S) = \text{const}$ or $\eta(\Omega_S) \propto \cos\vartheta_S$, the surface S' is also spherical, but, compared to S, its radius is decreased ($R' = R - \eta$) or its center is shifted

along the polar axis. To first order in the small deviation η, the correlation function $G_{S'}$ for the deformed surface S' is related to correlation functions for the non-deformed spherical surface S via

$$G_{S'}(t;\mathbf{r}_A,\mathbf{r}_B) = G_S(t;\mathbf{r}_A,\mathbf{r}_B) + \int dS\,\eta(\Omega_S)\,\{\frac{1}{2}(\partial_n\phi(\mathbf{r}_S))^2\cdot\phi(\mathbf{r}_A)\,\phi(\mathbf{r}_B)\,\}_S \quad . \tag{A.1}$$

Here ∂_n is a derivative perpendicular to S, and

$$\{\frac{1}{2}(\partial_n\phi(\mathbf{r}_S))^2\cdot\phi(\mathbf{r}_A)\,\phi(\mathbf{r}_B)\,\}_S \;=\; \{\partial_n\phi(\mathbf{r}_S)\,\phi(\mathbf{r}_A)\}_S\,\{\partial_n\phi(\mathbf{r}_S)\,\phi(\mathbf{r}_B)\}_S \quad , \tag{A.2}$$

due to Wick's theorem. Obviously $G_{S'}$ in (A.1) satisfies the Ornstein-Zernike type equation (2.46) for arbitrary points $\mathbf{r}_A$, $\mathbf{r}_B$ off the surface. As is shown below,

$$G_{S'}(t;\mathbf{r}_A,\mathbf{r}_B) \;\to\; [r_A-(R-\eta(\Omega_A))]\,\{\partial_n\phi(\mathbf{r}_A)\,\phi(\mathbf{r}_B)\}_S \tag{A.3}$$

as $\mathbf{r}_A$ approaches the surface and $\mathbf{r}_B$ is off the surface. Thus $G_{S'}$ vanishes at the deformed surface S'.

To derive (A.3) one has to use the explicit form of G_S, which for a sphere in d dimensions is given by [22, 7]

$$G_S(t;\mathbf{r}_A,\mathbf{r}_B) \;\equiv\; \{\phi(\mathbf{r}_A)\phi(\mathbf{r}_B)\}_S \;=\; \sum_{l=0}^{\infty} W_l^{(\alpha)}(\vartheta)\,\hat{G}_l(t;\mathbf{r}_A,\mathbf{r}_B;R) \quad . \tag{A.4}$$

Here $\alpha=(d-2)/2$, ϑ is the angle between $\mathbf{r}_A$ and $\mathbf{r}_B$, and

$$W_l^{(\alpha)} \;=\; (2\pi^{d/2})^{-1}\,\Gamma(\alpha)\,(l+\alpha)\,C_l^{(\alpha)}(\cos\vartheta) \quad , \tag{A.5}$$

where $C_l^{(\alpha)}$ are Gegenbauer polynomials, and

$$\hat{G}_l \;=\; (r_< r_>)^{-\alpha}\, K_{\alpha+l}(\sqrt{t}\, r_>)\Big(I_{\alpha+l}(\sqrt{t}\, r_<) - \frac{I_{\alpha+l}(\sqrt{t}\, R)}{K_{\alpha+l}(\sqrt{t}\, R)}\, K_{\alpha+l}(\sqrt{t}\, r_<)\Big) \quad , \tag{A.6}$$

where $r_< = \min(r_A, r_B)$, $r_> = \max(r_A, r_B)$ and I, K are modified Bessel functions. This implies

$$\{(\partial_n \phi(\mathbf{r}_S))\, \phi(\mathbf{r}_A)\}_S \;=\; \sum_{l=0}^{\infty} W_l^{(\alpha)}(\vartheta_{\mathbf{r}_S,\mathbf{r}_A})\, R^{-1-\alpha}\, r_A^{-\alpha}\, K_{\alpha+l}(\sqrt{t}\, r_A) \,/\, K_{\alpha+l}(\sqrt{t}\, R) \quad . \tag{A.7}$$

Eq. (A.3) now follows since (A.7) for $r_A \to R$ becomes a $\delta-$function in the solid angle, i.e.

$$\lim_{r_A \to R} R^{d-1} \int d\Omega_S\, f(\Omega_S)\, \{(\partial_n \phi(\mathbf{r}_S))\, \phi(\mathbf{r}_A)\}_S \;=\; f(\Omega_A) \tag{A.8}$$

for arbitrary smooth test functions f. While $\{(\partial_n \phi(\mathbf{r}_S))\, \phi(\mathbf{r}_A)\}_S$ vanishes because of the Dirichlet condition if $\mathbf{r}_A$ approaches a point on the surface S which is *different* from $\mathbf{r}_S$, the Dirichlet condition is broken for $\mathbf{r}_A \to \mathbf{r}_S$ by the operator $\partial_n \phi(\mathbf{r}_S)$.

With the help of Eq. (A.1) one can express the change in free energy of a polymer with two fixed ends on deforming the particle surface

$$\frac{F_{S'} - F_S}{k_B T} \;=\; -\ln \frac{\mathcal{L}^{-1} G_{S'}}{\mathcal{L}^{-1} G_S} \;=\; -\int dS\, \eta(\Omega_S)\, \frac{p(S)}{k_B T} \tag{A.9}$$

in terms of the local polymer pressure $p(S)$ which acts on a surface element dS of the non-deformed spherical surface S. Here again $\mathcal{L}^{-1}$ denotes the inverse

of the Laplace transform in Eq. (2.45). Since the two ends are fixed at $\mathbf{r}_A$, $\mathbf{r}_B$,

$$\frac{p(S)}{k_BT} = \frac{p(\mathbf{r}_S\,;\,\mathbf{r}_A\,,\mathbf{r}_B)}{k_BT} = \frac{\mathcal{L}^{-1}\{\frac{1}{2}(\partial_n\phi(\mathbf{r}_S))^2\,\cdot\,\phi(\mathbf{r}_A)\,\phi(\mathbf{r}_B)\,\}_S}{\mathcal{L}^{-1}\{\phi(\mathbf{r}_A)\,\phi(\mathbf{r}_B)\}_S} \quad . \tag{A.10}$$

If only one end is fixed at $\mathbf{r}_A$ and the other end is free,

$$\frac{p(S)}{k_BT} = \frac{p(\mathbf{r}_S\,;\,\mathbf{r}_A)}{k_BT} = \frac{\mathcal{L}^{-1}\{\frac{1}{2}(\partial_n\phi(\mathbf{r}_S))^2\,\cdot\,\phi(\mathbf{r}_A)\int d\mathbf{r}_B\,\phi(\mathbf{r}_B)\,\}_S}{\mathcal{L}^{-1}\{\phi(\mathbf{r}_A)\int d\mathbf{r}_B\,\phi(\mathbf{r}_B)\}_S} \quad . \tag{A.11}$$

A simple explicit result follows for a *long* chain with one end fixed at $\mathbf{r}_A$ outside the sphere. In this case R, $r_A \ll \mathcal{R}_x$, the Bessel functions in Eq. (A.7) can be expanded for small argument, and one finds

$$\frac{p(\mathbf{r}_S\,;\,\mathbf{r}_A)}{k_BT} = \frac{(d-2)\Gamma(d/2)}{2\pi^{d/2}}\,\frac{(r_A/R)^2-1}{1-(R/r_A)^{d-2}}\,\frac{1}{|\mathbf{r}_A-\mathbf{r}_S|^d} \quad . \tag{A.12}$$

In $d=3$ the derivative of the polymer free energy with respect to the radius of the sphere is given by

$$\int dS\,\frac{p(\mathbf{r}_S\,;\,\mathbf{r}_A)}{k_BT} = \frac{1}{r_A-R} \tag{A.13}$$

and the repulsive force between the fixed point and the sphere by

$$\int dS\,\cos\vartheta_{\mathbf{r}_S,\mathbf{r}_A}\,\frac{p(\mathbf{r}_S\,;\,\mathbf{r}_A)}{k_BT} = \frac{R/r_A}{r_A-R} \quad . \tag{A.14}$$

Both results are consistent with the free energy cost

$$\frac{F_S}{k_BT} = -\ln\left(1-\frac{R}{r_A}\right) \tag{A.15}$$

of introducing the spherical obstacle S.

The pressure in Eqs. (A.10) and (A.11) is related to the density of polymer material near the surface point $\mathbf{r}_S$. For example for an ideal chain with two ends fixed at $\mathbf{r}_A$ and $\mathbf{r}_B$, the fraction of monomers

$$\vartheta(\mathbf{r})\, d\mathbf{r} \equiv \frac{1}{N} \sum_{j=1}^{N} \delta(\mathbf{r} - \mathbf{r}_j)\, d\mathbf{r} \tag{A.16}$$

in a volume element $d\mathbf{r}$ is related to the partition function $Z^{[\mathcal{W}]}$ of a chain subject to an external potential $\mathcal{W}$ by [19]

$$\frac{\mathcal{R}_x^2}{2} \langle \vartheta(\mathbf{r}) \rangle_{A,B} = -\Big(\frac{\delta}{\delta \mathcal{W}(\mathbf{r})} \ln Z^{[\mathcal{W}]}(L;\, \mathbf{r}_A,\, \mathbf{r}_B\,;\, R) \Big)_{\mathcal{W}=0} \quad . \tag{A.17}$$

Here $Z^{[\mathcal{W}]}$ satisfies the diffusion-like equation (2.9) with $L', \mathbf{r}, \mathcal{V}$ replaced by $L, \mathbf{r}_A, \mathcal{W}$. The derivative of $Z^{[\mathcal{W}]}$ is related by

$$-\Big(\frac{\delta}{\delta \mathcal{W}(\mathbf{r})} Z^{[\mathcal{W}]}(L;\, \mathbf{r}_A,\, \mathbf{r}_B\,;\, R) \Big)_{\mathcal{W}=0} = \mathcal{L}^{-1} \{ \frac{1}{2} \phi^2(\mathbf{r}) \cdot \phi(\mathbf{r}_A)\, \phi(\mathbf{r}_B) \}_S \tag{A.18}$$

to the Ginzburg-Landau correlation function with ϕ^2 inserted. When $\mathbf{r}$ approaches the surface $\mathbf{r}_S$ of the spherical particle,

$$\frac{1}{2} \phi^2(\mathbf{r}) \;\to\; (r - R)^2\, \frac{1}{2} \left(\partial_n \phi(\mathbf{r}_S)\right)^2 \quad , \tag{A.19}$$

and Eq. (A.10) leads to the density-pressure relation

$$\langle\, \vartheta(\mathbf{r} \to \mathbf{r}_S) \,\rangle_{A,B} \;\to\; 2 \frac{(r-R)^2}{\mathcal{R}_x^2}\, \frac{p(\mathbf{r}_S\,;\, \mathbf{r}_A\,, \mathbf{r}_B)}{k_B T} \quad . \tag{A.20}$$

For later use I record the relation

$$-\frac{d}{dR} Z^{[0]}(L\,;\, \mathbf{r}_A, \mathbf{r}_B\,;\, R) = \int dS \left(-\frac{\delta}{\delta \mathcal{W}(\mathbf{r})} Z^{[\mathcal{W}]}(L\,;\, \mathbf{r}_A, \mathbf{r}_B\,;\, R)/(r-R)^2 \right)_{\mathbf{r} \to \mathbf{r}_S, \mathcal{W}=0} \quad , \tag{A.21}$$

which follows from (A.1) with an angular-independent $\eta = -dR$ and from Eqs. (A.18) and (A.19).

The relations (A.1), (A.3), (A.8)-(A.11) and (A.21) can be generalized in an obvious way to other surfaces S such as cylinders or ellipsoids. In particular, Eq. (A.21) applies to a cylinder of radius R and infinite length if r is replaced by the distance $r_\perp$ of point $\mathbf{r}$ from the axis of the cylinder.

A.2 Density-pressure identity for mutually repelling chains in the mean-field approximation

To derive (1.3) it is convenient to use the grand canonical ensemble. The derivative of the free energy for a cylinder in Eq. (3.16) is given by

$$\frac{d}{dR}\frac{F/\lambda}{k_BT} = \sum_{\mathcal{N}=1}^{\infty} \frac{\zeta^{\mathcal{N}}}{\mathcal{N}!}\left[-\frac{d}{dR}\,\mathcal{Z}_c^{(\mathcal{N})}/\lambda\right] \tag{A.22}$$

and the density profile of free polymers by Eq. (3.3). There is an obvious correspondence between tree diagrams of Eq. (A.22) shown in Fig. A.1 and tree diagrams (with $\mathbf{r}$-insertions) of Eq. (3.3). Using Eq. (A.21) for each ideal polymer line in Eq. (A.22) generates all the corresponding diagrams of Eq. (3.3), with prefactors such that Eq. (1.3) holds in the form of Eq. (3.44).

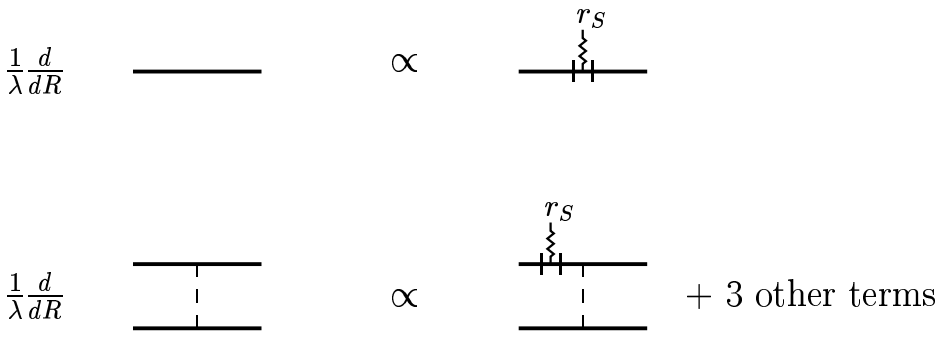

Figure A.1: Diagrammatic representation of the derivative of the free energy cost with respect to the radius of the cylindrical particle (Eqs. (A.21), (A.22)). Each diagram has its counterpart in the fugacity expansion (3.3) of the polymer density near the surface.

Appendix B

Solution of self-consistent equations

In order to solve the system of equations (2.20)-(2.23), one uses the Laplace transform of the partition function $Z^{[\mathcal{V}]}(L, \mathbf{r})$ introduced in Section 2.5

$$\chi^{[\mathcal{V}]}(t; \mathbf{r}) = \mathcal{L}\, Z^{[\mathcal{V}]}(L, \mathbf{r})\,. \tag{B.1}$$

If one now introduces the dimensionless quantities

$$\tilde{\rho} = r_\perp/\sqrt{L}, \;\; \tau = Lt + \mathcal{S} \tag{B.2}$$

and

$$\tilde{\chi}_\tau(\tilde{\rho}) = \chi^{[\mathcal{V}]}(t; \mathbf{r})/L \quad , \tag{B.3}$$

then Eqs. (2.20) and (2.21) lead to

$$-\tilde{\chi}''_\tau(\tilde{\rho}) - \frac{d_\perp - 1}{\tilde{\rho}}\tilde{\chi}'_\tau(\tilde{\rho}) + \left[\tau + \delta\tilde{\mathcal{V}}(\tilde{\rho})\right]\tilde{\chi}_\tau(\tilde{\rho}) = 1 \tag{B.4}$$

with

$$\delta\tilde{\mathcal{V}}(\tilde{\rho}) = \mathcal{S}\left[-1 + \mathcal{M}(r_\perp)\right] \ . \tag{B.5}$$

According to Eq. (2.23),

$$\mathcal{M}(r_\perp) = \int_\gamma \frac{d\tau}{2\pi i}\, e^\tau \tilde{\chi}_\tau^2(\tilde{\rho}) \quad , \tag{B.6}$$

where the integration path γ is parallel to the imaginary axis and to the right of all singularities of the integrand. For the explicit calculation of the inverse Laplace transform one can use Cauchy's integral theorem to deform the integration path as indicated in Fig. B.1.

The integrations over the large quarter circles (γ_2, γ_6) vanish if the radius goes to infinity and on making the angle α arbitrarily small, one remains with an integration of the imaginary part of $\tilde{\chi}_\tau^2$ along the negative real axis (γ_3, γ_5) and an integration along the small circle around the origin (γ_4). The boundary condition (2.22) now reads

$$\tilde{\chi}_\tau(\tilde{\rho} \to R/\sqrt{L}) \to 0 \quad , \tag{B.7}$$

and the bulk limit is given by

$$\lim_{\tilde{\rho}\to\infty} \tilde{\chi}_\tau(\tilde{\rho}) = \frac{1}{\tau}. \tag{B.8}$$

Since the density profile reaches its bulk value 1 at a distance of a few times the correlation length, one can assume that the range of the potential $\delta\tilde{\mathcal{V}}$ is finite, i.e. there exists a $\tilde{\rho}_0$ with $\delta\tilde{\mathcal{V}}(\tilde{\rho}) \equiv 0$ for $\tilde{\rho} \geq \tilde{\rho}_0$. Thus, in the range $\tilde{\rho} \geq \tilde{\rho}_0$ the relevant linear differential equation is

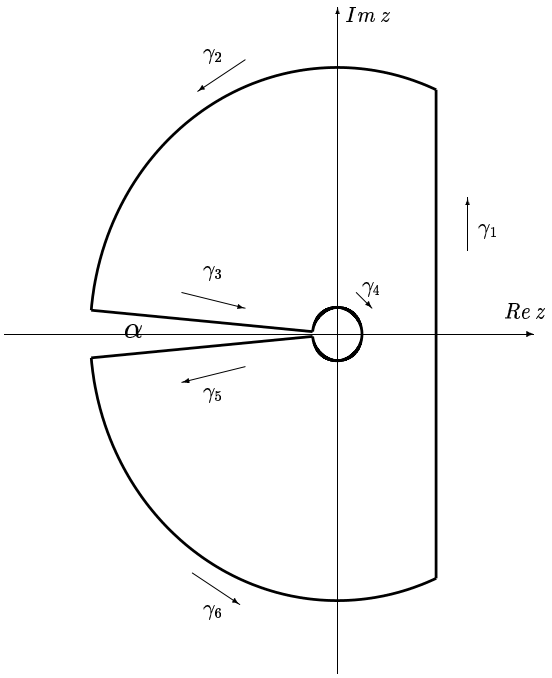

Figure B.1: Deformation of the integration path. γ_1 is the original path, an integration along γ_2 and γ_6 vanishes if the large radius goes to infinity. For $\alpha \to 0$ the integration over γ_3 and γ_5 is an integration along the negative real axis.

$$-\tilde{\chi}_\tau''(\tilde{\rho}) - \frac{d_\perp - 1}{\tilde{\rho}}\tilde{\chi}_\tau'(\tilde{\rho}) + \tau\tilde{\chi}_\tau(\tilde{\rho}) = 1 \tag{B.9}$$

with the boundary condition (B.8), whereas in the range $\tilde{\rho}_s \equiv R/\sqrt{L} \leq \tilde{\rho} < \tilde{\rho}_0$ one has to solve numerically the initial value problems

$$-g_\tau''(\tilde{\rho}) - \frac{d_\perp - 1}{\tilde{\rho}}g_\tau'(\tilde{\rho}) + \left[\tau + \delta\tilde{\mathcal{V}}(\tilde{\rho})\right] g_\tau(\tilde{\rho}) = 1$$

$$g_\tau(\tilde{\rho}_s) = 0, \quad g_\tau'(\tilde{\rho}_s) = 0 \tag{B.10}$$

and

$$-h_\tau''(\tilde{\rho}) - \frac{d_\perp - 1}{\tilde{\rho}} h_\tau'(\tilde{\rho}) + \left[\tau + \delta\tilde{\mathcal{V}}(\tilde{\rho})\right] h_\tau(\tilde{\rho}) = 0$$

$$h_\tau(\tilde{\rho}_s) = 0, \quad h_\tau'(\tilde{\rho}_s) = 1. \tag{B.11}$$

The solution to Eq. (B.4) is given by

$$\begin{aligned} \tilde{\chi}_\tau(\tilde{\rho}) \quad &= \quad \left(g_\tau(\tilde{\rho}) + c_1 h_\tau(\tilde{\rho}) \, , \, \frac{1}{\tau} + c_2 \tilde{\rho}^{-\alpha} K_\alpha(\tilde{\rho}\sqrt{\tau})\right) \\ &\text{for} \quad \left(R/\sqrt{L} \leq \tilde{\rho} < \tilde{\rho}_0 \, , \, \tilde{\rho}_0 < \tilde{\rho}\right) \end{aligned} \tag{B.12}$$

where $\alpha = (d_\perp - 2)/2$ and K_α is a modified Bessel function. The constants c_1 and c_2 are calculated from the continuity condition of $\tilde{\chi}_\tau$ and $\tilde{\chi}_\tau'$ at $\tilde{\rho} = \tilde{\rho}_0$.

Thus, after choosing a starting potential [1] $\delta\tilde{\mathcal{V}}_0(\tilde{\rho})$, one calculates, with the steps described above, a solution $\tilde{\chi}_\tau^0$, which by means of Eqs. (B.6) and (B.5) yields a new potential $\delta\tilde{\mathcal{V}}_1(\tilde{\rho})$. Solving the problem (B.4)-(B.8) again with $\delta\tilde{\mathcal{V}}(\tilde{\rho})$ replaced by $\delta\tilde{\mathcal{V}}_1(\tilde{\rho})$ and following the same steps leads to a potential $\delta\tilde{\mathcal{V}}_2(\tilde{\rho})$ and so on. The sequence $\delta\tilde{\mathcal{V}}_i(\tilde{\rho})$ then converges to the self-consistent potential $\delta\tilde{\mathcal{V}}(\tilde{\rho})$, which yields the monomer density $\mathcal{M}(r_\perp)$ directly from Eq. (B.5).

[1] In practise $\delta\tilde{\mathcal{V}}_0(\tilde{\rho})$ was always chosen to be zero so that the solution $\tilde{\chi}_\tau^0$ is the well known analytical result for the dilute limit

Appendix C

Susceptibility for the ellipsoid problem

Here the integration of the Green's function that leads to the susceptibility in Eq. (5.23) is shown in detail. Starting point is the relation

$$\chi(t;\mathbf{r}) = \int_0^{2\pi} d\phi \int_{-1}^{1} d\eta \int_{\xi_0}^{\infty} d\xi f^3(\xi^2-\eta^2) G(\eta,\xi,\phi;\eta',\xi',\phi') \ , \qquad \text{(C.1)}$$

where for G one has to insert Eq. (5.21). The integration over the angle variable ϕ leads to a factor $2\pi\delta_{m0}$, as expected from the symmetry requirements. Therefore the sum over m reduces to the one addend with $m = 0$, and one gets

$$\begin{aligned}\chi(t;\mathbf{r}) \ &= \ ik \int_{-1}^{1} d\eta \int_{\xi_0}^{\infty} d\xi f^3(\xi^2-\eta^2) \sum_{n=0}^{\infty} \frac{1}{N_n} S_n(c,\eta) S_n(c,\eta') \cdot \\ &\cdot \begin{cases} R_n^{(1)}(c,\xi) R_n^{(3)}(c,\xi') - \dfrac{R_n^{(1)}(c,\xi_0)}{R_n^{(3)}(c,\xi_0)} R_n^{(3)}(c,\xi) R_n^{(3)}(c,\xi') \ , \ \xi < \xi' \\ R_n^{(1)}(c,\xi') R_n^{(3)}(c,\xi) - \dfrac{R_n^{(1)}(c,\xi_0)}{R_n^{(3)}(c,\xi_0)} R_n^{(3)}(c,\xi) R_n^{(3)}(c,\xi') \ , \ \xi > \xi' \ . \end{cases} \qquad \text{(C.2)}\end{aligned}$$

The integration over η can also be carried out independently yielding

$$\int_{-1}^{1} d\eta\,(\xi^2-\eta^2)S_n(c,\eta) \;=\; {\sum_{r=0,1}^{\infty}}' d_r^n(c)\int_{-1}^{1} d\eta\,(\xi^2-\eta^2)P_r(\eta)$$

$$= \begin{cases} \sum_{r=0}^{\infty} d_{2r}^{2l}(c)\int_{-1}^{1} d\eta\,(\xi^2-\eta^2)P_{2r}(\eta) & ,n=2l \\ \sum_{r=0}^{\infty} d_{2r+1}^{2l+1}(c)\int_{-1}^{1} d\eta\,(\xi^2-\eta^2)P_{2r+1}(\eta) & ,n=2l+1 \end{cases}$$

$$= \begin{cases} 2\xi^2 d_0^{2l} - (\frac{2}{3}d_0^{2l} + \frac{4}{15}d_2^{2l}) & ,n=2l \\ 0 & ,n=2l+1\;. \end{cases} \qquad \text{(C.3)}$$

To simplify the integration over ξ one needs the recursion formula for the coefficients d_r^n that is given by [45]

$$\frac{(r+2)(r+1)c^2}{(2r+3)(2r+5)}d_{r+2}^n(c) + \left[r(r+1) - \lambda_n(c) + \frac{2r(r+1)-1}{(2r-1)(2r+3)}c^2\right] d_r^n(c)$$

$$+ \frac{r(r-1)c^2}{(2r-3)(2r-1)}d_{r-2}^n(c) = 0\;. \qquad \text{(C.4)}$$

For $r=0$ this leads to

$$\frac{2}{15}c^2\,d_2^n(c) \;+\; (\frac{1}{3}c^2 - \lambda_n(c))\,d_0^n(c) = 0\;. \qquad \text{(C.5)}$$

Inserting this result into Eq. (C.3) gives for the η-integration the result

$$\int_{-1}^{1} d\eta\,(\xi^2-\eta^2)S_n(c,\eta) \;=\; \frac{2d_0^n(c)}{c^2}(c^2\xi^2 - \lambda_n(c))\delta_{n,2l} \qquad \text{(C.6)}$$

so that only even values of n survive. For the sphere limit in Eq. (5.25) I

need also the behavior of the coefficients for $f \to 0$. This is equivalent with $c \to 0$, and in this limit the recursion formula reduces to

$$\begin{aligned} 0 &= [r(r+1) - \lambda_n(0)]\, d_r^n(0) \\ &= [r(r+1) - n(n+1)]\, d_r^n(0) \quad . \end{aligned} \tag{C.7}$$

The $c \to 0$ result $\lambda_n(0) = n(n+1)$ is taken from Reference [45]. From the last line it follows that $d_r^n(0) = \text{const} \cdot \delta_{rn}$, and from the normalization of the coefficients it follows that const $= 1$.

The remaining ξ-integration decomposes into two parts. One gets for $\xi < \xi'$

$$\begin{aligned} &\int_{\xi_0}^{\xi'} d\xi\, (c^2\xi^2 - \lambda_n(c)) \left[R_n^{(1)}(c,\xi) R_n^{(3)}(c,\xi') - \frac{R_n^{(1)}(c,\xi_0)}{R_n^{(3)}(c,\xi_0)} R_n^{(3)}(c,\xi) R_n^{(3)}(c,\xi') \right] \\ &\quad = -R_n^{(3)}(c,\xi') \left[(\xi^2-1) \frac{d}{d\xi} \left(R_n^{(1)}(c,\xi) - \frac{R_n^{(1)}(c,\xi_0)}{R_n^{(3)}(c,\xi_0)} R_n^{(3)}(c,\xi) \right) \right]_{\xi_0}^{\xi'} \end{aligned} \tag{C.8}$$

and for $\xi > \xi'$

$$\begin{aligned} &\int_{\xi'}^{\infty} d\xi\, (c^2\xi^2 - \lambda_n(c)) \left[R_n^{(1)}(c,\xi') R_n^{(3)}(c,\xi) - \frac{R_n^{(1)}(c,\xi_0)}{R_n^{(3)}(c,\xi_0)} R_n^{(3)}(c,\xi) R_n^{(3)}(c,\xi') \right] \\ &\quad = -\left(R_n^{(1)}(c,\xi') - \frac{R_n^{(1)}(c,\xi_0)}{R_n^{(3)}(c,\xi_0)} R_n^{(3)}(c,\xi') \right) \left[(\xi^2-1) \frac{d}{d\xi} R_n^{(3)}(c,\xi) \right]_{\xi'}^{\infty} , \end{aligned} \tag{C.9}$$

where the differential equation for R_n (Eq. (5.13)) was used. From Eq. (4.1.17) in reference [45] one knows that

$$R_n^{(3)}(c,\xi) \quad \stackrel{c\xi \to \infty}{\longrightarrow} \quad \frac{\mathrm{e}^{ic\xi}}{c\xi} \quad . \tag{C.10}$$

Thus, for $c = i\sqrt{t}f$ $R_n^{(3)}(c,\xi)$ vanishes exponentially, and the insertion of the upper bound in Eq. (C.9) yields no contribution. Inserting the other boundaries and combining Eqs. (C.2), (C.6), (C.8), (C.9) gives

$$\chi(t;\mathbf{r}) \;=\; -\frac{2ikf^3}{c^2}\sum_{l=0}^{\infty}\frac{d_0^{2l}(c)}{N_{2l}(c)}\,\frac{S_{2l}(c,\eta')}{R_{2l}^{(3)}(c,\xi_0)}\cdot$$

$$\cdot\left\{R_{2l}^{(3)}(c,\xi')\left[i(\xi'^2-1)\left(R_{2l}^{(2)}(c,\xi_0)\left(\tfrac{d}{d\xi'}R_{2l}^{(3)}(c,\xi')\right)-\left(\tfrac{d}{d\xi'}R_{2l}^{(3)}(c,\xi')\right)R_{2l}^{(1)}(c,\xi_0)\right)+\frac{i}{c}\right]\right.$$

$$\left.-\left(\tfrac{d}{d\xi'}R_{2l}^{(3)}(c,\xi')\right)(\xi'^2-1)\left(R_{2l}^{(3)}(c,\xi_0)R_{2l}^{(1)}(c,\xi')-R_{2l}^{(1)}(c,\xi_0)R_{2l}^{(3)}(c,\xi')\right)\right\}, \quad \text{(C.11)}$$

where I used Eq. (5.18) and the Wronskian

$$R_n^{(1)}(c,\xi)\left(\frac{d}{d\xi'}R_n^{(2)}(c,\xi)\right)-R_n^{(2)}(c,\xi)\left(\frac{d}{d\xi'}R_n^{(1)}(c,\xi)\right)=\frac{1}{c(\xi^2-1)}\quad . \quad \text{(C.12)}$$

Applying again the same tools one gets

$$\chi(t;\mathbf{r}) \;=\; -\frac{1}{k^2}\sum_{l=0}^{\infty}\frac{2d_0^{2l}(c)}{N_{2l}(c)}\,\frac{S_{2l}(c,\eta)}{R_{2l}^{(3)}(c,\xi_0)}\left\{R_{2l}^{(3)}(c,\xi_0)-R_{2l}^{(3)}(c,\xi)\right\}, \quad \text{(C.13)}$$

and by using Eq. (5.27) and setting $k = i\sqrt{t}$ one finally arrives at

$$\chi(t;\mathbf{r}) \;=\; \frac{1}{t}\left\{1-\sum_{l=0}^{\infty}\frac{2d_0^{2l}(i\sqrt{t}f)}{N_{2l}(i\sqrt{t}f)}S_{2l}(i\sqrt{t}f,\eta)\frac{R_{2l}^{(3)}(i\sqrt{t}f,\xi)}{R_{2l}^{(3)}(i\sqrt{t}f,\xi_0)}\right\}\quad . \quad \text{(C.14)}$$

Appendix D

Transformation of the Meijer function

In the derivation of the center of mass density profile near a planar wall in Chapter 6 occurs a Meijer G-function. Since this is no standard function one is interested to express it in terms of more well known functions if possible. In this appendix I show how this can be done in the present case. Inserting the definition of the Meijer function, given in Ref. [43] one finds

$$G^{3,0}_{2,3}\left(x\left|\begin{array}{lll} 0, & 1/2 & \\ 0, & 1/3, & 2/3 \end{array}\right.\right) = \frac{1}{2\pi i}\int_{L_{i\infty}} \frac{\Gamma\left(\frac{2}{3}+s\right)\Gamma\left(\frac{1}{3}+s\right)}{\Gamma\left(\frac{1}{2}+s\right)}\, x^{-s}\, ds$$

$$= \frac{1}{2\pi i}\int_{L_{i\infty}} \frac{\frac{1}{2}\left(\frac{1}{3}+s+\frac{2}{3}+s\right)}{\frac{1}{2}+s} \frac{\Gamma\left(\frac{2}{3}+s\right)\Gamma\left(\frac{1}{3}+s\right)}{\Gamma\left(\frac{1}{2}+s\right)}\, x^{-s}\, ds$$

$$= \frac{1}{2}\,\frac{1}{2\pi i}\int_{L_{i\infty}} \left[\frac{\Gamma\left(\frac{4}{3}+s\right)\Gamma\left(\frac{2}{3}+s\right)}{\Gamma\left(\frac{3}{2}+s\right)} + \frac{\Gamma\left(\frac{5}{3}+s\right)\Gamma\left(\frac{1}{3}+s\right)}{\Gamma\left(\frac{3}{2}+s\right)}\right] x^{-s}\, ds$$

$$= \frac{1}{2}\frac{1}{2\pi i}\int_{L_{i\infty}}\left[\frac{\Gamma\left(\frac{1}{3}+t\right)\Gamma\left(-\frac{1}{3}+t\right)}{\Gamma\left(\frac{1}{2}+t\right)}+\frac{\Gamma\left(\frac{2}{3}+t\right)\Gamma\left(-\frac{2}{3}+t\right)}{\Gamma\left(\frac{1}{2}+t\right)}\right]x^{-t}\,x\,dt$$

$$= \frac{x}{2}\left[G^{2,0}_{1,2}\left(x\left|\begin{array}{ll}1/2 & \\ 1/3, & -1/3\end{array}\right.\right)+G^{2,0}_{1,2}\left(x\left|\begin{array}{ll}1/2 & \\ 2/3, & -2/3\end{array}\right.\right)\right] \quad . \qquad \text{(D.1)}$$

$L_{i\infty}$ denotes a way in the complex plane parallel to the imaginary axis and to the right of all singularities of the integrand, and in the fourth step I substituted $s+1$ by t. Again from Ref. [43] one can find that the Meijer functions in the last expression are directly related to the modified Bessel function via

$$G^{2,0}_{1,2}\left(x\left|\begin{array}{ll}1/2 & \\ \alpha, & -\alpha\end{array}\right.\right) = \frac{1}{\sqrt{\pi}}\mathrm{e}^{-x/2}\,K_\alpha\left(\frac{x}{2}\right) \qquad \text{(D.2)}$$

which leads directly to the result used in Eq. (6.17)

$$G^{3,0}_{2,3}\left(x\left|\begin{array}{lll}0, & 1/2 & \\ 0, & 1/3, & 2/3\end{array}\right.\right) = \frac{1}{\sqrt{\pi}}\frac{x}{2}\mathrm{e}^{-x/2}\left[K_{1/3}\left(\frac{x}{2}\right)+K_{2/3}\left(\frac{x}{2}\right)\right] \quad . \qquad \text{(D.3)}$$

Bibliography

[1] S. Asakura and F. Oosawa, J. Chem. Phys. **22**, 155 (1954).

[2] R. Tuinier et al., Phys. Rev. E **60**, 848 (1999).

[3] J. Janzen and D.E. Brooks, Clinical Hemorheology **9**, 695 (1989).

[4] A.M. Kulkarni, A.P. Chatterjee, K.S. Schweizer, and C.F. Zukoski, Phys. Rev. Lett. **83**, 4554 (1999); J. Phys. (London) C **12**, A301 (2000).

[5] A.P. Minton, Current Opinion in Biotechnology **8**, 65 (1997).

[6] P.R. Wills et al., Biophys. Chem. **57**, 37 (1995).

[7] A. Hanke, E. Eisenriegler, and S. Dietrich, Phys. Rev. E **59**, 6853 (1999).

[8] A.P. Chatterjee and K.S. Schweizer, J. Chem. Phys. **109**, 10464 (1998).

[9] A.P. Chatterjee and K.S. Schweizer, J. Chem. Phys. **109**, 10477 (1998).

[10] A. Bringer, E. Eisenriegler, F. Schlesener and A. Hanke, Eur. Phys. J. B, **11**, 101 (1999).

[11] M. Fuchs and K.S. Schweizer, Europhys. Lett. **51**, 621 (2000)

[12] R. Tuinier, G.A. Vliegenthart and H.N.W. Lekkerkerker, J. Chem. Phys. **113**, 10768 (2000).

[13] R. Tuinier, G.A. Vliegenthart and H.N.W. Lekkerkerker, Macromolecules **34**, 4636 (2001).

[14] F. Schlesener, A. Hanke, R. Klimpel and S. Dietrich, Phys. Rev. E **63**, 041803 (2001).

[15] P. G. Bolhuis, A. A. Louis, J. P. Hansen, E. J. Meijer, J. Chem. Phys. **114**, 4296 (2001).

[16] P.G. de Gennes, *Scaling Concepts in Polymer Physics* (Cornell University, Ithaca, 1979).

[17] J. des Cloizeaux and G. Jannink, *Polymers in Solution* (Clarendon, Oxford, 1990).

[18] L. Schaefer, *Excluded Volume Effects in Polymer Solutions* (Springer Berlin Heidelberg New York, 1999).

[19] E. Eisenriegler, *Polymers near Surfaces* (World Scientific, Singapore, 1993).

[20] T.M. Birshtein and O.V. Borisov, Polymer **32**, 916 (1991).

[21] T. Odijk, Macromolecules **29**, 1842 (1996); J. Chem. Phys. **106**, 3402 (1996); Physica A **278**, 347 (2000).

[22] E. Eisenriegler, A. Hanke, and S. Dietrich, Phys. Rev. E **54**, 1134 (1996).

[23] E. Eisenriegler, J. Physics (London) C **12**, A227 (2000).

[24] K.M. Jansons and C.G. Phillips, J. Colloid Interface Sci. **137**, 75 (1990).

[25] K.R. Myers and K.F. Freed, J. Chem. Phys. **98**, 2437 (1993).

[26] P.G. de Gennes, C.R. Acad. Sc. Paris B **288**, 359 (1979).

[27] J.F. Joanny, L. Leibler and P.G. de Gennes, J. Polym. Sci., Polym. Phys. Ed. **17**, 1073 (1979).

[28] E. Eisenriegler, Phys. Rev. E **55**, 3116 (1997).

[29] E. Eisenriegler, in: *Field Theoretical Tools in Polymer- and Particle-Physics*, (H. Meyer-Ortmanns, A. Klümper eds.), Lecture Notes in Physics **508** (Springer, Berlin, 1998).

[30] M. Abramowitz and I. Stegun, *Handbook of Mathematical Functions* (Dover Publications, New York 1965).

[31] R. Maassen, E. Eisenriegler and A. Bringer, J. Chem. Phys. **115**, 5292 (2001).

[32] E. Eisenriegler and R. Maassen, J. Chem. Phys. **116**, 449, (2002).

[33] P.G. de Gennes, Phys. Lett. **38A**, 339 (1972).

[34] T.W. Burkhardt and E.Eisenriegler, Phys. Rev. Lett. **74**, 3189 (1995).

[35] E.Eisenriegler and U. Ritschel, Phys. Rev. B **51**, 13717 (1995).

[36] W. Helfrich, Z. Naturforsch. C **28**, 693 (1973).

[37] E. Eisenriegler, J. Chem. Phys. **79**, 1052 (1983).

[38] J. van der Gucht, N. A. M. Besseling, J. van Male, and M. A. Cohen Stuart, J. Chem. Phys. **113**, 2886 (2000).

[39] D. R. Nelson, Phys. Rev. B **14**, 1123 (1976)

[40] M. Daoud and P.G. de Gennes, J. Phys. (Paris) **38**, 85 (1977).

[41] A.A. Louis, P.G. Bolhuis, E.J. Meijer and J.P. Hansen, J. Chem. Phys. **116**, 10547 (2002).

[42] C.R. Chester, *Techniques in partial differential equations*, International series in pure and applied mathematics, McGraw-Hill Book Company (1971).

[43] A. Prudnikov, Yu. Brychkov, and O. Marichev, *Integrals and Series*, Vol. 3, (Gordon and Breach, London 1992).

[44] A. Prudnikov, Yu. Brychkov, and O. Marichev, *Integrals and Series*, Vol 5, (Gordon and Breach, London 1992).

[45] C. Flammer, *Spheroidal wave functions*, stanford university press (1957).

[46] J.Meixner, F.W.Schäfke, *Mathieusche Funktionen und Sphäroidfunktionen* (Springer, Berlin 1954).

List of Figures

Danksagung

Die vorliegende Arbeit wurde am Institut für Festkörperforschung des Forschungszentrums Jülich angefertigt. Mein Dank gilt allen, die zum Gelingen dieser Arbeit beigetragen haben. Insbesondere danke ich Herrn Prof. Dr. E. Eisenriegler für die stete Hilfsbereitschaft und die anregende Betreuung der Arbeit. Desweiteren danke ich Herrn Dr. A. Bringer für wertvolle Diskussionen und zahlreiche Ratschläge und meinen Kollegen für den freundschaftlichen Austausch während des Mittagessens und bei anderen Gelegenheiten. Allen meinen Freunden danke ich für Ihr Verständnis und Ihren Zuspruch.

Ganz besonderer Dank gilt meinen Eltern und meiner Freundin Ines für Ihre Unterstützung und Aufmunterung, ohne die das Ganze nicht möglich gewesen wäre.